COMPUTER ENHANCED SPECTROCHEMICAL AND CHROMATOGRAPHIC ANALYSIS APPLIED TO PROBLEMS IN ANALYTICAL AND FORENSIC CHEMISTRY

By

UNDUGODAGE DON NUWAN THARANGA PERERA

Bachelor of Science
University of Kelaniya
Kelaniya, Sri Lanka
2006

Post Graduate Diploma in Analytical Chemistry
University of Peradeniya
Peradeniya, Sri Lanka
2009

Submitted to the Faculty of the
Graduate College of the
Oklahoma State University
in partial fulfillment of
the requirements for
the Degree of
DOCTOR OF PHILOSOPHY
July, 2015

COMPUTER ENHANCED SPECTROCHEMICAL AND CHROMATOGRAPHIC ANALYSIS APPLIED TO PROBLEMS IN ANALYTICAL AND FORENSIC CHEMISTRY

Dissertation Approved:

Dr. Barry K. Lavine

Dissertation Adviser

Dr. Ziad El Rassi

Dr. Nicholas Materer

Dr. Sadagopan Krishnan

Dr. Kaan Kalkan

ACKNOWLEDGEMENTS

First and foremost, I would like to express my deepest gratitude to my advisor, Dr. Barry K. Lavine, for his continuous support, excellent guidance, caring, patience, motivations and immense knowledge, without whom none of this would have been possible.

I would also like to thank my graduate advisory committee Dr. Ziad El Rassi, Dr. Nicholas Materer, Dr. Sadagopan Krishnan, Dr. John Gelder, and Dr. Kaan Kalkan for their guidance, advices and valuable comments.

I am thankful to my lab mates Collin, Sandhya, Tao and Kaushalya for the friendship and help gave to me when needed. Special thanks goes to former lab mates Dr. Ayuba Fasasi and Dr. Nikhil Mirjankar for their helpful discussions and guidance.

Finally, I wish to thank my family for their unconditional love, tremendous support and encouragement. My parents, Ranjan Perera and late Gnanawathie Aluthgedara, and my two sisters, Nilushi and Dilushi, have provided unending support for my career choice, without whom I would not be where I am today. Thank you my son Vinuka for becoming the origin of my happiness and the spirit of my hope for the future. Finally, I would like to thank my wife Rangika for cheering me up and standing by me through the good times and bad. Thank you for being with me all these years and making them the best years of my life.

Name: UNDUGODAGE DON NUWAN THARANGA PERERA

Date of Degree: JULY, 2015

Title of Study: COMPUTER ENHANCED SPECTROCHEMICAL AND CHROMATOGRAPHIC ANALYSIS APPLIED TO PROBLEMS IN ANALYTICAL AND FORENSIC CHEMISTRY

Major Field: CHEMISTRY

Abstract:

The main objectives of the research described in this dissertation are: (1) to develop powerful separation methods for the analysis of complex mixtures by systematically adjusting parameters related to selectivity, (2) to better understand polymer swelling as a transduction mechanism for chemical sensing, and (3) to address the issue of distortions in attenuated total reflection (ATR) spectra when compared to transmission spectra of the same samples. Using medium chain length alcohols as mobile phase modifiers in reversed phase liquid chromatography to improve selectivity through enhanced stationary phase solvation, better resolution is achieved in the separation of vanillin and its isomers with water rich mobile phases. This can be attributed to butanol partitioning into the bonded alkyl phase, increasing the contact surface area of the stationary phase and thereby increasing the selectivity of the separation. Copolymers of *N*-isopropylacrylamide and alkyl acrylic acids are shown to swell reversibly in both low and high ionic strength buffer solutions at ambient and physiological temperatures. The pK_a of these particles can be tuned to respond sharply in the physiological pH range (5.0 to 7.4) by varying the degree of cross-linking, the amount of *N*-tertbutylacrylamide in the formulation or the alkyl chain length of the pH sensitive co-monomer. The ATR correction algorithm to convert transmission spectra from the PDQ library into ATR spectra is shown to address distortion issues such as the relative intensities and broadening of the bands, and introduction of wavelength shifts at lower frequencies, which prevent library searching of ATR spectra using archived IR transmission data. To assess the efficacy of the ATR correction algorithm, search prefilters were successfully developed from simulated ATR spectra for the purpose of identifying the assembly plant of a vehicle from an ATR spectrum of its clear coat. Clear coats whose ATR spectra were obtained using a Nicolet iS50 FTIR spectrometer were correctly classified on the basis of the vehicle's assembly plant using these search prefilters. For some of these validation set samples, there were marked differences between the experimental ATR spectrum and the computed ATR spectrum derived from the corresponding transmission spectrum of the same sample obtained from the Paint Data Query forensic database which can be attributed to weathering. By exposing a fresh surface of the clear coat automotive paint layer to the ATR probe, interference due to weathering was obviated which will facilitate library matching of these samples.

TABLE OF CONTENTS

Chapter Page

LIST OF TABLES

LIST OF FIGURES

Figure Page

Figure Page

CHAPTER I

INTRODUCTION

The research described in this thesis is directed towards three specific goals: (1) characterization of swellable polymer particles that respond to changes in pH of aqueous solutions in contact with them, (2) development of reversed phase liquid chromatographic methods for complex mixture analysis based on selectivity enhancement through stationary phase solvation, and (3) application of attenuated total reflection spectroscopy in forensic automotive paint analysis. The significance of this research lies in the development of new methods to address problems of widespread interest in the areas of chemical sensing, food chemistry and forensic science.

Microgels developed from *N*-isopropylacrylamide and prepared as monodispersed colloids have attracted considerable attention because of their ability to undergo large changes in size and water content over a narrow temperature range. The characterization of their unique properties is crucial towards advancing our understanding of polymer swelling and to the discovery of new applications for these materials. Our current understanding of polymer swelling and how the composition of the polymer directly correlates to its swelling behavior is inadequate. Further studies are necessary to elucidate the relationship between monomer type and content, particularly how incorporation of pH sensitive functional comonomers into polyNIPA imparts unique properties that allow

swelling to be triggered by pH. Complex formulations of polyNIPA, which include the use of pH sensitive functional comonomers, allows investigation of variables other than temperature which trigger polymer swelling. Characterization of several copolymers of *N*-isopropylacrylamide such as acrylic acid, methacrylic acid, ethacrylic acid and propacrylic acid which is discussed in Chapter 3 reveal polymer pK_a values in the pH range of 4 to 6. There are many advantages in using polymers for sensing applications. As polymers are composed of repeating monomer units, the substitution of these monomer units and changes in their relative percent composition can provide a large reservoir of material with tailored properties. The ability to tune the properties of materials readily prepared through free-radical dispersion photopolymerization provides a facile pathway towards preparing materials that meet the specific requirements of sensing materials. In addition, the polymers which utilize swelling as their transduction mechanism, can be coupled with existing technologies such as fiber optics for remote sensing.

Reversed phase liquid chromatography (RPLC) is the method of choice for the analysis of many chemical and biological molecules because of the selectivity, efficiency, and broad range of substances that can be chromatographed using this technique. Although significant advances continue to be made in the application of RPLC, there has been far less progress in the development of mechanistic models, which describe in detailed molecular terms, the separation process in RPLC. Control and manipulation of the separation process is crucial and requires an understanding of retention and knowledge of the role played by the composition of the mobile phase in this process. In Chapter 4, the results from a study involving the separation of vanillin and its isomers using medium

chained length alcohols as mobile phase modifiers to improve selectivity through enhanced stationary phase solvation is presented.

As modern automotive paints are using thinner undercoat and color coat layers protected by a thicker clear coat layer, a clear coat paint smear is, all too often, the only layer of paint left at the crime scene. PDQ, a database created specifically for forensic automotive paint analysis, will not be able to develop an accurate hit-list of potential suspects from the clear coat paint smear as PDQ employs a text based search system to search clear coats based on their formulation and modern automotive clear coats applied to automotive substrates have only one of two possible formulations: acrylic melamine styrene or acrylic melamine styrene polyurethane. Although commercial library search algorithms can be applied to the digital libraries of transmission spectra in PDQ, clear coat formulations are too similar for these algorithms to generate accurate hit lists by direct searching. Furthermore, forensic laboratories in the United States are turning to attenuated total reflection to collect infrared absorbance spectra and this further complicates the analysis of clear coat spectra due to distortions present in attenuated total reflection spectra when compared to the corresponding transmission spectra of the same automotive paint samples. Methodology to address this problem is discussed in Chapter 5 of this dissertation.

This thesis is divided into six chapters. The first chapter is the introduction which provides an overview of the research problems pursued in this dissertation. Chapter 2 provides the necessary theory and background and the three research problems described in this dissertation are outlined and discussed in Chapters 3, 4, and 5. A summary of the results obtained in this dissertation research are outlined in Chapter 6.

CHAPTER II

THEORY

2.1 Polymer Swelling

A crosslinked polymer can absorb a large quantity of solvent and swell when the polymer is placed in a compatible solvent [1]. As swelling occurs, solvent molecules will penetrate into the polymer network. Absorption of solvent molecules causes the chains comprising the crosslinked polymer to elongate. However, stretching of the polymer chains generates an elastic retractive force (due to crosslinking) which opposes the deformation of the polymer network. This retractive force will increase until equilibrium is achieved. The extent of polymer swelling depends upon the degree of crosslinking and the compatibility of the solvent for the polymer.

Swelling cannot occur unless the polymer is crosslinked as an uncrosslinked polymer will dissolve in a compatible solvent. The presence of cross-linking provides the polymer network with a permanent structure since it allows the polymer chains to return to their previous state after being deformed.

Polymer swelling was first characterized by Flory and Rehner in 1943 [2]. They treated the Helmholtz free energy change of the polymer swelling process as a sum of two terms: free energy of mixing of the polymer network with the solvent and the elastic free

energy due to the expansion of the polymer network. Flory expressed (nonionic) swelling [3] for uncharged polymers as

$$Q_m^{5/3} \cong \frac{(\bar{\nu} M_c)\left(\frac{1}{2} - \chi_1\right)}{\left(1 - \frac{2M_c}{M}\right) V_1} \tag{2.1}$$

where Q_m is the ratio of the final to the initial volume of the polymer, $\bar{\nu}$ is the specific volume of the polymer, M_c is the molecular weight per cross-linked unit, M is the molecular weight of the polymer network, χ_1 is the polymer-solvent interaction parameter, and V_1 is the molar volume of the solvent. M_c denotes the amount of crosslinking, $(1\text{-}2M_c/M)$ is a correction factor for polymer network imperfections due to chain ends and χ_1 accounts for the interaction of the polymer with the solvent. From Equation 1 it is evident that swelling decreases as the degree of cross-linking in the polymer increases. Furthermore, χ_1 is the dominant factor governing the swelling and shrinking of nonionic polymers. If $\chi_1 < 0.5$, Q_m is positive and the polymer swells. If $\chi_1 > 0.5$, Q_m is negative and the polymer shrinks.

Flory used a lattice model to describe the thermodynamics of mixing of the polymer chains with the solvent. According to this model, the interactions between the polymer and solvent molecules are van der Waals forces, hydrogen bonding, and dipole-dipole interactions. The lattice model only describes interactions between neighboring lattice sites. Furthermore, the enthalpy of mixing due to changes in these interactions governs the miscibility of the system as the entropy of mixing is small. In Flory's model, the polymer-solvent interaction parameter χ_1 is related to the change in the free energy change of the system. For interactions of the solvent molecules and the polymer, the energetic and

entropic contributions to the mixing can be correlated through the Helmholtz free energy. For this system, the Helmholtz free energy is equal to the Gibbs free energy as the mixing occurs at constant temperature, volume, and pressure. An increase in χ_1 means that polymer-solvent interactions are less favored than polymer-polymer and solvent-solvent interactions. A decrease in χ_1 means that polymer-solvent interactions are stronger than polymer-polymer and solvent-solvent interactions.

For crosslinked polymers with little or no charge, swelling is nonionic. If the base monomer of the polymer is charged, contributions arising from electrostatic repulsion between the polymer chains and the osmotic pressure arising from the counter-ions necessary to preserve the neutrality of the polymer will influence swelling. Flory [3] expressed ionic swelling as

$$Q_m^{5/3} \cong \frac{\left(\frac{i}{2V_u\sqrt{S}}\right)^2 + \left(\frac{\frac{1}{2} - \chi_1}{V_1}\right)}{\frac{V_e}{V_0}} \tag{2.2}$$

where, Q_m is the ratio of the final to initial volume of the polymer, i is the number of electronic charges per polymer unit, V_u is the molecular volume of polymer repeating unit., S is the ionic strength of the solution in contact with the polymer, χ_1 is the polymer-solvent interaction parameter. V_1 is the molecular volume of the solvent, V_e is the effective number of chains in network, and V_0 is the volume of unswollen polymer network. Ionic swelling is dependent upon the ionic strength of the solution in contact with the polymer. Low ionic strength (S) solutions promote polymer swelling, whereas high ionic strength solutions

suppress polymer swelling. By increasing the ionic strength of the solution in contact with the polymer, ionic swelling and nonionic swelling can be distinguished since nonionic swelling is not influenced by the ionic strength of the solution in contact with the crosslinked polymer.

To characterize polymer swelling, the swellable polymer can be embedded in a PVA hydrogel membrane [4]. 90% of the PVA membrane is comprised of water. The refractive index of the swellable polymer will undergo a change with swelling and shrinking, whereas the refractive index of the PVA remains constant. The relationship between the light reflected by the membrane and the refractive indices of the media is given by the following equation

$$R = \left(\frac{n_1 - n_2}{n_1 + n_2}\right)^2 \tag{2.3}$$

where R is the light reflected by the membrane, n_1 is the refractive index of the swellable polymer and n_2 is the refractive index of PVA. In Figure 2.1, the change that occurs in the turbidity of a PVA hydrogel membrane containing pH sensitive polyNIPA particles is shown.

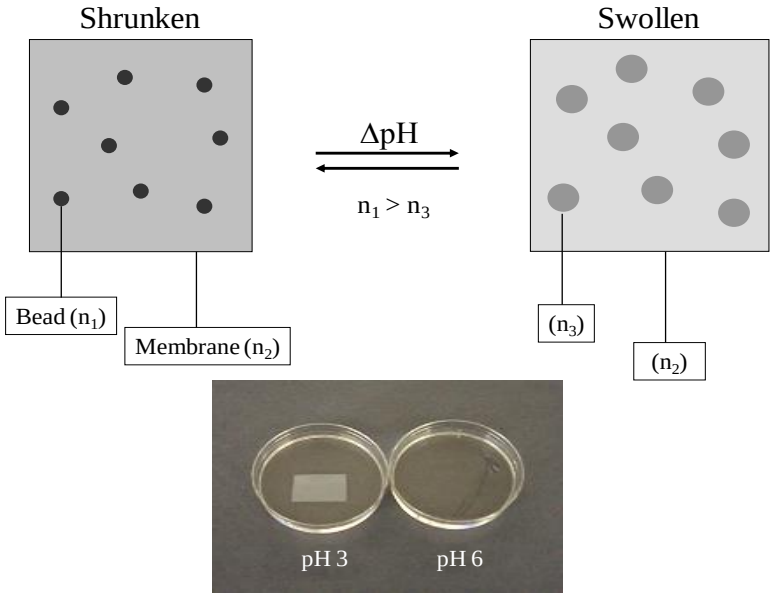

Figure 2.1. pH induced swelling of the polyNIPA particles embedded in the PVA hydrogel membrane changes the refractive index of the particles and the corresponding turbidity of the membrane. The pH sensitive polyNIPA particles exist in a shrunken (turbid) state at low pH but at high pH exist in a (transparent) swollen state.

At pH 3.0, the polyNIPA particles are in a shrunken state and the refractive index of the polymer particles (n_1) is higher than the refractive index of the hydrogel membrane (n_2). This causes the membrane to appear turbid because the light transmitted through the membrane has been attenuated because of reflection. At pH 6.0, the polyNIPA particles swell which increases their water content. The refractive index (n_3) of the polymer particle decreases until these particles approach the refractive index (n_2) of the hydrogel used to prepare the membrane. As the difference between the refractive index of the polymer particles and the PVA is close to zero, the light loss due to reflection is less. For this reason, the polymer membrane is less turbid at pH 6.0. The change in the refractive index of NIPA

polymer is the dominant optical effect which allows us to monitor polymer swelling by turbidity.

Surface plasmon resonance spectroscopy was used to verify our explanation given about the changes in the turbidity of the membrane that occur due to pH induced polymer swelling of the polyNIPA particles embedded in the hydrogel membrane. Figure 2.2 (A) shows the change in the refractive index of the pH sensitive polyNIPA particles spin coated directly onto the surface of the gold SPR substrate. The refractive index of the polymer particles for each pH buffer solution was calculated using SPALL (Wolfgang Knoll, Max Plank Institute) which is based on Fresnel's equations to model the SPR data. The procedure used for modeling this data can be found elsewhere [5]. Figures 2.2 (B) shows a similar plot with these same particles spin-coated onto the gold surface covered by a PVA membrane. Figures 2.2 (C) shows the changes in refractive index of the PVA hydrogel membrane directly deposited on the SPR slide in the absence of the pH sensitive polymer particles. Clearly, the results shown in Figure 2 are consistent with the explanation given about the reasons for the change in the turbidity of the hydrogel membrane shown in Figure 2.1.

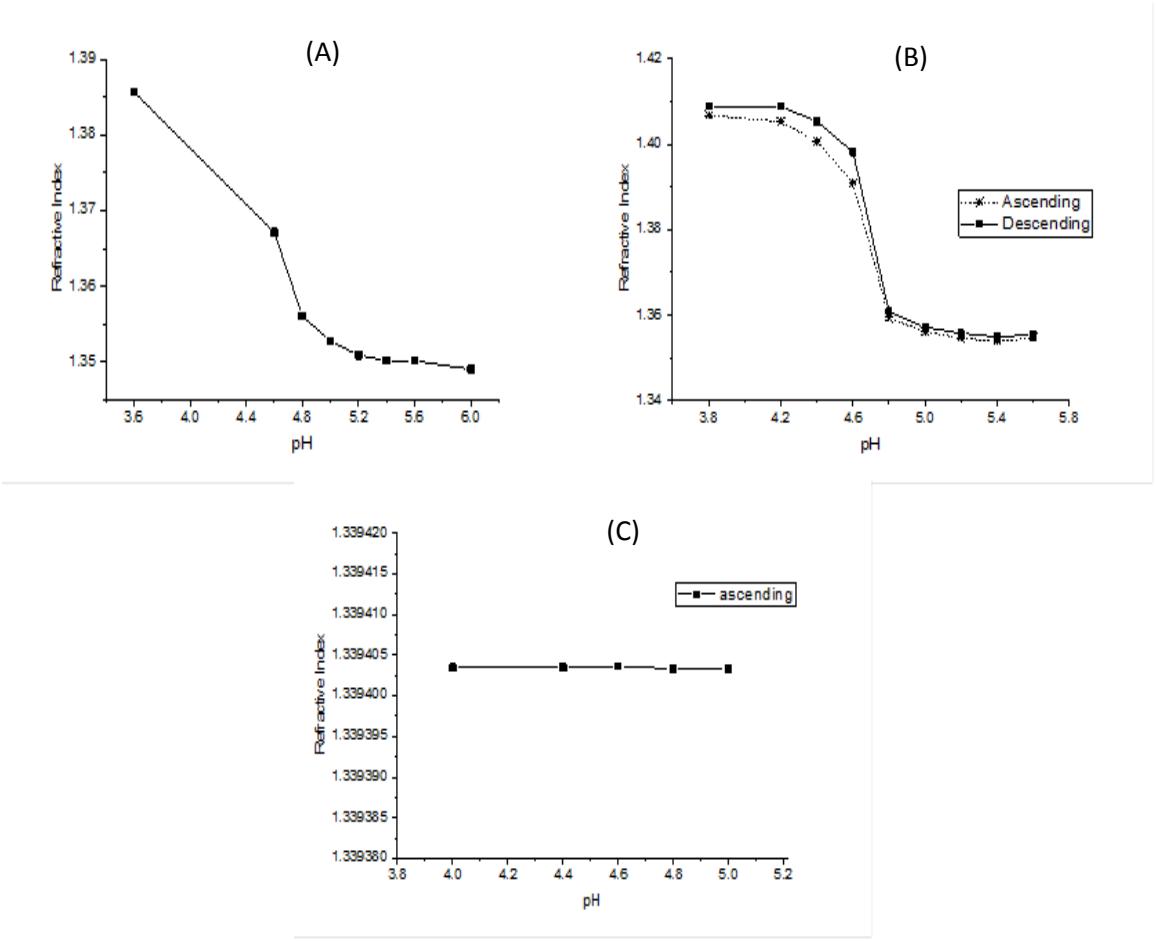

Figure 2.2 (A) Changes in the refractive index of the pH sensitive polyNIPA particles spin coated directly onto the surface of the gold SPR substrate. (B) Changes in the refractive index of the pH sensitive polyNIPA particles spin coated directly onto the surface of the gold SPR substrate and covered by a PVA membrane. (C) Changes in refractive index of the PVA hydrogel membrane directly deposited on the SPR slide in the absence of the pH sensitive polymer particles.

2.2 Bonded Alkyl Stationary Phases in Reversed Phase Liquid Chromatography

The majority of liquid chromatographic separations are performed in the reversed phase mode using columns packed with alkyl bonded phases. In reversed phase liquid chromatography (RPLC), the mobile phase is a hydro-organic solvent mixture. Chemically bonded phases used in RPLC are inherently stable and offer many advantages including

reproducible retention times, and long column lifetimes. Mobile phases can be changed or varied to optimize a separation as there are few limitations on mobile phase composition. Mixtures containing compounds of varying polarity can be separated in a single run by changing the composition of the mobile phase using gradient elution techniques. The ease of use, convenience, economy, and the wide applicability of bonded phase columns have resulted in the dominance of the RPLC technique in analytical chemistry.

Although significant advances continue to be made in the applications of RPLC, there has been far less progress in understanding retention on alkyl bonded phases. There have been a variety of mechanistic models and viewpoints expressed by researchers in the literature. Halasz [6] postulated that bonded alkyl moieties extend vertically from the silica surface forming a molecular bristle. Others believe that solvent interactions with bonded alkyl phases force the bonded chains to lie horizontally against the surface. Lochmuller [7] proposed that bonded alkyl chains on the sorbent-mobile phase interface are associated in clusters of 10 or more molecules forming pseudo-liquid areas called liquid droplets. Several NMR, IR and fluorescent studies [8-12] have been undertaken by a number of workers either confirming or disputing these proposed structures.

Solute retention by alkyl bonded surfaces has been described as solute partitioning between two liquids, with the chemically modified surface considered by some workers to be a bulk liquid [13, 14]. However, an alkyl bonded phase differs from the corresponding bulk liquid. Bonded phases are more ordered than liquids. Furthermore, bonding reduces the number of degrees of freedom restricting both the translational and rotational motions of the bonded moieties. Distances between the alkyl chains comprising the bonded phase are greater than distances between molecules in a bulk liquid. The solvation of the solute

by the bonded phase is greatly dependent upon the size of the solute and the length of the chemical moiety bonded to the surface of the silica. Evidently, chain organization of the alkyl bonded stationary phase plays a major role in solute retention. The current view of partitioning is that a full embedding of the solute between the chains comprising the stationary phase occurs [15]. This partitioning is driven by the differences in chemical potential of the solute between the mobile and stationary phases as well as by the energetics of the solute in each phase.

Retention in RPLC is probably more than solute interactions with the n-alkyl chains of the bonded phase. The organic modifier intercalates into the bonded phase, and the amount of organic modifier within the stationary phase is thought to change as a function of the mobile phase composition. Furthermore, the organic modifier can saturate the stationary phase when its volume percentage in the mobile phase reaches a threshold value. For methanol, the volume percentage is 50% whereas acetonitrile saturates the stationary phase at lower acetonitrile volumes [16, 17]. The stationary phase has been described as a mixture of bonded organic chains, residual silanols, adsorbed water, and molecules of organic modifier [18]. It has been found that increased associations between bonded alkyl chains and water are a result of water forming hydrogen bonds with residual silanols when mobile phases with high concentrations of organic modifier are used as eluent.

Clearly, the stationary phase will be enriched in organic modifier, with the extracting solvent interacting with the solute. The nature of this interaction is not well understood. Some workers hold the view that organic modifier when sorbed or partitioned into the bonded stationary phase changes its sorbent properties [19-25]. They believe that an understanding of stationary phase solvation is important because changes in selectivity

are known to occur as a result of changes in the concentration of the organic modifier in the mobile phase or from changes in the type of organic modifier used in the mobile phase, which in turn influences the amount of organic modifier dissolved in the stationary phase. The presence of organic modifier in the mobile phase has considerable influence on the conformation of the alkyl bonded phase. Alkyl chains appear to assume a more ordered state when the mobile phase has a high organic modifier content [26]. With increasing concentration of the organic modifier, there is a concomitant increase in the hydrocarbonaceous surface area available for interactions with the solute. However, solute retention generally decreases with increasing organic content of the mobile phase - solute partitioning into the stationary phase is favored at lower organic modifier concentrations. As the volume fraction of water in the mobile phase increase, nonpolar solutes interact with nonpolar alkyl chains and the retention increases [27].

A thorough and detailed understanding of retention in alkyl bonded phases at the molecular level is crucial for improving separations in RPLC as the stationary phase is not a passive entity that plays no role in the separation process as suggested by proponents of solvophobic theory [28, 29]. The importance of the stationary phase in the retention process is demonstrated by the shape selectivity of polyaromatic hydrocarbons which varies widely among commercial columns [30, 31]. Second, chromatographic selectivity is highly dependent upon the chain density of the alkyl bonded phase [32, 33]. Solvophobic theory cannot account for these differences because of the reliance of this theory to model retention in terms of the solvation of the solute instead of the transfer of the solute between solvent systems (i.e., mobile phase and stationary phase).

2.3 Attenuated Total reflection in Fourier Transform Infrared Spectroscopy (FTIR)

Attenuated total reflection (ATR) has become the most widely practiced sampling technique in Fourier transform infrared (FTIR) spectroscopy [34]. ATR requires very little sample preparation and consistent results can be obtained with relatively little expertise on the part of the user. ATR is known by a number of other names, such as multiple internal reflection, evanescent wave, and internal reflection spectroscopy. In the last section of this chapter, the theory underlying ATR will be reviewed and compared to transmission spectroscopy. Problems preventing ATR spectra from being matched to a library of transmission spectra will also be discussed.

2.3.1 Theory of ATR

In a typical ATR-FTIR experiment, the sample is directly placed on the sensing element which is known as the internal reflection element (IRE). The IRE has a higher refractive index compared to that of the sample. In other words, the IRE is optically dense and the sample is optically rare. The refraction of light through these two media is explained by Snell's law (see Figure 2.3)

$$n_1 \sin \theta_1 = n_2 \sin \theta_2 \tag{2.4}$$

where n_1 is the refractive index of the optically dense medium, n_2 is the refractive index of the optically rare medium, θ_1 is the angle of incidence and θ_2 is the angle of refraction

measured from the normal of the boundary between the two media. In ATR, the beam originates from an optically dense medium with a refractive index of n_1. Therefore, the angle of refraction θ_2 is always larger than the angle of incidence θ_1. When θ_1 is adjusted to a value such that the angle of refraction (θ_2) must equal to 90^0, the beam will travel along the interface of the two media. This angle of incidence is known as the critical angle (θ_c). When the angle of incidence is greater than the critical angle, the angle of refraction is greater than 90^0, and the beam is reflected internally back into the optically dense medium.

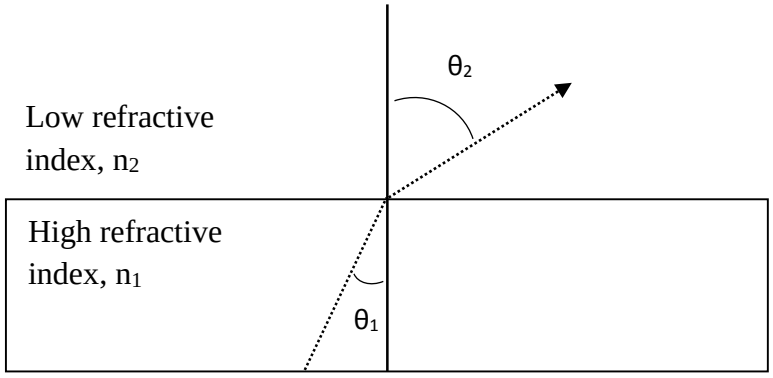

Figure 2.3. Refraction of light at the interface of optically dense medium of refractive index of n1 and optically rare medium of refractive index of n_2. θ_1 is the angle of incidence and θ_2 is the angle of refraction measured from the normal of the boundary

The critical angle for the IRE can be calculated from Snell's law using Equation 5 which was developed from Equation 4.

$$\theta_c = sin^{-1}\frac{n_2}{n_1} \tag{2.5}$$

For most organic compounds, the refractive index of the sample (n_2) is approximately 1.5. Using Equation 5, one can calculate the critical angle of the internal reflection elements. For example, the critical angle of the Germanium (Ge) IRE, which has a refractive index of 4.00, is 22^0, and the critical angle of the Diamond IRE (refractive index of 2.41) is 40^0. If the incident angle is greater than the critical angle of the material comprising the internal reflection element, the beam is completely reflected back into the IRE. This is known as total internal reflection.

When total internal reflection occurs, the beam will be restricted to the IRE. However, the electromagnetic field of the photons of the incident beam will extend from the optically dense medium to the optically rare medium at the point of incidence. This is known as the evanescent wave. The relationship between the electric field strength of the evanescent wave and its distance from the surface of the optically dense medium is given by Equation 6 [35]

$$E = E_0 e^{-\gamma z} \tag{2.6}$$

where E_0 is the strength of the electric field at the surface of the optically dense medium, γ is a constant, and E is the strength of the electric field at a distance z from the surface of the optically dense medium. The distance corresponding to the strength of the field

decaying to e^{-1} of its intensity at the surface of the optically dense medium is called the depth of penetration (d_p). For any distance less than d_p, the evanescent wave is able to interact effectively with the optically rare medium. The value of d_p corresponding to this distance is equal to $1/\gamma$, see Equation 6. d_p is a function of the wavelength of the incident radiation (λ), angle of incidence (θ), refractive index of the IRE (n_1) and the refractive index of the sample (n_2), see Equation 7 [36].

$$d_p = \frac{\lambda}{2\pi n_1 \sqrt{sin^2\theta - (n_1/n_2)^2}} \quad (2.7)$$

d_p for germanium and diamond IREs are 0.66 μm and 2.00 μm respectively when the incident angle of 45^0 is used, and 0.51 μm and 1.1 μm when the incident angle is 60^0 IREs. If it is desired to restrict the study to the surface, an IRE with a high refractive index material and a high angle of incidence should be employed (e.g., Ge IRE with 60^0 incident angle). For analyses involving only the bulk sample, using an IRE with a comparatively lower refractive index value and a low angle of incidence would be recommended (e.g., diamond with angle of incidence of 45^0).

2.3.2 ATR versus Transmission Spectra

Due to differences in the optical configuration and the process used to measure IR absorption, ATR spectra differ from transmission spectra in the band shapes, relative

intensities and the peak frequencies. This poses a problem when performing spectral library searching as spectra in most commercial IR libraries are collected in transmission mode. A precise comparison of ATR spectra to transmission spectra will be precluded by these differences. Figure 2.4 shows an ATR spectrum measured using a diamond ATR accessory and a transmission spectrum of the same automotive clear coat paint sample (CONT1049), which consists of the polymer acrylic melamine styrene. When comparing the ATR spectrum with the transmission spectrum, the absorbance values for the bands in the lower wavenumber region are higher and the absorbance values for the bands in the higher wavenumber region are lower than the corresponding absorption bands in the transmission spectrum. This is due to the wavelength dependence of the penetration depth of the evanescent wave (see Equation 7) which defines the optical path length in Beers law for the ATR experiment. In other words, d_p is smaller at higher wavenumbers and larger at lower wavenumbers. Since the depth of penetration is a linear function of wavelength, the wavelength dependence of the optical path length of the sample in ATR can be corrected by either dividing the absorbance values by their corresponding wavelength or multiplying them by their corresponding wavenumber.

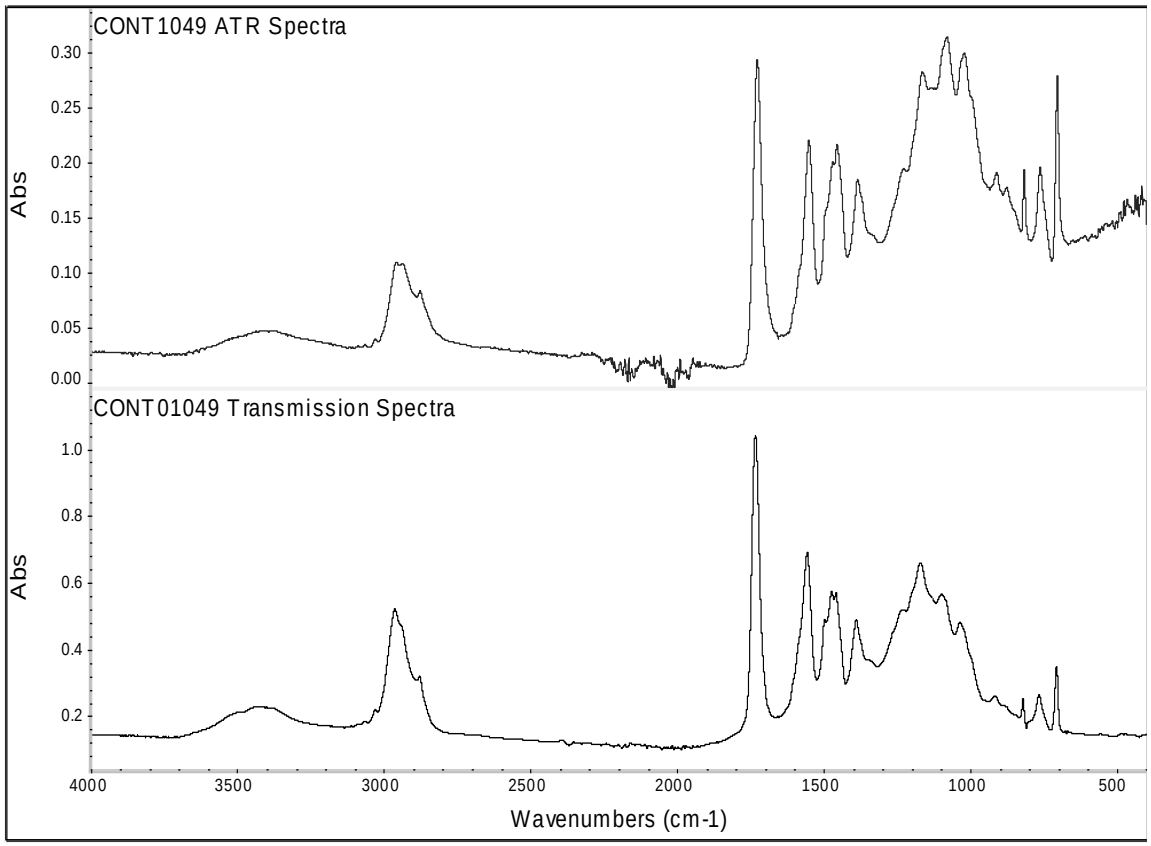

Figure 2.4. FTIR spectra of an automobile clear coat sample designated as CONT1049 in the PDQ database. The sample is an acrylic melamine styrene polymer. Both the ATR (upper) and transmission (lower) spectra are shown

Although absorption band intensities in ATR spectra can be corrected using the approach described above, differences in the shapes of the spectral bands will remain (see Figure 2.5) due to the variation in the refractive index across an absorption band which is known as anomalous dispersion. For very strong absorption bands, absorption maxima are shifted to a lower wavenumber in ATR spectra. Furthermore, strong absorption bands in ATR spectra appear asymmetric when compared with their transmission counterparts.

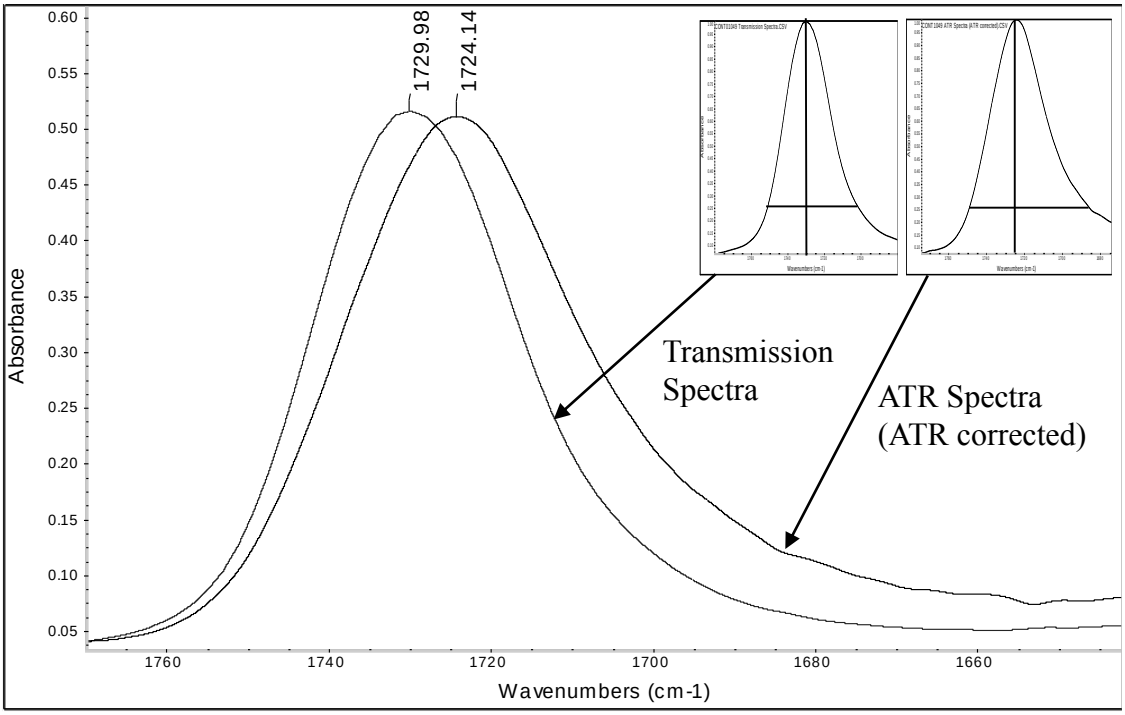

Figure 2.5. Carbonyl band from an automobile clear coat paint sample (CONT1049) obtained from an ATR corrected spectrum (diamond IRE) and from a transmission spectrum.

Absorbance of radiation is governed by the complex refractive index of the sample, which consists of both a real and imaginary component as shown in Equation 8 [37]

$$\tilde{n}(\tilde{\nu}) = n(\tilde{\nu}) + ik(\tilde{\nu}) \tag{2.8}$$

where $n(\tilde{\nu})$ is the real refractive index (or the refractive index from Snell's Law) and $k(\tilde{\nu})$ is the imaginary refractive index (or absorption index) at $\tilde{\nu}$ which is the wavenumber. For any sample, the absorption index (i.e., the k- index) is given by Equation 9 [37] where $\alpha(\tilde{\nu})$ is the linear absorption coefficient.

$$k = \frac{\alpha(\tilde{\nu})}{4\pi\tilde{\nu}} \tag{2.9}$$

The penetration depth of the evanescent wave across an absorption band can be computed from Equation 7 with the complex refractive index inserted for the refractive index of the sample and the IRE crystal, see Equation 10 [38].

$$d_p = \frac{\lambda}{2\pi}\left[\frac{\sqrt{\left(n_1^2.sin^2\theta - n_2^2 + k_2^2\right)^2 + (2.n_2.k_2)^2} + \left(n_1^2.sin^2\theta - n_2^2 + k_2^2\right)}{2}\right]^{-1/2} \tag{2.10}$$

The spectrum of both n and k for poly(methyl methacrylate) across the carbonyl stretching band is shown in Figure 2.6.

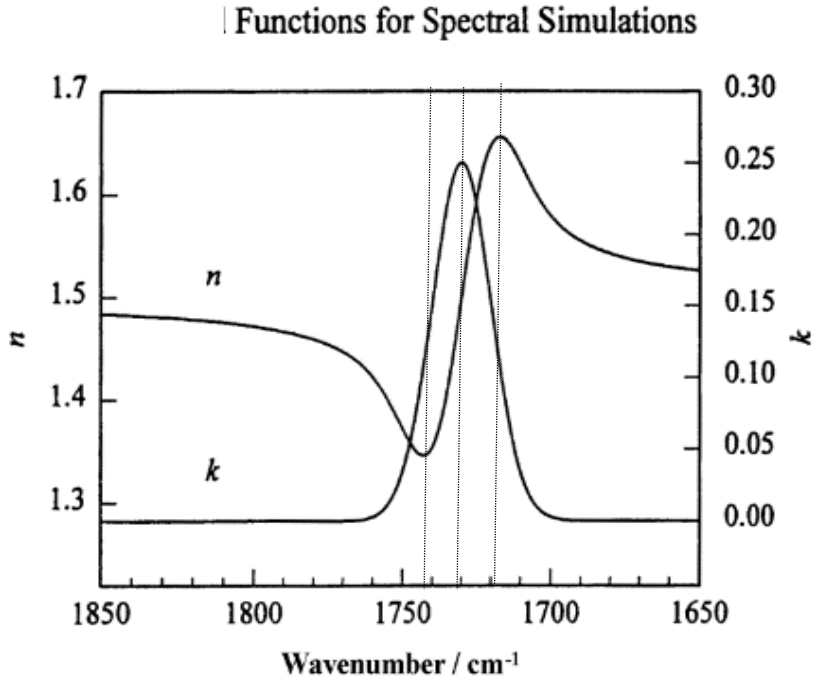

Figure 2.6. Variation of the refractive index (n) and the absorption index (k) of the carbonyl stretching band of PMMA. Reproduced from P. R. Griffiths and J. A. de Haseth, Fourier Transform Infrared Spectroscopy, 2nd Edition, John Wiley & Sons, NY 2007, pp. 297.

The refractive index of the sample increases across an absorbance band, and the $\sin^{-1}(n_2/n_1)$, which is the critical angle (see Equation 5) can become greater than the angle of incidence. In these cases (the absorbance maxima corresponding to a strong absorption band), the beam does not undergo internal reflection and is completely refracted. This effect is pronounced when the critical angle of the IRE material is close to the incident angle. For example, this effect is larger for diamond ($\theta_c = 40^0$) than Ge ($\theta_c = 22^0$). For a wavenumber that does not show any absorbance, (e.g., 1850 cm^{-1} in Figure 5), we can assign values to k and n of 0 and 1.5 respectively. Therefore, the depth of penetration of the evanescent wave calculated using Equation 7 is 1.16 μm for diamond.

The penetration depth of the evanescent wave across the absorbance band dramatically changes due to the large change in both the refractive index and the absorbance index in the optically rare medium (i.e., the sample). Consider 1740 cm^{-1} in Figure 5 where the refractive index of n is at a minimum. The calculated penetration depth of the evanescent wave would be the minimum (0.86 μm for diamond) due to the small values of n and k. At wavenumber 1730 cm^{-1} the calculated penetration depth would be higher as the n and k values are larger (0.96 μm for diamond). The largest d_p value is achieved around 1720 cm^{-1} (1.68 μm for Diamond IRE). Clearly, the penetration depth of the evanescent wave varies across the absorption band which in turn distorts the peak causing asymmetry. This distortion will also shift the wavenumber of the absorbance maxima to lower values further complicating a library search using transmission spectral libraries.

Recently, an algorithm has been developed to transform IR transmission spectra into ATR spectra [39]. The ATR conversion algorithm addresses the issues contributing to spectral distortion including lower relative intensities at higher wavenumbers due to the lower depth of penetration of the evanescent wave, and the band broadening and wavenumber shifts due to anomalous dispersion. In this procedure, the surface reflection phenomenon of the incident beam at the boundary between the sample and the IRE is characterized using Fresnel's equations. To calculate the reflectance of the p- and s-polarized light, it is necessary to compute the optical constants (i.e., the n- and k- indices) of the sample, and to provide the refractive index of the IRE, the sample thickness, incident angle of the beam and the number of internal reflections. ATR spectra for p- and s-polarized light are averaged to obtain absorbance values for unpolarized light.

The n- and k- indices of the sample are computed at each wavelength from the transmission spectra expressed in absorbance units. First the k– indices are computed using Equation 11 [40]

$$k(v) = \frac{2.303A(v)\lambda}{4\pi d} \qquad or \quad k(v) = \frac{2.303A(v)}{4\pi v d} \tag{2.11}$$

where A(v) is the absorbance value of the transmission spectrum as a function of wavenumber (v), λ is the corresponding wavelength (which equals 1/ v), and d is the sample thickness. The complex refractive index, which is a function of both real and imaginary components as shown in Equation 8, are mutually related through the Kramers-Kronig relationship [41]. Once the imaginary part (k-index) has been calculated using Equation 11, the n- index can be calculated by Kramers-Kronig integration of the k- index using Equation 9. Here, the refractive index at high wavenumbers where there is no sample absorbance is used as an anchor value, see Equation 12

$$n(v_a) = n(\infty) + \frac{2}{\pi} P \int_0^\infty \frac{vk(v)}{v^2 - v_a^2} dv \tag{2.12}$$

where P is the principle value of the integral, n(∞) is the refractive index at high wavenumber where there is no absorbance. The double Fourier method is used to perform the calculations outlined in Equation 12. After the complex refractive index of the sample has been computed, the coefficients for p- and s-polarized light at each wavenumber are calculated after providing the n- and k- indices to Equations 13 and 14 [42]

$$r_s = \frac{n_0 \cos(\theta_0) - \tilde{n}_1 \cos(\theta_1)}{n_0 \cos(\theta_0) + \tilde{n}_1 \cos(\theta_1)} \tag{2.13}$$

$$r_p = \frac{\tilde{n}_1 \cos(\theta_0) - n_0 \cos(\theta_1)}{\tilde{n}_1 \cos(\theta_0) + n_0 \cos(\theta_1)} \tag{2.14}$$

where n_0 and $\tilde{n}_1$ are the refractive indices of the IRE and the sample, and θ_0 and θ_1 are the angles formed between the incident beam and the normal in the IRE and in the sample. Reflectance values for the corresponding ATR spectrum are calculated using Equation 15.

$$R = \frac{(R_p + R_s)}{2} = \left(|r_p|^2 + |r_p|^2\right) \tag{2.15}$$

Using this procedure, the first step is to calculate the k- index and n-index from the transmission spectra using Equations 11 and 12. The computed k- and n- coefficients are placed in Equations 13 and 14 to calculate the Fresnel's reflection coefficients. The

reflectance at each wavelength in the ATR spectrum is computed using Equation 15. Figure 2.7 shows the comparison of an experimentally obtained ATR spectrum for a clear-coat paint sample contains acrylic melamine styrene polymer and the ATR spectrum simulated from the transmission spectrum of the same sample using the aforementioned procedure. The only difference between these two spectra is the region that corresponds to absorption of IR radiation by the diamond cell (2000-2200 cm^{-1}) which is not conveyed in the simulated ATR spectrum.

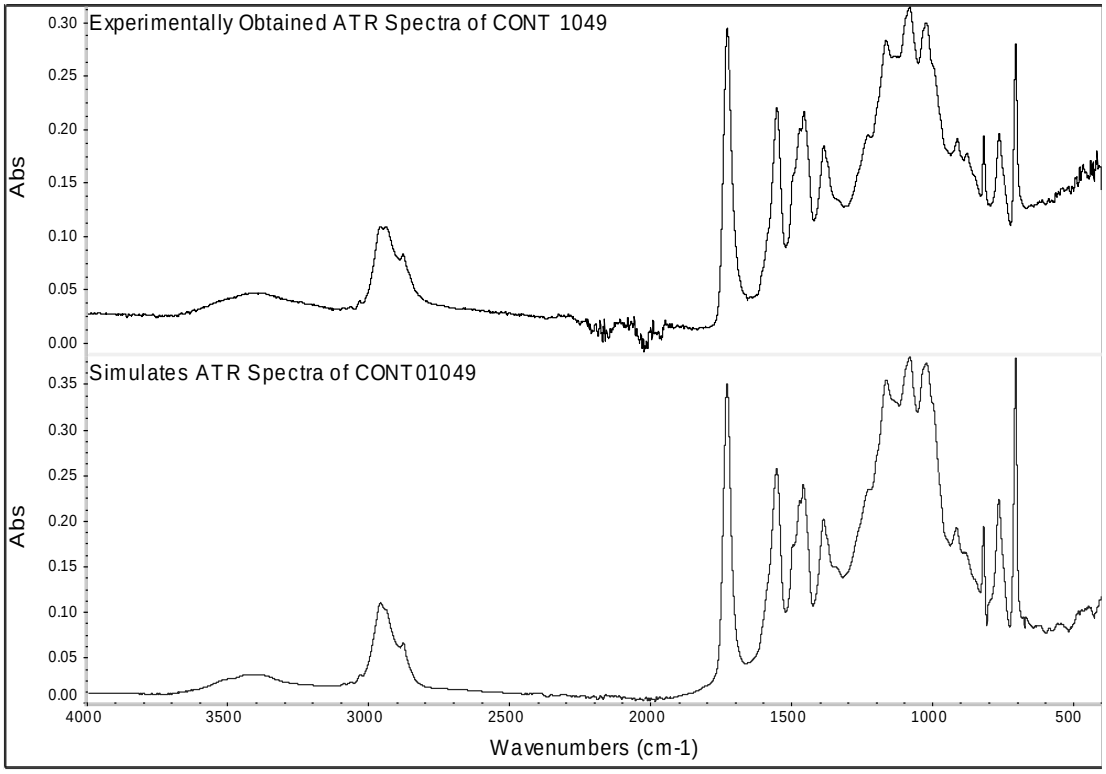

Figure 2.7. FTIR spectra of automobile clear coat paint sample designated as CONT1049: experimental ATR spectrum (upper), and simulated ATR spectrum of CONT1049 (lower).

References

1. H. G. Elias, Introduction to Polymer Science, VCH, New York, 1997.

2. P. J. Flory and J. Rehner, Statistical Mechanics of Crosslinked Polymer Networks II Swelling, J. Chem. Phys., 1943, 11, 521-526

3. P. J. Flory, Principles of Polymer Chemistry, Cornell University Press, New York 1953.

4. B. K. Lavine, L. Oxenford, M. Kim, N. Kaval, M. Benjamin, and W. R. Seitz, "Novel Turbidimetric Method to Study Polymer Swelling," Microchem. J., 2012, 103, 97-104.

5. B. K. Lavine, G. Mwangi, N. Mirjankar, and M. Kim, "Characterization of Swellable Molecularly Imprinted Polymer Particles by Surface Plasmon Resonance Spectroscopy," Appl. Spectros., 2012, 66(4), 440-446.

6. K. Kach, I. Sebastian, and I. Halasz, "Preparation and properties of reversed phases" J. Chromatogr. 1976, 122, 3-16.

7. C. H. Lochmuller and D. R. Wilder, "The Sorption Behavior of Alkyl Bonded Phases in Reverse-Phase, High Performance Liquid Chromatography" J. Chromatogr. Sci., 1979, 17, 574-579.

8. D. M. Bliesner and K. B. Sentell, "Deuterium nuclear magnetic resonance spectroscopy as a probe for reversed-phase liquid chromatographic bonded phase solvation: methanol and acetonitrile mobile phase components" J. Chromatogr., 1993, 631, 23-35.

9. M. E. Gangoda and R. K. Gilpin, "NMR Investigations of 13C Labeled Alkyl Modified Silica" J. Magn. Reson, 1983, 63, 140-143.

10. K. B. Sentell, D. M. Bliesner, and S. T. Shearer, "^{2}H and ^{13}C NMR studies of reveresed phase liquid chromatographic stationary phases: solvation and temperature effects "Spec. Publ. R. Soc. Chem. (Chem. Mod. Surf.), 1994, 139, 191-202.

11. M. E. J. Montgomery and M. J. Wirth, "Spectroscopic Study of the Molecular Basis of Wetting of a C18 Surface by Long-Chain n-Alcohols" Anal. Chem., 1994, 66, 680-684.

12. Y. D. Men and D. B. Marshall, "Relationship between surface polarity, retention of moderately polar solutes, and mobile-phase composition in reversed-phase high-performance liquid chromatography" Anal. Chem., 1990, 62, 2606-2610.

13. G. E. Berendsen and L. de Galan, "A Geometrical Model for Chemically Bonded TMS and PDS Phases" J. Liquid Chromatogr., 1978, 1, 403-426.

14. G. E. Berendsen and L. de Galan, "Preparation and Chromatographic Properties of Some Chemically Bonded Phases for Reversed-Phase Liquid Chromatography" J. Liquid Chromatogr., 1978, 1, 561-568.

15. J. G. Dorsey and K. A. Dill, The Molecular Mechanism of Retention in Reversed Phase Liquid Chromatography, Chem. Rev., 1989, 89, 331-338.

16. E. D. Katz, K. Ogan, and R.P. W. Scott, "Distribution of a solute between two phases: The basic theory and its application to the prediction of chromatographic retention" J. Chromatogr., 1986, 352, 67-90.

17. P. Zhu, Chromatographia, "On the chromatography mechanism of reversed-phase liquid chromatography" 1986, 21, 229-233.

18. L. C. Tan and P. W. Carr, "Study of retention in reversed-phase liquid chromatography using linear solvation energy relationships: II. The mobile phase" J. Chromatogr. A., 1998, 799, 1-19

19. R. M. McCormick, and B. L. Karger, "Distribution phenomena of mobile-phase components and determination of dead volume in reversed-phase liquid chromatography" Anal. Chem., 1980, 52, 2249-2257.

20. K. G. Wahlund and I. J. Beijersten, "Stationary phase effects in reversed-phase liquid chromatography of acids and ion pairs" J. Chromatogr., 1978, 149, 313-320.

21. K. G. Wahlund and I. J. Beijersten, "Adsorption of 1-pentanol on alkyl-modified silica and its effect on the retention mechanism in reversed-phase liquid chromatography" Anal. Chem., 1982, 54, 128-137.

22. N. Felitsyn and F. Cantwell, "Stationary-Phase Contribution of 1-Propanol Organic Modifier to Changes in Sorption of 1-Hexanol on an ODS-Bonded Phase" Anal. Chem., 2000, 72, 1031-1036.

23. N. Felitsyn and F. Cantwell, "Effect of Stationary-Phase Sorption of Organic Modifier from a Water-Rich Mobile Phase on Solute Retention by an ODS Bonded Phase" Anal. Chem., 1999, 71, 1862-1870.

24. L. Glavina and F. Cantwell, "Role of the compact part of the electrical double layer in the simultaneous sorption of different ions of the same charge on a reversed-phase bonded-phase liquid chromatography packing" Anal. Chem., 1993, 65, 3299-3308.

25. A. Alvarez-Zepeda, B. N. Barman, and D. M. Matire, "Thermodynamic study of the marked differences between acetonitrile/water and methanol/water mobile-phase systems in reversed-phase liquid chromatography" Anal. Chem., 1992, 64, 1978-1984.

26. M. E. J. Montgomery, M. A. Green, and M. J. Wirth, "Orientational dynamics of a hydrophobic guest in a chromatographic stationary phase: effect of wetting by alcohol" Anal. Chem., 1992, 64, 1170-1175.

27. A. M. Stalcup, D. E. Martire, and S. A. Wise, "Thermodynamic comparison of monomeric and polymeric C_{18} bonded phases using aqueous methanol and acetonitrile mobile phases" J. Chromatogr., 1988, 442, 1-14.

28. C. Horvath, W. Melander and I. Molnar, "Solvophobic interactions in liquid chromatography with nonpolar stationary phases", J.Chromatogr. A, 1976, 125, 129-156.

29. A. Vailaya and C. Horvath, "Retention in reversed-phase chromatography: partition or adsorption?" J. Chromatogr. A, 1998, 829, 1-20.

30. L. C. Sander and S. A. Wise, "Synthesis and characterization of polymeric C18 stationary phases for liquid chromatography" Anal. Chem., 1984, 56, 504-512.

31. L. C. Sander and S. A. Wise, "Evaluation of shape selectivity in liquid chromatography" LC-GC, 1990, 8, 378-384.

32. K. B. Sentell, and J. G. Dorsey, "Retention mechanisms in reversed-phase liquid chromatography. Stationary-phase bonding density and partitioning" Anal. Chem., 1989, 61, 930-935.

33. K. B. Sentell and J. G. Dorsey, "Retention mechanisms in reversed-phase chromatography : Stationary phase bonding density and solute selectivity" J. Chromatogr., 1989, 461, 193-200.

34. J. A. Reffner and P. A. Martoglio, Uniting Microscopy and Spectroscopy in Practical Guide to Infrared Microspectroscoy, H. J. Humecki (Eds), Marcel Dekker, NY 1995, pp. 59-62.

35. M. Milosevic, Internal Reflection and ATR Spectroscopy, John Wiley & Sons, NY 2012.

36. P. Griffiths and J. A. de Haseth, Fourier Transform Infrared Spectrometer, John Wiley & Sons, New York, 2007, pp. 324.

37. M. Born, W. Emil, A. B. Bhatia, P. C. Clemmow, D. Gabor, A. R. Stokes, A.M. Taylor, P. A. Wayman, W. L. Wilcox, Principals of Optics: Electromagnetic Theory of Propagation, Interference, and Diffraction of Light, Cambridge, UK, Cambridge University Press, 2002, 7th edition.

38. H. Hosono, "Fourier transform infrared attenuated total reflection spectra of ion-implanted silica glasses" J. Applied Physics, 1991, 69, 8079-8085.

39. B. K. Lavine, A. Fasasi, N. Mirjankar, K. Nishikida, J. Campbell, Simulation of Attenuated Total Reflection Infrared Absorbance Spectra: Application to Automotive Clear Coat Forensic Analysis, Appl. Spectroscop., 2014, 68, 608-615.

40. A. G. Marshall, Biophysical Chemistry: Principles, Techniques, and Applications, John Wiley & Sons, NY 1978.

41. R. M. A. Azzam, N. M. Bashira, Ellipsometry and Polarized Light, Amsterdam, The Netherlands, Elsevier BV 1977.

42. F. Wooten, Dispersion Relations and Sum Rules, in F. Wooten (editor) Optical Properties of Solids, New York, Academic Press, NY 1972, pp. 173-185.

CHAPTER III

SWELLABLE N-ISOPROPYLACRYLAMIDE POLYMER PARTICLES WITH TUNED pH RESPONSES

3.1 Introduction

pH is one of the most common laboratory measurements made. Many different methods exist for the measurement of pH ranging from colorimetric indicators to glass and metal electrodes. The glass electrode is the most widely used method for measuring pH. Due to the well-established nature of the glass electrode, it has been used to prepare pH buffer solutions in the pH profiling experiments described in this chapter. Accurate and precise measurements of pH for buffer solutions were critical for the investigation of the pH response properties of the pH sensitive copolymers of *N*-isopropylacryamide described in this chapter.

Although glass electrodes have been used in a variety of laboratory and field settings, the size of the electrode and its need for continued recalibration, often the result of drift, will limit its application to analysis problems in biological and environmental sensing, e.g., gastric pH sensing that requires indwelling pH electrode systems to continuously monitor ruminal acidosis in dairy cows [43], continuous *in vivo* measurement

of pH sensing of blood in arteries and muscles for patients suffering from tissue ischemia [44], pH sensing to study gastro-esophageal reflux disease, a digestive disorder related to the retrograde movement of gastric acid into the esophagus [45], and monitoring of the rising acidity level of the oceans because of the water becoming enriched in carbon dioxide from global warming [46].

Fiber optic pH sensing [47-50] has been investigated as an alternative to the glass electrode for these types of sensing applications. A pH indicator is immobilized at the distal end of an optical fiber by adsorption, covalent bonding, or entrapment. Interaction of the indictor with the sample solution leads to changes in its optical properties which is detected through the optical fiber by absorbance or fluorescence. However, the pH indicators are usually dyes and can photodegrade over time or leach out if immobilized by adsorption or entrapment. Furthermore, their response is limited to a very specific wavelength region which places constraints on the instrument used.

To overcome these disadvantages, swellable polymer particles functionalized to respond to pH and embedded in a PVA hydrogel membrane can be utilized as pH indicators for optical fibers**.** This approach to chemical sensing involves measuring the change in membrane turbidity that results from changes in the refractive index of the microspheres that accompany their swelling and shrinking. The turbidity of the membrane is measured as absorbance at 700 nm using a conventional spectrophotometer and a cuvette with a custom built membrane holder. The indicator phase consists of lightly crosslinked polyNIPA particles (approximately 1μm in diameter) that have been pH sensitized because acrylic acid, methacrylic acid, ethacrylic acid or propacrylic acid has been included in the polymer formulation as a comonomer. The microspheres swell and shrink with changing

hydrogen ion concentration in the aqueous solution in contact with the membrane. When the membrane is exposed to an alkaline solution, the microspheres swell due to deprotonation of the carboxylic acid group, which introduces a negative charge onto the polymer causing the water content of the polymer to increase. This reduces the refractive index of the polyNIPA particles, so it is closer to the refractive index of the hydrogel, leading to a decrease in the amount of light reflected and hence reduced turbidity because the percentage of light reflected at an interface increases with the difference in the refractive index of the two media.

Polymer swelling utilizing hydrogel membranes containing swellable polymer particles that have been sensitized to pH offers several important advantages for sensing. The hydrogel membrane can serve as a "filter" to block out larger molecules, e.g. humic acid that might otherwise foul the microspheres. The polymer microspheres will not leach out of the membrane as compared to reagent phases. Another advantage of this approach to sensing is that it can be implemented at any wavelength including the near infrared wavelengths used in telecommunications. It enables a true coupling of state of the art fiber optic technology with chemical sensing. These membranes have been shown to be stable for several years. They are not subject to photo-degradation and can undergo multiple swelling and shrinking cycles without degrading. Furthermore, swelling and shrinking of the microspheres has a minimal effect on the size of the hydrogel, and does not generate enough force to affect adhesion of the hydrogel to a substrate.

In the study described in this chapter, swellable polymer particles that respond to pH have been prepared by free radical dispersion polymerization using *N*-isopropylpolyacrylamide (NIPA), methylene-bis acrylamide, 2-dimethoxy-2 phenyl-

acetophenone, *N*-tert-butylacrylamide (NTBA), and acrylic acid, methacrylic acid, ethacrylic acid or propacrylic acid. The polymer particles are incorporated into hydrogel membranes prepared by mixing the pH sensitive polyNIPA particles with aqueous polyvinyl alcohol solutions followed by cross linking with glutaric dialdehyde. When the polymer particles are dispersed in a hydrogel, there are large changes in the turbidity of the membrane as the pH of the solution in contact with the membrane is varied. These changes can be monitored using visible and near infrared absorbance spectroscopy, surface plasmon resonance, or the quartz crystal microbalance. The polymer particles show a large response over a narrow pH range. Both the degree of swelling and the apparent pK_a of the polymer particles are observed to increase with temperature, and the degree of swelling and apparent pK_a of the particles is independent of the ionic strength of the solution in contact with the membrane if the polymer particles are sufficiently cross-linked. The apparent pK_a of the polymer particles can be tuned to respond sharply in the physiological pH range by varying the degree of cross-linking, the amount of NTBA used in the formulation and the alkyl chain length of the pH sensitive co-monomer.

3.2 Experimental

N-isopropylacrylamide (NIPA) and acetontrile were obtained from Acros (New Jersey, USA). Acrylic acid (AA), methacrylic acid (MAA), *N, N*'-methylenebis (acrylamide) (MBA), Theophylline, 2, 2 dimethhoxy-2-phenyl-acetophenone (DMPA), poly(vinyl alcohol) (Mw 85,000 – 146,000, 98-99 % hydrolyzed), and glutaric dialdehyde (50 w % solution in water) were purchased from Aldrich Chemical Co. (Milwaukee, WI, USA). Glutaric dialdehyde was diluted to 10 % with DI water. All reagents and solvents

were used as received. Ethacrylic acid (EAA) and propacrylic acid (PAA) were prepared using a previously published literature procedure [51].

Polymer microspheres were synthesized by free radical dispersion polymerization. In a typical synthesis, NIPA (14 mmol), MAA (2 mmol), MBA (2 mmol), Theophylline (1 mmol) and DMPA (0.2 g) were transferred to a 500 mL 3-neck round bottom Pyrex flask and dissolved in 100 mL acetonitrile. Monomer solution was simultaneously sonicated using a Branson 1510 ultrasonicater and purged with dry nitrogen gas for 20 minutes in order to remove dissolved oxygen. Free radical photoreaction was performed at room temperature in a Rayonet photoreactor equipped with G4T5 type mercury lamps and a cooling fan. Since the UV cutoff of the Pyrex flask is less than 260 nm, monomer solution was radiated in the UV-A (315 nm to 400 nm) region. When a quartz flask was used which allowed radiation at shorter wavelengths to pass through, polymer particles were not produced probably due to photodegradation of reagents. After a 12 hour reaction period, a turbid polymer suspension was transferred into two 50 mL polypropylene centrifuge tubes and centrifuged at 3000 RPM for 10 min. After separating the decant, particles were resuspended in 25 mL aliquots of 90/10 (v/v) mixture of methanol and glacial acetic acid, sonicated for 30 minutes and centrifuged at 3000 RPM for 10 min. This washing procedure was repeated for 4 times in order to remove theophylline and unreacted reagents. Finally, particles were washed 3 times with 25 mL aliquots of methanol, resuspended in a small amount of methanol and stored in glass vials until use.

Hydrogel membranes were prepared by mixing the polyNIPA particles with aqueous PVA solution and cross-linking using glutaric dialdehyde. In a typical membrane preparation, 2 g of mixture of microspheres (1%, w/w) and PVA solution (8% w/w) was

prepared in a 4 mL glass vial and the mixture was magnetically stirred overnight in order to homogeneously disperse the particles in the PVA solution. 50 μL of 10% aqueous glutericdialdehyde was then added using a micropipette and stirring continued for another one hour. Finally 25 μL of 4 M HCl was added as an initiator and after approximately 1 min of stirring the mixture was cast between two glass slides that were separated by 127 μm thick Teflon spacers. (Teflon spacers determine the thickness of the membrane). After about one hour gelatin period, the membrane was separated from the slides, washed with plenty of DI water and stored in DI water until use.

The membrane was mounted on a membrane holder (see Figure 3.1) placed in the sample cuvette. DI water was present in the reference cuvette of the double beam spectrometer. The sample cuvette was filled with buffer solution. By changing the buffer solutions in contact with the membrane, its pH response profile was obtained. The buffer solutions were prepared using chloroacetic acid (pH range 3-3.8), acetic acid (pH 3.9-5.4), 2-(*N*-morpholino) ethanesulfonic acid (pH range 5.5-7.3), 3-(*N*-morpholino) propanesulfonic acid (pH range 7.4-8.0) or TRIS (pH range 7.2-9.0). To prepare buffer solutions with different ionic strengths, a known amount of NaCl was added to each buffer solution. An online buffer calculator (www.liv.ac.uk/buffers/buffercalc.html) was used to determine the composition of each buffer for a specific pH and ionic strength.

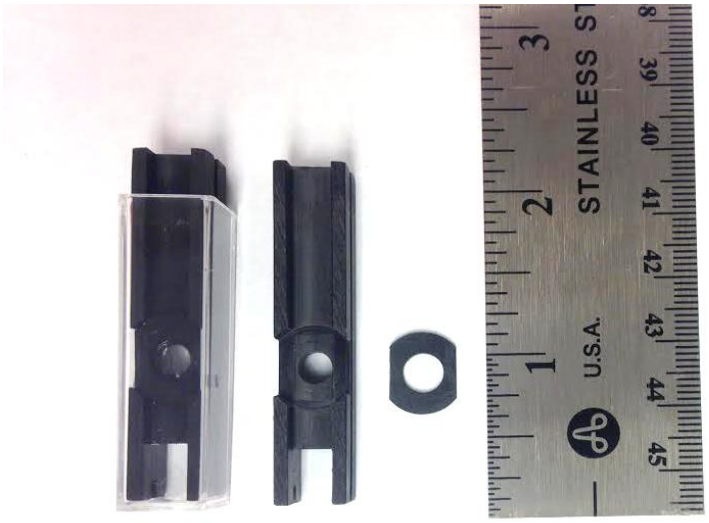

Figure 3.1. Picture of sample holder used to mount membrane segment for turbidity measurements.

3.3 Results and Discussion

Figure 3.2 shows the pH response profile for the poly (*N*-isopropylacrylamide) synthate NK 1-60 (14 mmol NIPA, 2 mmol MAA, 2 mmol NTBA, and 2 mmol MBA) prepared by copolymerization with MAA and embedded in PVA hydrogel membrane. For each data point shown in the figure, the membrane was rinsed three times with buffer solution and allowed to equilibrate for 5 min prior to analysis by turbidity. Absorbance values (i.e., turbidity) were obtained at 700 nm and plotted against pH of each buffer.

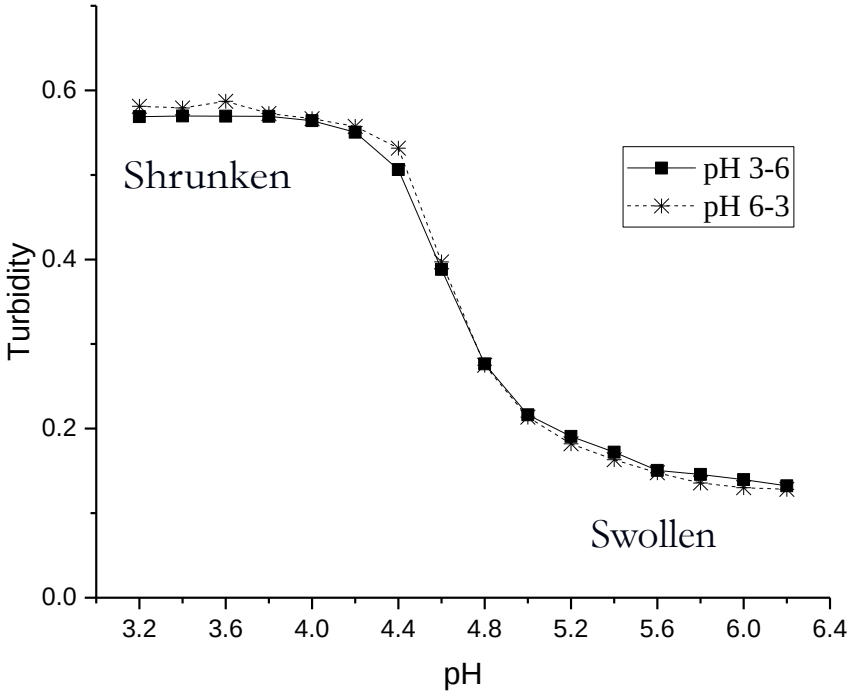

Figure 3.2. Ascending and descending pH response profiles of NK 1-60 at ambient temperature. Solid line = ascending (forward) pH profile. Dashed line = descending (reverse) pH profile

The pH response profile is reversible as both the ascending (sold line) and descending (dashed line) response curves are superimposable. At low pH, the polymer exists in the shrunken state and the water content of the NK 1-60 particles is lower than that of the PVA hydrogel. The turbidity of the membrane as measured by the spectrometer is high because of the higher amount of light reflected due to the refractive index of the particles being higher than the refractive index of PVA. At higher pH values, the water content of the polymer particles increases due to swelling induced by the deprotonation of the pH sensitive comonomer. The refractive index of the particles decreases as the particles

swell and approaches the refractive index of PVA. The membrane becomes less turbid because less light is reflected. The turbidity reaches a limiting value corresponding to complete deprotonation of the functional comonomer.

The inflection point in the turbidity versus pH plot shown in Figure 3.2 is the apparent pK_a of the polymer. At the inflection point, there are approximately equal amounts of the protonated and deprotonated form of the carboxylate group of the functional comonomer. The term "apparent pKa" which refers to the inflection point in the pH profile where the response is midway between the response at lower pH and higher pH is used here as turbidity versus pH has not yet been described by theory in a manner that would allow the calculation of pK_a from the observed data.

Figure 3.3 shows the batch to batch variability of pH sensitive polymers prepared using the same formulation as was used to prepare NK 1-60. Care was taken to fix the reaction temperature during the preparation of these polymers. The pH profiles obtained were reversible as the ascending profile and descending profile (not shown in the figure) were reversible. Although the apparent pKa of each batch was the same, the total absorbance change indicative of pH induced swelling over the pH range 3 to 7 was not equivalent to the other membranes suggesting that batch to batch variability exists for polymer particles prepared using the NK 1-60 formulation.

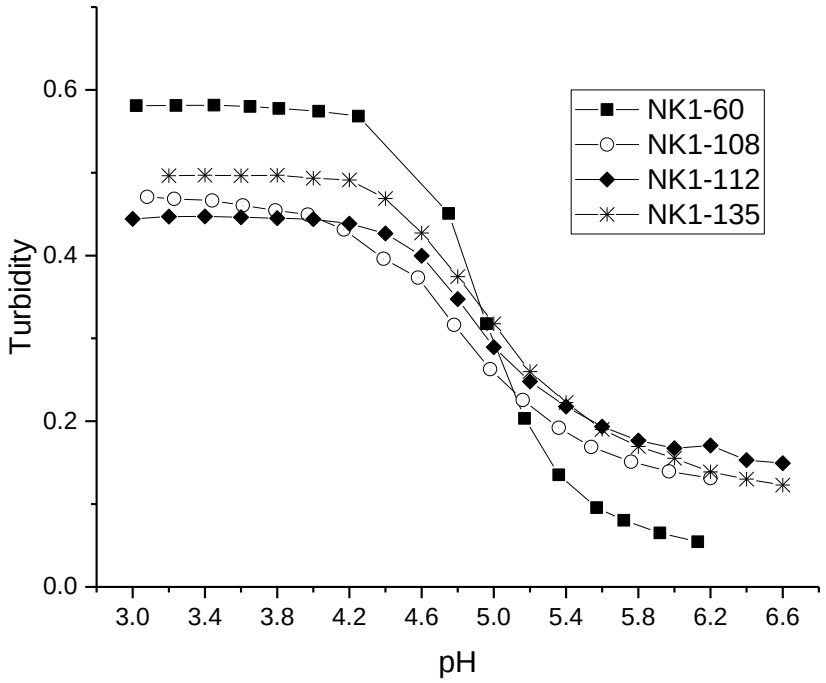

Figure 3.3. pH profile of different polymer batches prepared using the NK 1-60 formulation at ambient temperature

The swelling behavior of the NK 1-60 particles was also investigated in low and high and ionic strength media to better understand the effect of ionic strength on pH induced polymer swelling. The NK 1-60 polymer test segment was exposed to buffers of increasing ionic strength. pH profiles were collected at 0.05 M, 0.1 M, 0.5 M, and 1.0 M ionic strength over the pH range of 3.0 to 6.6 at 0.2 increments starting at pH 3.0. The ionic strength of each buffer was adjusted by adding known amounts of NaCl to an aliquot of

the 0.1 M buffer solution. Figure 3.4 shows the four pH profiles at the ionic strengths tested. There are no observable difference in the total swelling response, nor were there any significant differences in the overall shape of the pH profiles or in the location of their inflection points. Furthermore, polymer swelling was nonionic (see Equations 2.1 and 2.2) and the swelling behavior of NK 1-60 at the different ionic strengths was reversible as the ascending profile and descending profile (not shown in the figure) were superimposable.

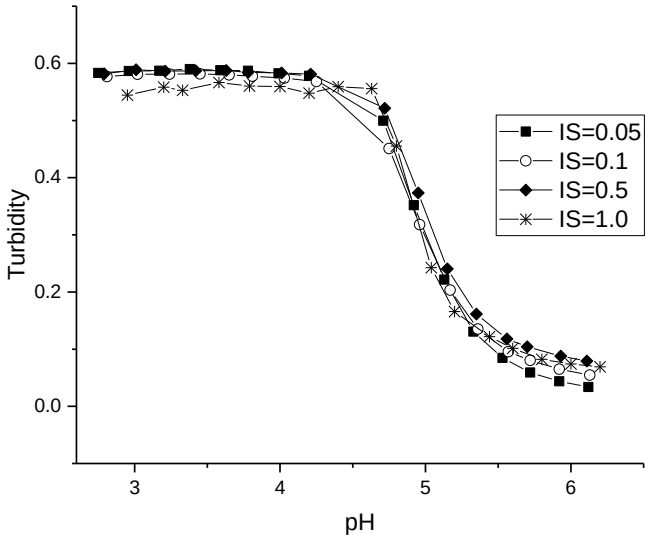

Figure 3.4. pH profiles of NK 1-60 at 0.05 M, 0.10 M, 0.50 M, 1.0 M ionic strength at ambient temperature.

The effect of ionic strength on other copolymers of NIPA and MAA was also investigated. Figures 3.5 and 3.6 show pH response curves for NK 1-28 (17 mmol NIPA, 2 mmol MAA and 1 mmol MBA) and NK 1-77 (16 mmol NIPA, 1mmol MAA, 2 mmol NTBA, and 1 mmol MBA) generated at an ionic strength of 0.1 M and 1.0 M. There is an increase in the apparent pKa of these pH response curves as the ionic strength of the buffer

solution in contact with these particles is increased (see Table 3.1). This can be attributed to the greater penetration of chloride anions into the polymer network which occurs as a result of higher ionic strength buffers. This, in turn, increases the amount of chloride anion on or in the vicinity of the polymer backbone, thereby increasing the amount of negative charge in the vicinity of the MAA monomer. The net result is a decrease in the tendency of the proton to dissociate from the carboxylic acid group of MAA. By increasing the degree of crosslinking between polymer chains (e.g., NK 1-60) in these synthates, this effect is probably mitigated. Clearly, the pH response of these polymer particles can be tuned to ionic strength by controlling the amount of crosslinking in these copolymers.

Table 3.1. Apparent pKa of NIPA and MAA Copolymers

NIPA Copolymer	Apparent pKa at 0.1 M IS	Apparent pKa at 1.0 M IS
NK 1-60 14 mmol NIPA, 2 mmol MAA, 2 mmol NTBA, and **2 mmol MBA**	4.88	4.90
NK 1-28 17mmol NIPA, 2mmol MAA and **1mmol MBA**	3.92	4.52
NK 1-77 16mmol NIPA, 1mmol MAA, 2mmol NTBA, and **1mmol MBA**	3.91	4.69

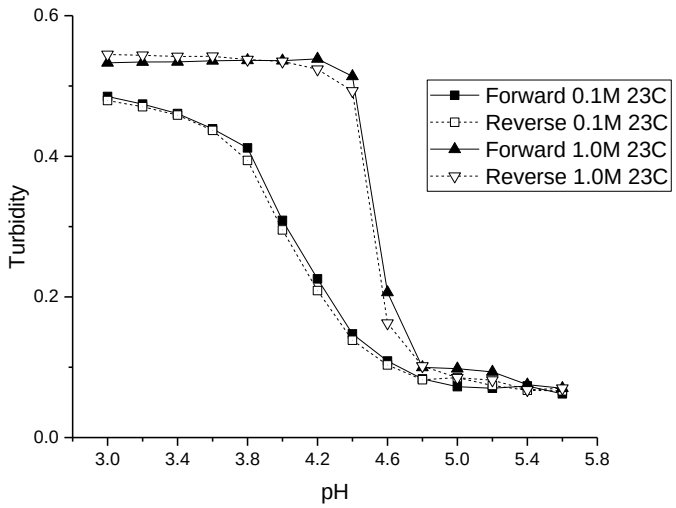

Figure 3.5. pH profiles of NK 1-28 at 0.10 M and 1.0 M ionic strength at ambient temperature.

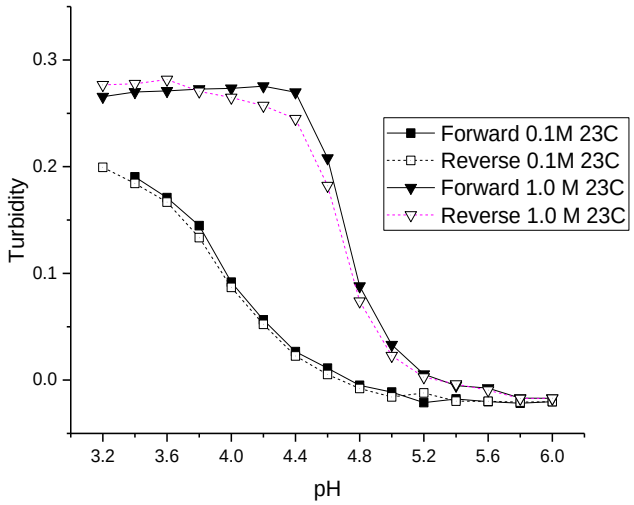

Figure 3.6. pH profiles of NK 1-77 at 0.10 M and 1.0 M ionic strength at ambient temperature.

Increasing the level of crosslinking in the copolymers of NIPA and MAA resulted in a decrease in polymer swelling (see Figure 3.7 and Table 3.2). The decrease in swelling with increased crosslinking can be attributed to increased structural rigidity, as the additional three-dimensional associations within the polymer physically resist swelling. From Equation 2.1, higher crosslinking corresponds to a higher value of ν_e, which is the effective number of chains in the polymer network. Since ν_e is inversely proportional to swelling, higher levels of crosslinking should reduce swelling. However, the use of low levels of cross linking (less than 5%) is not desirable, as the polymer will be amorphous. This prevents it from being reproducibly dispersed in the hydrogel. Although higher levels of crosslinking favor the formation of uniform monodispersed particles yielding reproducible membrane dispersions, 15% crosslinking has the drawback that total swelling is suppressed limiting sensitivity. 10% crosslinker in the formulation is a good compromise as the magnitude of the pH response profile is indicative of high sensitivity, and particle morphology is suitable for reproducible membrane dispersions.

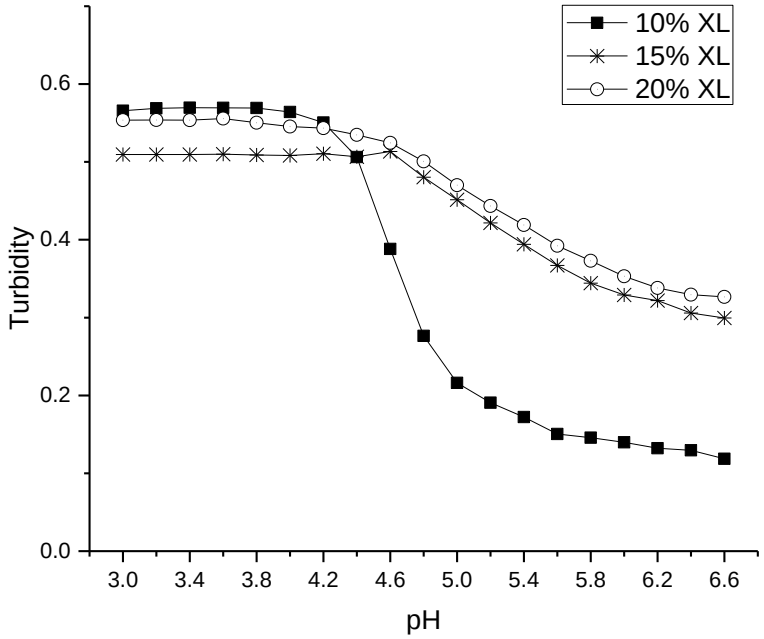

Figure 3.7. pH response profiles of NIPA copolymers of MAA at 10%, 15%, and 20% crosslinking at ambient temperature.

Table 3.2 Composition of the Copolymers used in the Crosslinking Study

NIPA Copolymer	NIPA	MAA	NTBA	MBA
NK 1-60 10% crosslinking	14 mmol	2 mmol	2 mmol	2 mmol
NK 1-148 15% crosslinking	13 mmol	2 mmol	2 mmol	3 mmol
NK 1-152 20% crosslinking	12 mmol	2 mmol	2 mmol	4 mmol

Increasing the NTBA content of the NIPA and MAA copolymers resulted in an increase in both polymer swelling and the apparent pK_a of the copolymers (see Figure 3.8

and Table 3.3). Swelling was reversible as the ascending profiles and descending profiles (not shown in Figure 3.8) were superimposable. NTBA is known to decrease the lower critical solution temperature of NIPA copolymers due to its hydrophobicity [52]. The increase in the apparent pK_a of these copolymers can probably be attributed to an increase in the hydrophobicity of the formulation used in their synthesis. The increase in pKa may be indirectly tied to the decrease in the lower critical solution temperature of the copolymers with increasing NTBA content.

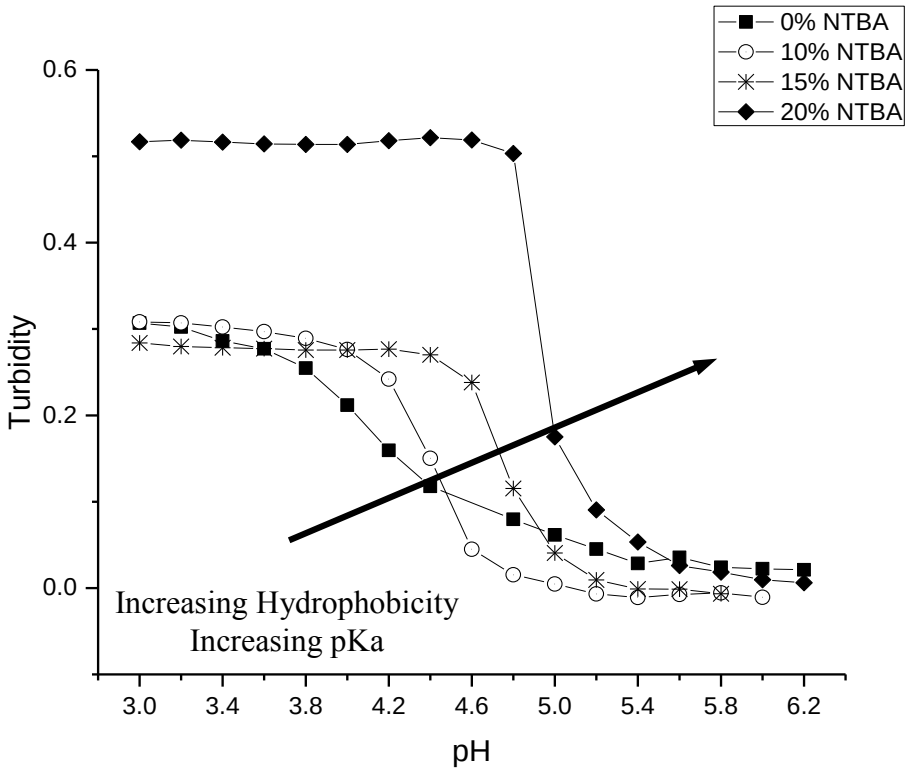

Figure 3.8. pH response profiles of NIPA copolymers of MAA at 10%, 15%, and 20% NTBA at 27^0 C.

Table 3.3 Composition of the Copolymers used in the NTBA Study

NIPA Copolymer	*Apparent pKa	NIPA	MAA	NTBA	MBA
NK 1-72 0% NTBA	4.10	16 mmol	1 mmol	0 mmol	1 mmol
NK 1-77 10% NTBA	4.43	15 mmol	1 mmol	2 mmol	1 mmol
NK 1-56 15% NTBA	4.73	14 mmol	1 mmol	3 mmol	1 mmol
NK 1-50 20% NTBA	4.91	14 mmol	1 mmol	4 mmol	1 mmol

*pKa of free MAA monomer as determined by titration with NaOH that was standardized with KHP is 4.65.

MAA plays a crucial role in defining the pH response of the polymer synthates previously discussed. Acrylates are generally used as comonomers because of their compatibility with NIPA. They have a terminal carboxylic acid that contributes to polymer swelling when deprotonated. To determine the optimal amount of MAA in the formulation, the pH response of the particles was determined for a series of NIPA-MAA polymers prepared with increasing MAA content (see Table 3.4). The pH profile of each polymer is shown in Figure 3.9. The 5%, 10%, 15%, 20%, and 25% polyNIPA-MAA particles exhibited reversible swelling, as the ascending profiles and descending pH profiles (not shown in Figure 3.9) were superimposable.

The increase in the apparent pKa of these polymer with increasing MAA content from approximately 4.7 for 10% 15%, and 20% MAA (which corresponds to the pKa of

the MAA monomer) to 5.2 for 25% MAA. The largest total absorbance change in the polymer series investigated occurred with 10% and 15% MAA (see Figure 3.9). If only 5%MAA is used, there is very little swelling and the pH response profile is not particularly distinct. By increasing the percent composition of MAA to 10% or 15%, there is a large increase in the total swelling and the pH profile is distinct. However, a further increase in the amount of MAA copolymerized with NIPA results in a reduction in swelling. Therefore, the optimum MAA composition is between 10% and 15% MAA.

Table 3.4 Composition of the Copolymers used in the MAA Study

NIPA Copolymer	Apparent pKa	NIPA	MAA	NTBA	MBA
NK 1-64 5% MAA	4.90	15 mmol	1 mmol	2 mmol	2 mmol
NK 1-60 10% MAA	4.57	14 mmol	2 mmol	2 mmol	2 mmol
NK 1-124 15% MAA	4.47	13 mmol	3 mmol	2 mmol	2 mmol
NK 1-119 20% MAA	4.66	12 mmol	4 mmol	2 mmol	2 mmol
NK 1-127 25% MAA	4.90	11 mmol	5 mmol	2 mmol	2 mmol

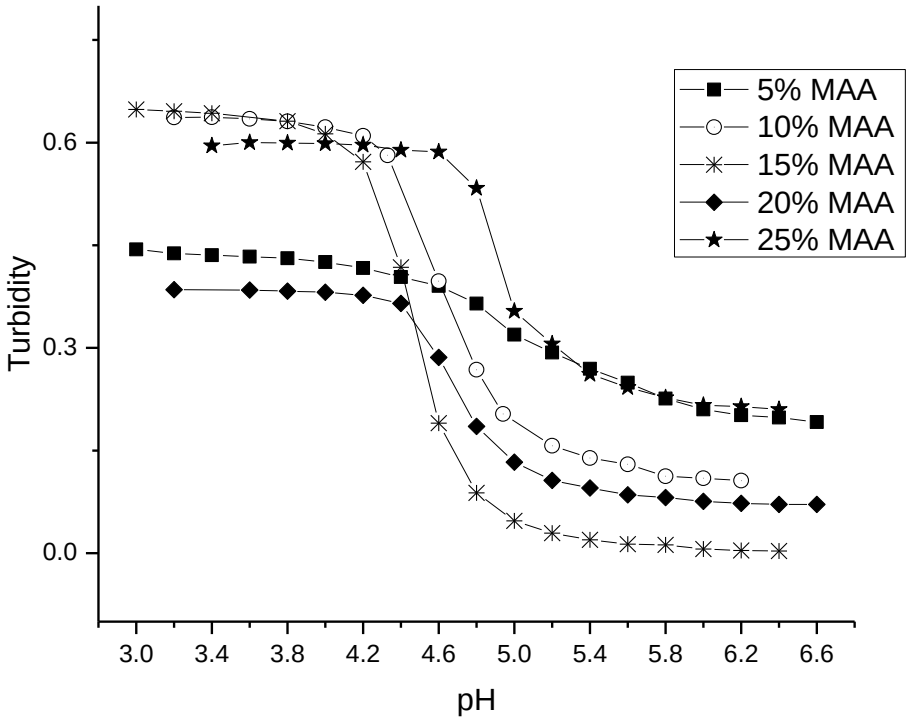

Figure 3.9. pH response profiles of NIPA copolymers of MAA at 5%, 10%, 15%, and 20% and 25% MAA at 27^0 C.

Although it is only a minor component in the polymer formulations investigated, MAA imparted the desired functionality to the microgel particles. Other functional co-monomers often reported in the literature for NIPA are also from the acrylate family, wherein a terminal carboxylic acid is deprotonated as the pH of the solution in contact with

the particles increases. A series of related acrylates were investigated to determine if incorporating a series of functional co-monomers of increasing pKa values will translate into higher pKa values for the NIPA copolymer synthates. Acrylates were selected because MAA is the functional comonomer incorporated into the majority of the polymers synthates investigated as part of the research performed in this study. Acrylates selected for this phase of the study included AA, MAA, EAA, and PAA. NIPA copolymers were prepared using 10% AA, 10% MAA, 10% EAA, or 10% PAA.

Figure 3.10 shows the pH response profiles of four poly (*N*-isopropylacrlyamide) synthates prepared by copolymerization of NIPA with AA, MAA, EAA, and PAA. Table 3.5 summarizes the formulation used for each synthate and its apparent pKa. The AA functionalized polymer has the lowest pKa of the copolymers investigated in this series, and a shift of 1.7 pH units in the pKa values are observed for the four polymers in this series. Clearly, the apparent pK_a of NIPA copolymers can be tuned by increasing the alkyl chain length (hydrophobicity) of the pH sensitive functional comonomer.

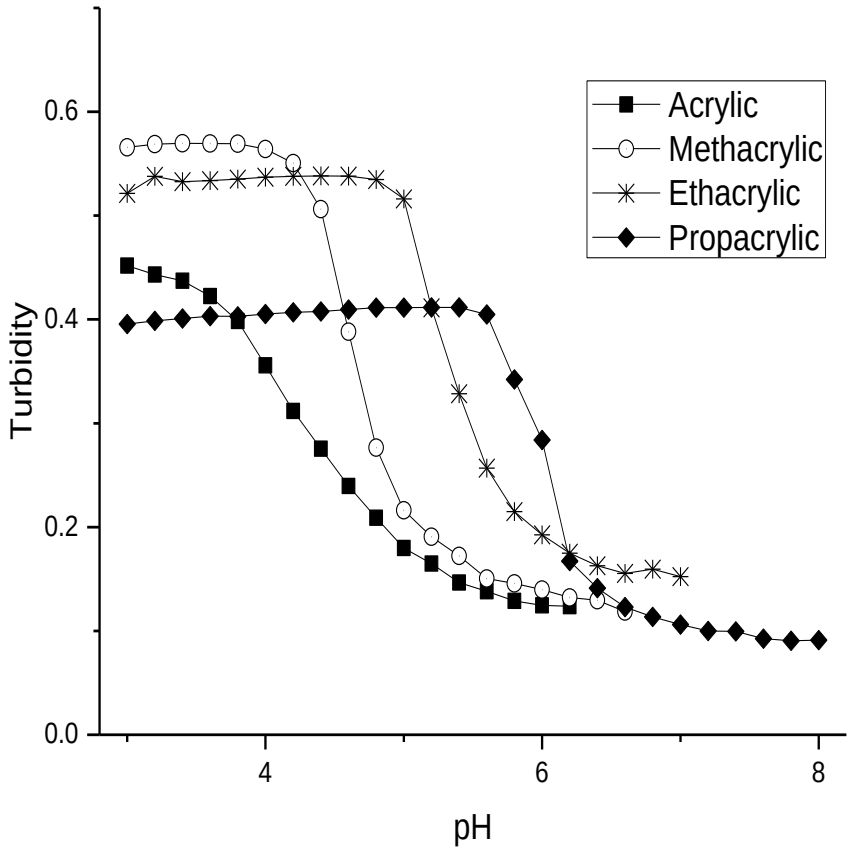

Figure 3.10. pH response profiles of NIPA copolymers of AA, MAA, EAA, and PAA at 23^0 C.

Table 3.5 Composition of the Copolymers used in the Functional Comonomer Study

NIPA Copolymer	Apparent pKa	pKa of functional comonomer	NIPA	Functional Comonomer	NTBA	MBA
NK 1-156	4.37	4.25	14 mmol	2 mmol of AA[1]	2 mmol	2 mmol
NK 1-60	4.70	4.65	14 mmol	2 mmol of MAA[2]	2 mmol	2 mmol
NK 1-146	5.39	4.65	14 mmol	2 mmol of EAA[3]	2 mmol	2 mmol
NK 1-155	6.07	4.84	14 mmol	2 mmol of PAA[4]	2 mmol	2 mmol

[1]Log P value of acrylic acid is 0.29
[2]Log P value of methacrylic acid is 0.93
[3]Log P value of ethacrylic acid is 1.08
[4]Log P value of propacrylic acid is 1.59

For AA and MAA functional comonomers, the apparent pKa is in agreement with the pKa of the corresponding free monomer. For EAA and PAA, the apparent pKa of the polymer is greater than the pKa of the corresponding free monomer. This can be attributed to the low reactivity ratios of EAA and PAA [53]. For these four NIPA copolymers, NIPA is the dominant monomer with only a small amount of the functional comonomer present. For AA and MAA, NIPA will be polymerized into chains containing well separated functional comonomer units since the reactivity ratios of all monomers comprising these two copolymers are the same. Because of the lower reactivity ratios of EAA and PAA, the corresponding copolymer will not contain well separated functional comonomer units resulting in higher pKa values.

Response curves were obtained at seven temperatures for each synthate to better understand the thermodynamics of pH induced polymer swelling. The apparent pK_a was computed for each response curve and the relationship between the apparent pK_a and temperature was modeled using the van't Hoff relationship, see Equation 3.1 where K_a is the acid dissociation constant of the copolymer, T is the temperature, ΔH^0 is the change in enthalpy for pH induced swelling of the poly (*N*-isopropylacrylamide) synthate, ΔS^0 is the change in the entropy associated with pH induced swelling of the poly (*N*-isopropylacrylamide) synthate, and R is the gas constant.

$$lnK_a = \frac{-\Delta H^0}{RT} + \frac{\Delta S^0}{R} \tag{3.1}$$

Table 3.6 lists the changes in enthalpy and entropy that occur due to pH induced swelling of the poly (*N*-isopropylacrylamide) synthates. For AA, MAA, and EAA, the increase in the hydrophobicity of the comonomer in the synthate (see Table 3.5) can be correlated to an increase in the enthalpy and entropy of swelling for these copolymers, whereas PAA does not follow this trend. The pH induced swelling behavior of AA, MAA, and EAA is reversible whereas the pH induced swelling behavior of PAA is irreversible as the ascending and descending pH curves do not overlap (see Figure 3.11). In all likelihood, the NIPA copolymer of PAA undergoes a conformational change when it swells and it does not return to the same initial shrunken state. This would readily explain why PAA appears to be a discordant data point.

Table 3.6. Enthalpy and Entropy Changes for pH Induced Swelling.

Functional Monomer	**ΔH (J/mol)**	**ΔS (J/mol*K)**
AA	-47,000 ± 2,300	-242 ± 7
MAA	-74,900 ± 4,400	-336 ± 15
EAA	-100,000 ± 3,300	-435 ± 11
PAA	-60,000 ± 2,400	-312 ± 8

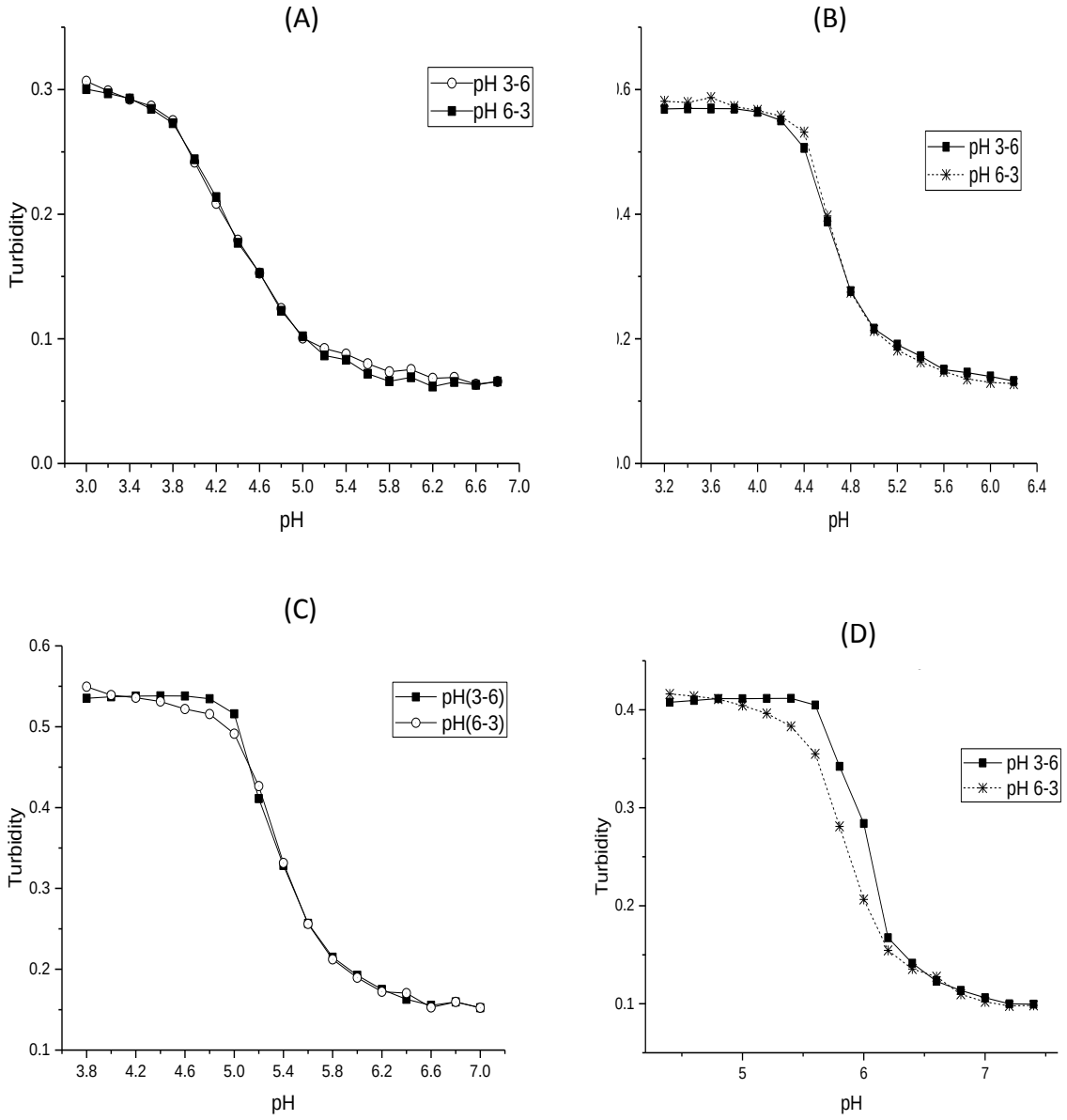

Figure 3.11. pH response curves of NIPA copolymers of (A) AA, (B) MAA, (C) EAA, (D) PAA

Protein binding experiments involving these four poly (*N*-isopropylacrylamide) synthates and hemoglobin (66.5 kDa) or γ-Globulin (150 kDa) were performed to determine if any carboxylic acid groups were present on the surface of these NIPA

copolymers. A procedure previously documented in the literature was adapted for this study [54]. The polyNIPA particles were spin coated onto a QCM gold substrate. After spin coating, the particles were exposed to pH 5.6 buffer and the resonance frequency of the QCM was recorded after 25 min. The QCM substrate was then exposed to a pH 5.6 buffer solution which contained 0.2 mg/mL of hemoglobin or γ-Globulin. (The pH of the buffer must be higher than the pKa of the polymer and less than the pI of the protein.) The frequency of the QCM crystal was recorded after 25 min for short time exposure and after 24 hr for long time exposure. Differences between the frequency of the crystal in contact with buffer solutions with and without protein are shown in Table 3.7 and 3.8. The data in both tables indicates that protein binding was restricted to the AA particles. Although the PAA particles could not undergo binding with either protein, the QCM frequency values recorded for these particles served as a baseline to establish frequency differences that would be indicative of binding. Clearly, the AA particles differ from the MAA and EAA particles in terms of the location of the carboxylic acid groups in the copolymer.

Table 3.7. Frequency Difference of QCM Crystal Before and After Exposure to γ-Globulin

Functional Comonomer	Difference in frequency (Hz) after short time exposure (25 min)	Difference in frequency (Hz) after long time exposure (24 hr)
AA	-2793	-8501
MAA	-94	-142

Table 3.8 Frequency Difference of QCM Crystal Before and After Exposure to Hemoglobin

Functional Comonomer	Difference in frequency (Hz) after short time exposure (25 min)	Difference in frequency (Hz) after long time exposure (24 hr)
AA	-4574	-5965
MAA	-221	-244
EAA	-277	-
PAA	-274	-

References

43. J. Gasteiner, T. Guggenberger, J. Hausler, and A. Steinwidder, Continuous and Long Term Measurement of Reticuloruminal pH in Grazing Dairy Cows by an Indwelling and Wireless Data Transmitting Unit, Vet. Med. International doi:10.1155/2012/236956

44. S. Zhang, B. R. Soller, and R. H. Micheels, Partial Least Squares Modeling of near Infrared Reflectance Data for Noninvasive in vivo Determination of Deep Tissue pH, Appl. Spectros., 1998, 52, 393-399.

45. H. M. Mousa, R. Rosen, F. W. Woodley, M. Ors, D. Armas, C. Faure, J. Fortunato, J. O'Connor, B. Skaggs, and S. Nurko, J. pediatr. Gastroenterol Nutr., 2011, 52(2), 129-139.

46. R. F. Service, Rising Acidity Brings an Ocean of Trouble, Science, 2016, 337, 146-148.

47. A. S. Jeevarajan, S. Vani, T. D. Taylor, M. M. Anderson, Continuous pH Monitoring in a perfused bioreactor system using an optical pH sensor, Biotechnology and Bioengineering, 78 (2002) 467-472.

48. K. Medlock, H. Harmer, G. Worsley, A. Horgan, J. Pritchard, pH-sensitive holograms for continuous monitoring in plasma, Anal Bioanal Chem, 389 (2007) 1533–1539.

49. M. J. P. Leiner, P. Hartmann, Theory and practice in optical pH sensing, Sensors and Actuators B 11 (1993) 281-289.

50. Fiber optic pH sensing. A. Ferguson, B. G. Healey, K. S. Bronk, S. M. Barnard, D. R. Walt, Simultaneous monitoring of pH, CO, and O using an optical imaging fiber, Anal. Chim. Acta. 340 (1997) 123-131.

51. M. Ferritto and D. A. Tirrell, Poly (2-Ethylacrylic Acid), Macromolecular Synthesis, 1992, 11, 59-63.

52. F. Seker and A. B. Ellis, Correlation of Chemical Structure and Swelling Behavior in N-Alkylacrylamide Hydrogels, Polym. Sci. Part A: Polym. Chem., 1998, 36, 2005-2012.

53. N. Murthy, J. R. Robichaud, D. A. Tirrell, P. S. Slayton, and A. S. Hoffman, "The design and synthesis of polymers for eukaryotic membrane disruption" Controlled Release, 1999, 61, 137-143.

54. X. Chen, S. Chen, and J. Wang, A pH-Responsive Poly (*N*-isopropylacrylamide-co-Acrylic Acid) Hydrogel for the Selective Isolation of Hemoglobin from Human Blood, Analyst, 2010, 135, 1736-1741.

CHAPTER IV

ANALYSIS OF VANILLA EXTRACT BY REVERSED PHASE LIQUID CHROMATOGRAPHY USING WATER RICH MOBILE PHASES

4.1 Introduction

Vanillin (4-hydroxy-3-methoxybenzaldehyde) is the major constituent of vanilla extract, a flavoring ingredient used in food and beverages. Natural vanilla extract prepared from the bean of the tropical orchid, *Vanilla planifolia*, is expensive due to the limited supply of the vanilla bean. For this reason, synthetic vanilla extracts are widely used. Synthetic vanilla extracts are less complex and usually contain vanillin, ethyl vanillin and other related compounds that are prepared from inexpensive starting materials.

Several reversed phase liquid chromatographic (RPLC) methods have been developed to quantitate coumarin, vanillin, and ethyl vanillin in vanilla products [55-58]. These RPLC methods, which employed isocratic or gradient elution, methanol, acetonitrile or tetrahydrofuran as the organic mobile phase modifier and diode array or mass spectrometer detection, are not able separate weakly retained compounds such as vanillic acid and isovanillin. The use of water rich mobile phases has been investigated in this study as a potential isocratic method to fully characterize the composition of synthetic

vanilla extract. Water rich mobile phases in RPLC are not generally used because of the long retention times involved. The problem of long retention times can be addressed using hydrophobic alcohols such as butanol in low quantities (approximately 1% v/v) as the organic modifier.

In an effort to gain insight into the relationship between stationary phase solvation and selectivity and to improve the chromatographic separation of water soluble compounds, Lavine [59] in a previous study had investigated the use of short and medium chained length alcohols (methanol, n-propanol, n-butanol, and n-pentanol) as mobile phase modifiers in RPLC to determine their impact on resolution. A wide range of mobile phase compositions was evaluated because of the large effect exerted by solvent strength on selectivity. Evidence was presented to support the view that an increase in the hydrophobicity of the organic modifier increases the selectivity of the C_{18} alkyl bonded phase by increasing its contact surface area due to improved wetting, which is a result of the greater hydrophobicity of the organic mobile phase modifier used.

Using aqueous rich mobile phases (e.g., 1% butanol in water acidified with 0.2% acetic acid), an RPLC and liquid chromatography/mass spectrometry (LC/MS) method capable of separating coumarin, vanillin, and derivatives of vanillin (e.g., vanillic acid, isovanillin, o-vanillin, ethyl vanillin) on an alkyl bonded C_{18} stationary phase column has been developed. Snyder's solvent strength model [60, 61] was used to provide a better understanding of the factors that influence the separation process and to offer insight into the retention mechanism when butanol is used as the organic mobile phase modifier on C_{18} and C_8 alkyl bonded phases. Because of the better resolution achieved in the separation of the vanillin compounds when butanol was used as the organic mobile phase modifier,

constituents of vanilla extract purchased from local supermarkets in the area were identified that hitherto had not been previously reported in the literature. Furthermore, vanilla extracts purchased from local supermarkets could be divided into distinct groups based on their composition as reflected by their RPLC profiles.

4.2 Experimental

The six retention probes used in this study, vanillic acid, isovanillin, o-vanillin, ethylvanillin, vanillin and coumarin were purchased from Aldrich and were used as received. The chemical structures of these six compounds are shown in Figure 1. Stock solutions of the vanillin compounds were prepared by weighing and dissolving the corresponding amount of the compound in methanol (Thermo-Fisher) followed by dilution to the appropriate working concentration (10^{-4} M) using doubly distilled water (prepared by a Barnstead NanoPure II System, Barnstead International, Dubuque, IA). If stored at 4 ^{0}C, the working solutions were stable for approximately one month. Since these compounds are weakly retained by alkyl bonded stationary phases, it was necessary to use water as the primary solvent to prepare the vanillin test mixtures. If a stronger solvent such as methanol were used to prepare the samples, the test mixtures would not have been deposited onto the head of the column as a thin plug during sample injection, with the result being increased band broadening.

Thirty-six vanillin extract products were obtained from local supermarkets in the area. Sample preparation consisted of pipetting 250 μL of vanillin extract into a 25 mL volumetric flask followed by the addition of 25% methanol in water solution with 1 % v/v/ acetic acid to volume and sonication of the flask. Methanol and butanol, the alcohols used

as organic modifiers in this study, were purchased from Thermo-Fisher and Aldrich. Glacial acetic acid, which was used to acidify the mobile phase, was obtained from Pharmaco. Doubly distilled water (purchased from Burdick & Jackson) was used to prepare all mobile phases, which were then filtered with 0.45 μm pore size filters (Varian). Varian Nylon 66 filters were used to remove particulate matter from the mobile phase. A transfer pipette was used to prepare mobile phases containing butanol because of the small volume of organic modifier used in the preparation of these solutions. Each mobile phase solution was degassed prior to use.

The chromatographic studies were performed on two LC instruments: (1) Varian High Performance Liquid Chromatograph equipped with a BDS-Hypersil C_{18} , C_8, or Cyanopropyl column (100× 4.6 mm, Particle Diameter 5 μm, Thermo-Fisher), Shimadzu column oven, ProStar reciprocating pump, and diode array detector, and (2) SHIMADZU 2010 LC-MS equipped with a 2010 Premier C_{18} column (100× 4.6 mm, Particle Diameter is 3 μm, Shimadzu), column oven, and two detectors (diode array and electro-spray mass spectrometer). The dead time of each column was determined by injecting different solutions (methanol, methanol-water, water, or KNO_3) onto the BDS or Premiere column, and the dead volume (1.1 mL for the Premiere column and 1.2 mL for the BDS column) was used in all retention factor calculations. All k' values determined in this study were averages of triplicate determinations, and deviations in individual k' values were never greater than 1%.

All mobile phases were percolated through the column at a flow rate of 1.0 mL/min (Varian Prostar HPLC) or 0.3 mL/min (Shimadzu LC/MS) for several hours to ensure reproducible solvation of the bonded phase. These flow rates were used in all of the studies

because of the desire to develop an RPLC or LC-MS analysis method for the analysis of vanillin extract. For the same reason, the temperature of the column was ambient. The injection volume was 5 μL. For the LC/MS runs, the ESI interface was operated in the negative ion mode, the nebulizing nitrogen gas flow rate for the LC-MS interface was set at 1.5 L/min, and the temperature of the curved desolvation line was set at 200 ˚C. Full-scan spectra were recorded from 50–500 m/z at a scan time of 500 amu/s.

4.3 Results and Discussion

4.3.1 Methanol versus Butanol as the Mobile Phase Modifier

A series of chromatograms were run to illustrate the advantages of using butanol as an organic modifier for the separation of vanillin, derivatives of vanillin and coumarin. The test mixture consisted of six compounds (see Figure 4.1).

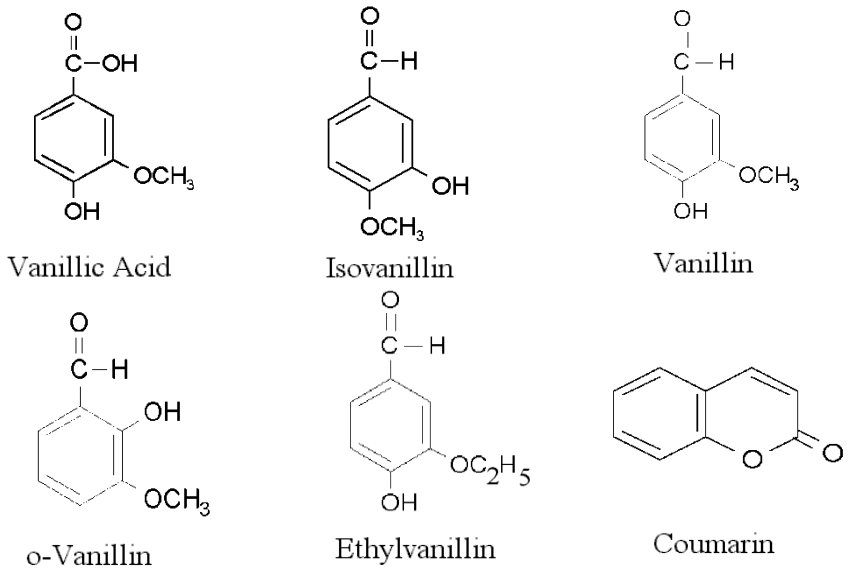

Figure 4.1. Chemical structures of the compounds comprising the vanillin test mixture.

Figure 4.2a shows a chromatogram of the vanillin test mixture using the methanol-water mobile phase (25% methanol in water with 0.2% acetic acid) that yielded the best separation on the BDS C_{18} column at ambient temperature. Figure 4.2b shows a chromatogram of the same test mixture on a butanol water mobile phase (1.0% butanol in water with 0.2% acetic acid) that yielded the best separation on the BDS C_{18} column at ambient temperature. The six components of the vanillin test mixture can be separated by the butanol-water mobile phase but not by the methanol-water mobile phase.

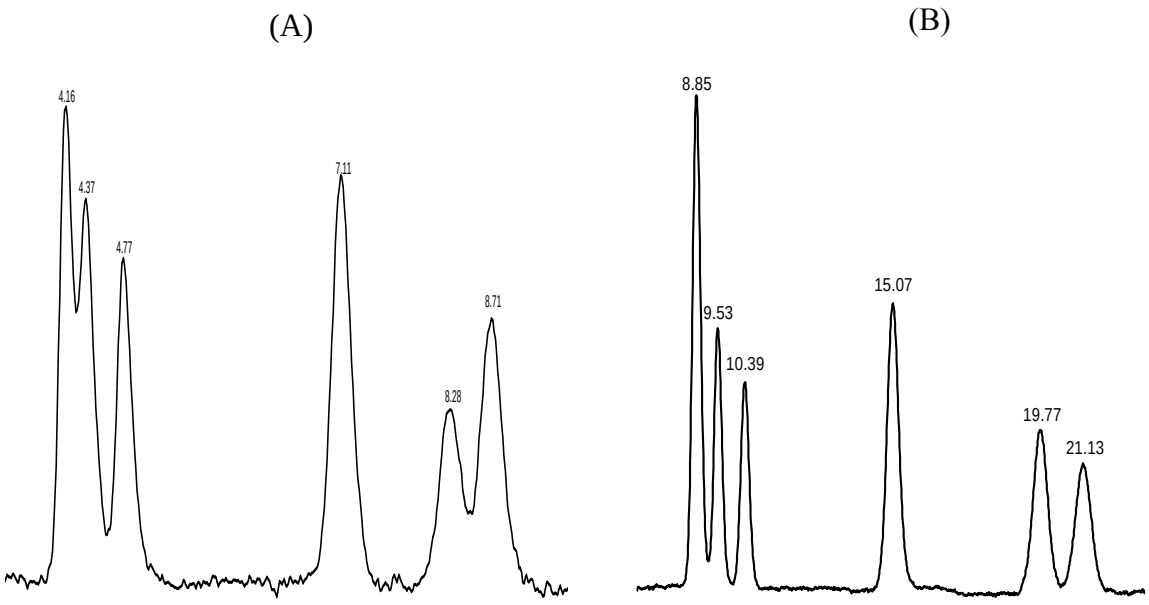

Figure 4.2. Chromatograms of the vanillin test mixture. Elution order was vanillic acid, isovanillin, vanillin, o-vanillin, ethylvanillin and coumarin. A) methanol-water mobile phase (25% methanol in water with 0.2% acetic acid) that yielded the best separation on the BDS C_{18} column at ambient temperature. B) butanol-water mobile phase (1.0% butanol in water with 0.2% acetic acid) that yielded the best separation of the test mixture on the BDS C_{18} column at ambient temperature.

To better understand the factors that contribute to better separations when butanol is used as the organic mobile phase modifier, it was necessary to examine retention factor data for each test mixture compound on the BDS C_{18} column in a systematic manner. In

RPLC, the factors which influence the separation process can be understood by a thorough analysis of k' data obtained for a set of compounds using Snyder's solvent strength plots (see Equation 1), where ln k_w is the logarithm of the retention factor for the compound in a purely aqueous medium, B is the slope of the plot, which is dependent on the solute and the chromatographic system investigated (mobile and stationary phase), and Φ is the volume percentage of organic modifier in the mobile phase. Snyder's solvent strength plots can also be used to predict selectivity and resolution for a particular separation over a narrow range of Φ [62].

$$\ln k' = \ln k_w - B\Phi \qquad (4.1)$$

Figure 4.3 shows a plot of ln k' versus ϕ for each compound of the vanillin test mixture eluted from the column using as mobile phases methanol in water with 0.2% acetic acid. Snyder solvent strength plots were generated using five methanol-water-acetic acid mobile phases: 15%, 20%, 25%, 30%, and 35% methanol in water with 0.2% acetic acid. (For this study, it was not possible to generate retention data using methanol-water mobile phases with less than 15% methanol because of difficulties encountered in eluting each component of the test mixture from the column.) The six compounds studied exhibited classical RPLC hydrophobic behavior. Plots of ln k' versus organic modifier concentration were linear for each test mixture compound investigated. Retention time decreases as the concentration of methanol increases because the stationary phase is saturated with methanol (i.e., the organic modifier) over the mobile phase composition range investigated.

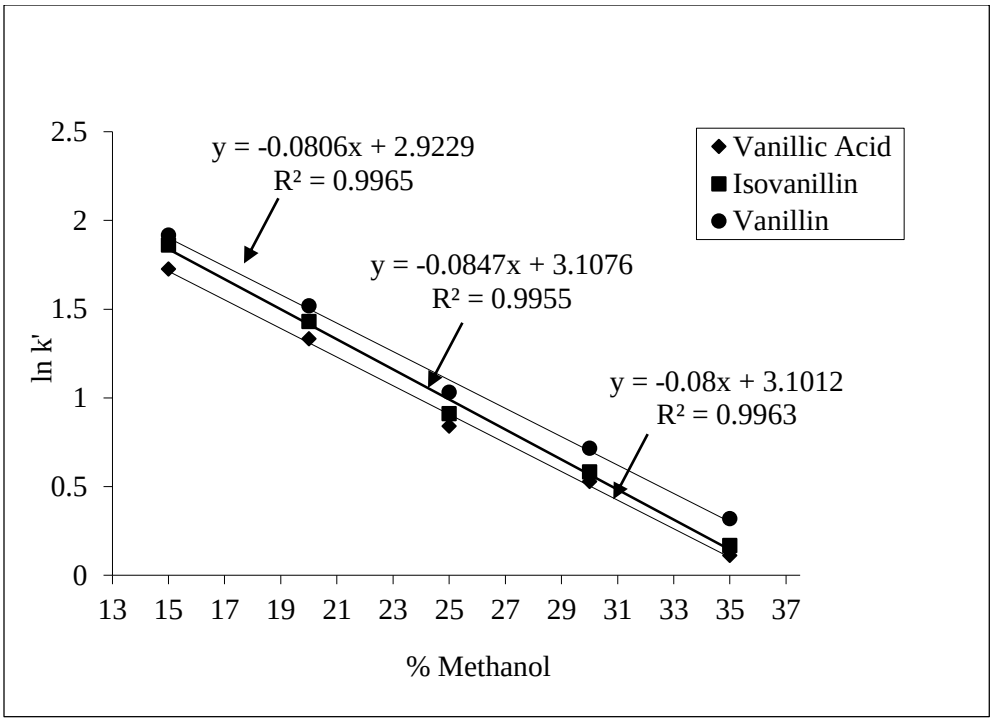

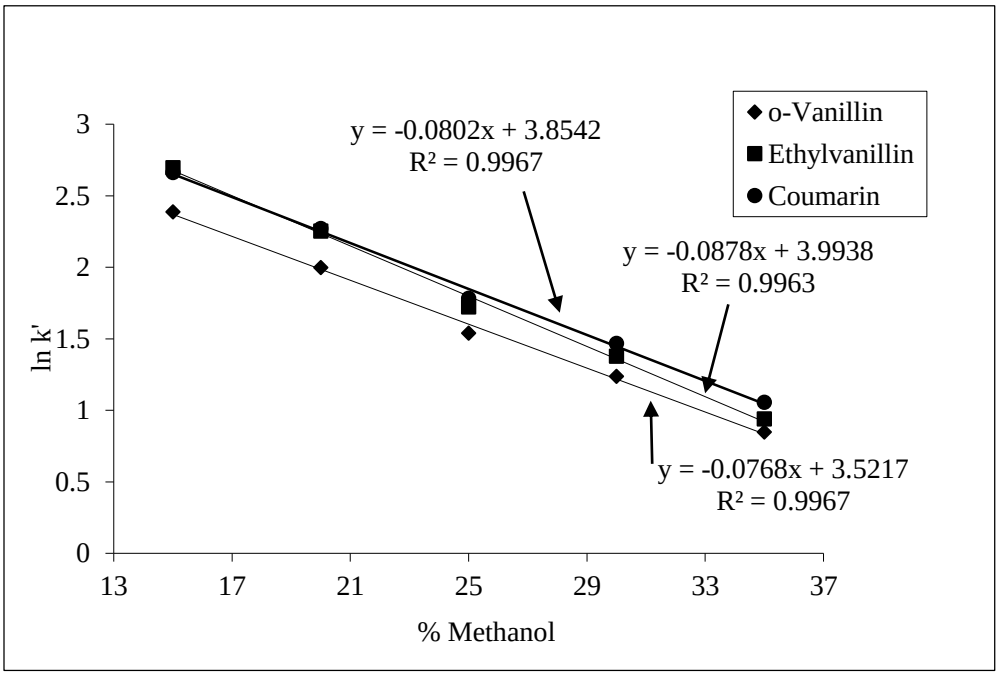

Figure 4.3. Plot of ln k' versus ϕ for each vanillin test mixture compound using as mobile phases methanol in water with 0.2% acetic acid

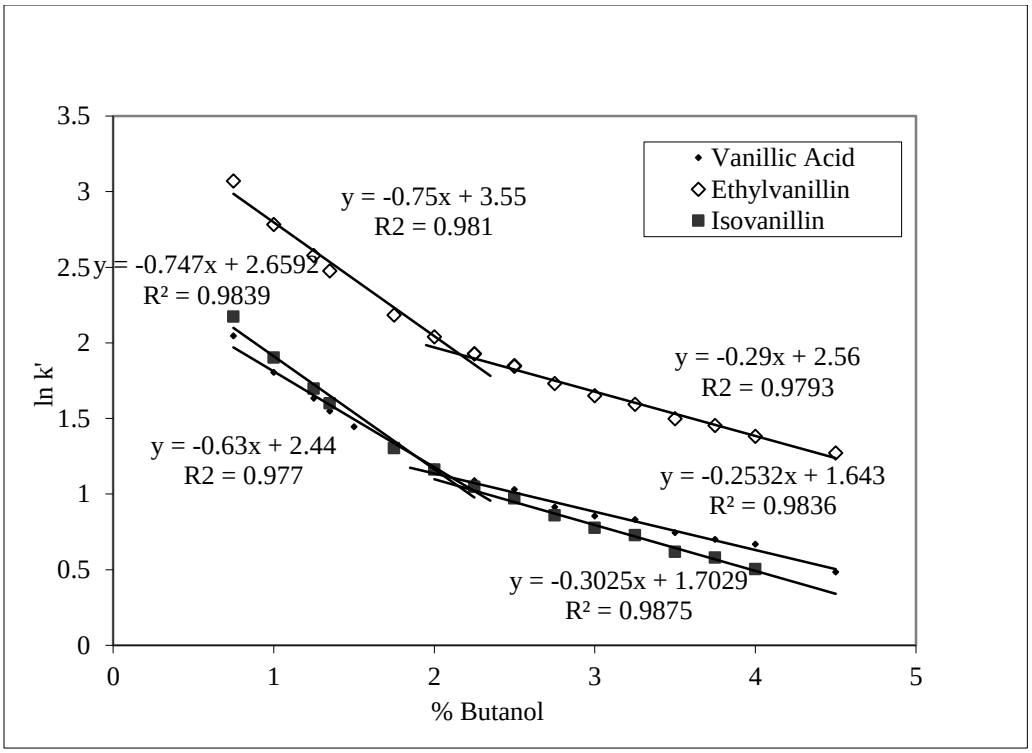

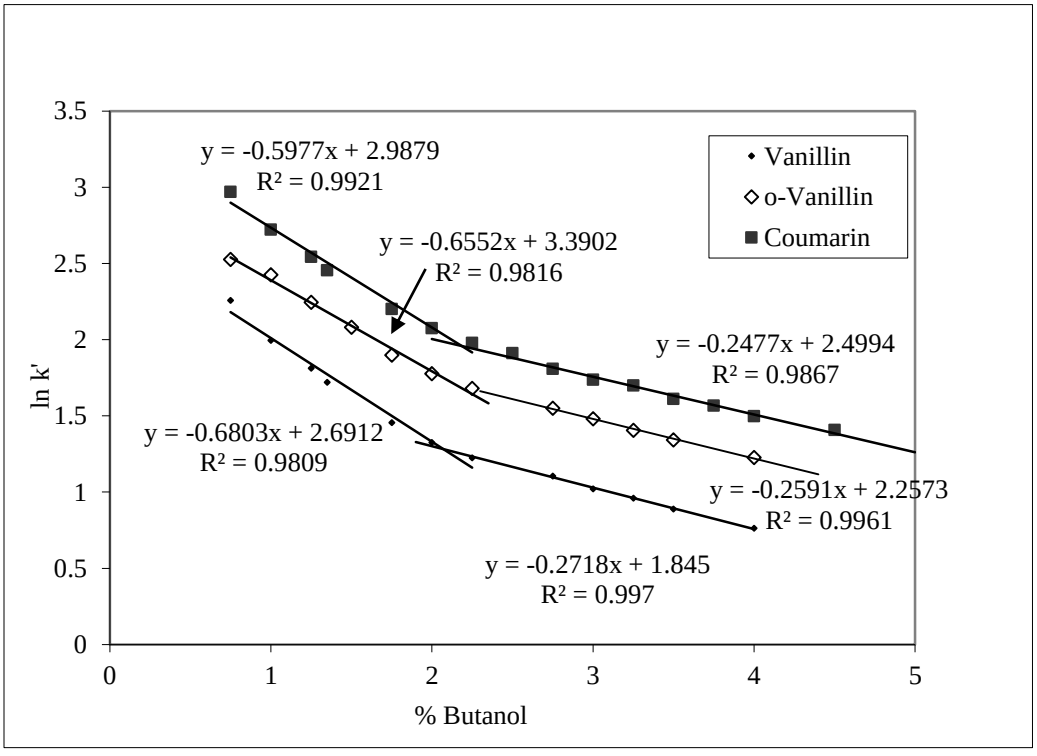

Figure 4.4. Plot of ln k' versus ϕ for each vanillin test mixture compound using as mobile phases butanol in water with 0.2% acetic acid

Figure 4.4 shows Snyder solvent strength plots generated for each test mixture compound using at least twelve butanol-water-acetic acid mobile phases with the concentration of butanol varying from 0.75%-4% v/v. All ln k' plots are bilinear, with the break occurring at the same mobile phase composition (2.5% butanol in water with 0.2% acetic acid) for each compound. Scott [63] has shown that saturation of the C_{18} stationary phase by butanol occurs at 2.5% v/v. Therefore, the break in each plot could be indicative of a change in the structure of the stationary phase [64]. The first linear segment of each plot denoted as "low butanol concentration" may correspond to a simultaneous change in both the mobile and stationary phases, whereas the second linear segment of each plot denoted as "high butanol concentration" may correspond to classical RPLC behavior - that is, a change in the composition of the mobile phase with increasing organic modifier (i.e., butanol) concentration, with the stationary phase remaining unchanged because it has been saturated by butanol.

All of the butanol ln k' plots were reproducible. The same results were obtained whether we started at higher organic modifier concentration and moved towards lower concentration or vice-versa. Clearly, the break in the ln k' plots cannot be attributed to a conformational effect involving the folding of the C_{18} chains.

For each vanillin test mixture compound, the computed k_w value in the regression equation developed from the "high alcohol concentration" butanol data is four to seven times less than the corresponding k_w value in the regression equation developed from the methanol water data. This result is not surprising because these k_w values do not represent true k_w values. Each represents what the capacity factor would be, if the conformation and composition of the stationary phase in pure water were the same as in the organic aqueous

mixtures used to generate these plots. Differences in these k_w values reflect differences in the solvation of the C_{18} alkyl bonded phase by methanol and butanol. These differences cannot be attributed to uncertainty in the least squares fitting of the data, which can be as high as 80% [65].

Schoemaker's solubility parameter model has been used by other workers to describe nonlinear behavior in ln k' versus ϕ plots [66, 67]. An $E\phi^{0.5}$ term, where E is a regression coefficient, is added to Snyder's solvent strength model to describe curvature at low concentrations ($\phi < 0.2$) of organic modifier. However, the functional form of the butanol data in the ln k' versus ϕ plots shown suggests that a bilinear model is more appropriate to fit this data, which is supported by residual plots of the regression. Furthermore, the data in these butanol plots is for $\phi < 0.04$. The degree of structure exhibited by these plots for the mobile phase composition range ($\phi < 0.2$) investigated cannot be attributed to differences in the solubility parameters of the solute, mobile phase and stationary phase.

Water rich mobile phases were also used to investigate C_8 and cyanopropyl bonded phase columns. Figure 4.5a shows the chromatogram of the vanillin test mixture using the methanol-water mobile phase (30% methanol in water with 0.2% acetic acid) that yielded the best separation on the BDS C_8 column at ambient temperature, and Figure 4.5b shows the chromatogram of the vanillin test mixture using the methanol water mobile phase (2.5% methanol in water with 0.2% acetic acid) that yielded the best separation on the BDS cyanopropyl bonded phase column at ambient temperature. Figure 4.5c shows the chromatogram of the vanillin test mixture using the butanol water mobile phase (0.75% butanol in water with 0.2% acetic acid) that yielded the best separation on the BDS C_8

column at ambient temperature, and Figure 4.5d shows the chromatogram of the vanillin test mixture using the butanol water mobile phase (2.5% butanol in water with 0.2% acetic acid) that yielded the best separation on the BDS cyanopropyl column at ambient temperature. When compared to C_{18}, C_8 yielded comparable results whereas the test mixture was poorly resolved on the cyanopropyl bonded using either methanol-water or butanol-water mobile phases.

4.3.2 C_{18} versus C_8

Snyder solvent strength plots were generated for methanol using five methanol-water-acetic acid mobile phases: 15%, 20%, 25%, 30%, and 35% methanol in water with 0.2% acetic acid and for butanol using at least twelve butanol-water-acetic acid mobile phases with the concentration of butanol varying from 0.75%,- 3% v/v. The methanol in water and butanol in water mobile phases yielded plots similar to C_{18}. Therefore, Log-Log plots of retention [68] for C_{18} and C_8 alkyl bonded phase columns were constructed to better understand the differences in behavior of these two alkyl bonded phases. Linear correlations with slopes of unity in such plots are termed "homoenergetic" and are indicative of the same retention mechanism for the two columns, whereas linear correlations with slopes different from unity are termed "homeoenergetic" and are indicative of similar but nonidentical thermodynamic retention behavior. Log-Log plots are shown in Figure 4.6 for methanol-water and in Figure 4.7 for butanol-water. It is evident from an examination of these plots that C_{18} and C_8 exhibit homeoenergetic behavior for both methanol-water and butanol water mobile phases. However, the slopes of the regression lines for methanol-water are closer to unity than butanol-water.

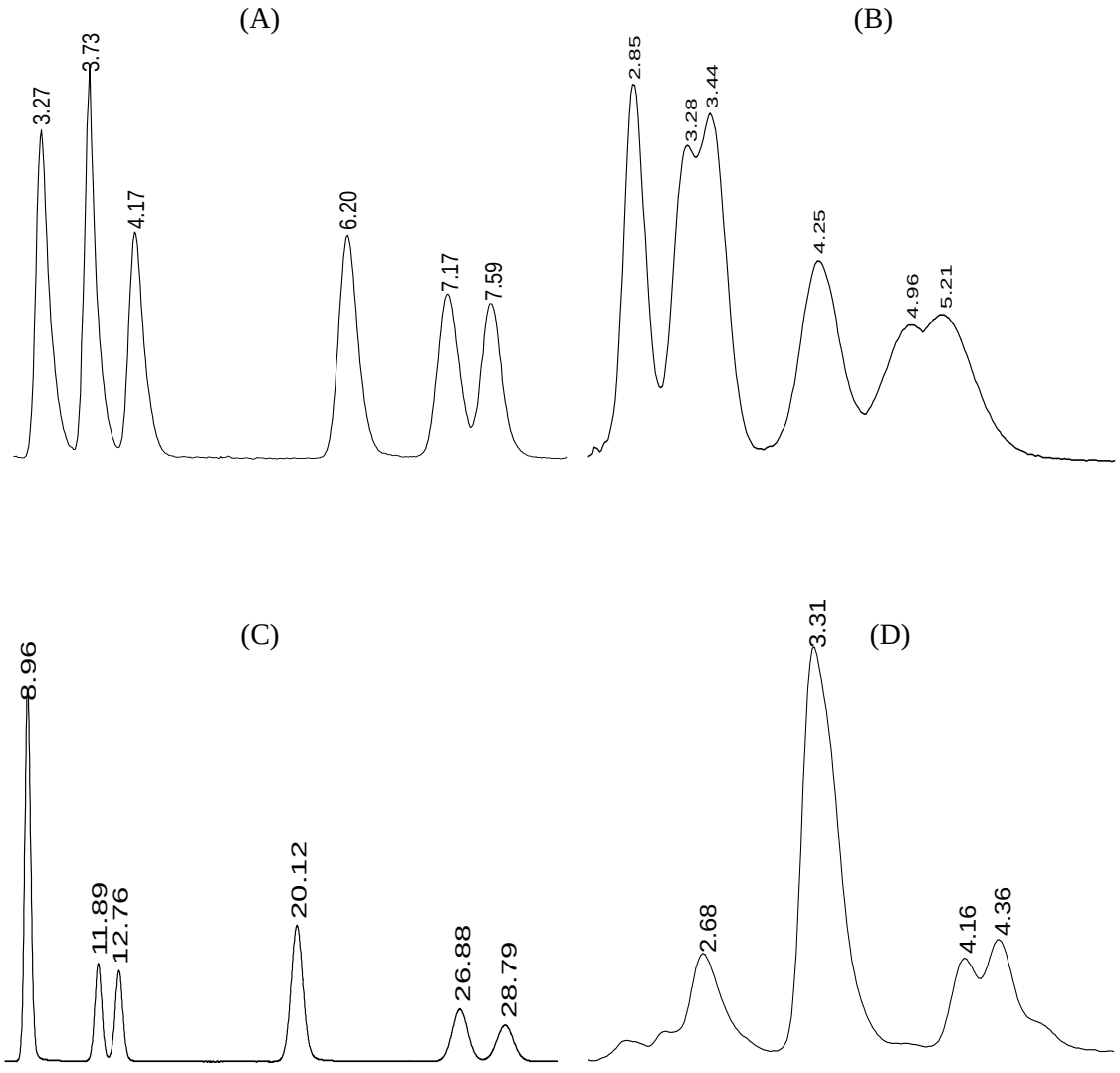

Figure 4.5. Chromatograms of the vanillin test mixture. Elution order was vanillic acid, isovanillin, vanillin, o-vanillin, coumarin, and ethylvanillin. A) methanol-water mobile phase (30% methanol in water with 0.2% acetic acid) that yielded the best separation on the BDS C_8 column at ambient temperature. B) methanol-water mobile phase (2.5% methanol in water with 0.2% acetic acid) that yielded the best separation on the BDS cyanopropyl bonded phase column at ambient temperature. C) butanol-water mobile phase (0.75% butanol in water with 0.2% acetic acid) that yielded the best separation on the BDS C_8 column at ambient temperature. D) butanol water mobile phase (2.5% butanol in water with 0.2% acetic acid) that yielded the best separation on the BDS cyanopropyl column at ambient temperature.

To better understand the reasons for homeoenergetic retention behavior as opposed to homoenergetic retention behavior, Log-Log plots of retention were generated for methanol-water and butanol-water mobile phases without acetic acid. Vanillic acid was excluded as it coeluted with the dead marker when acetic acid is not present in the mobile phase. Log-Log plots are shown for methanol-water in Figure 4.8 and are shown for butanol-water in Figure 4.9. The slopes of the regression lines for butanol-water are comparable to methanol-water. Furthermore, the slopes of the regression lines for methanol-water mobile phases with and without acetic acid are comparable. From the four sets of Log-Log plots generated, pH has a greater effect on retention with butanol-water mobile phases. This suggests that pH will have a greater impact on the separation of the vanillin test mixture when butanol is used as the organic mobile phase modifier.

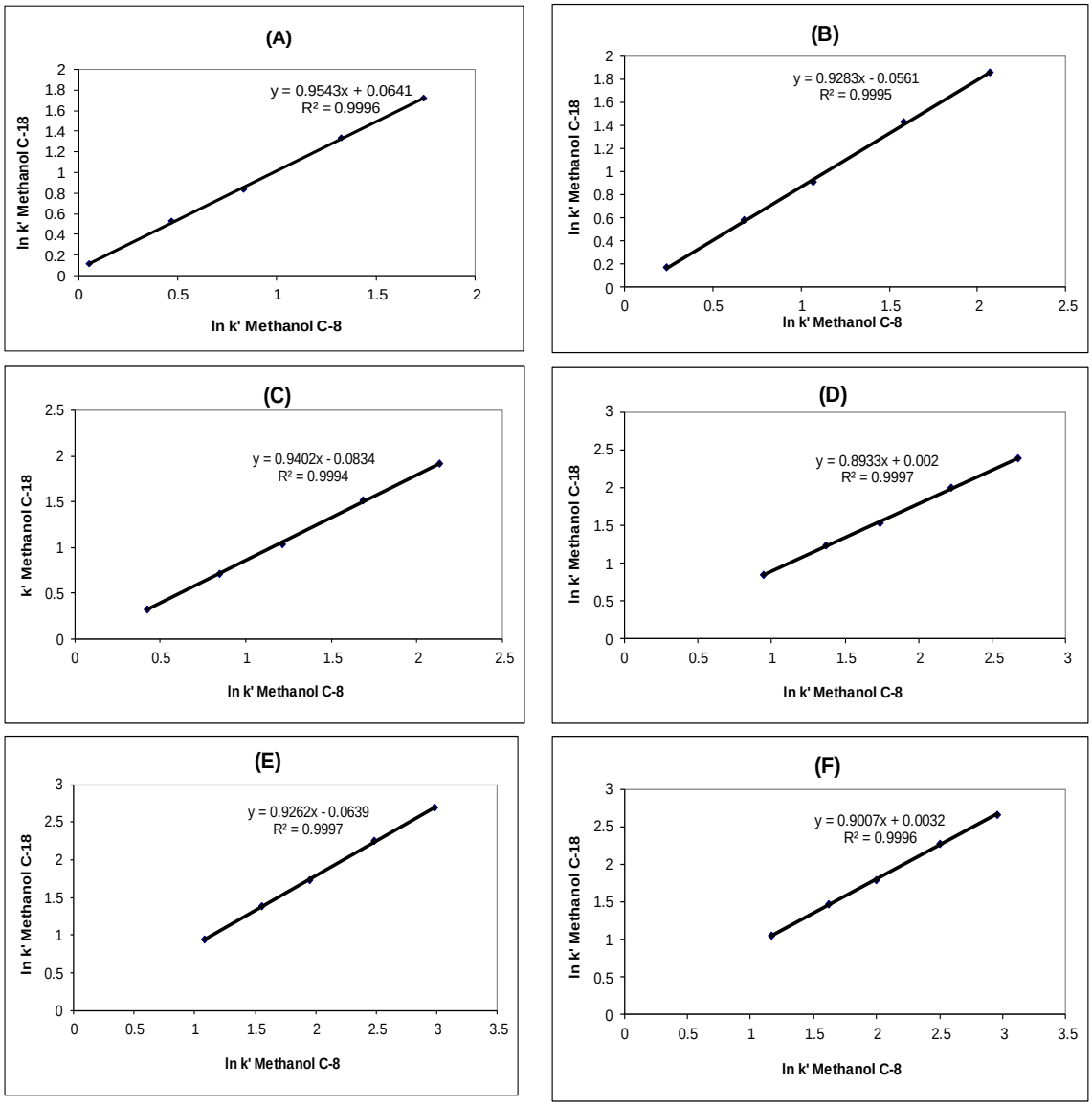

Figure 4.6. Log-Log plots for the vanillin test mixture compounds using methanol in water with 0.2% acetic acid as the mobile phase for A) vanillic acid, B) isovanillin, C) vanillin, D) o-vanillin, E) ethylvanillin, F) coumarin.

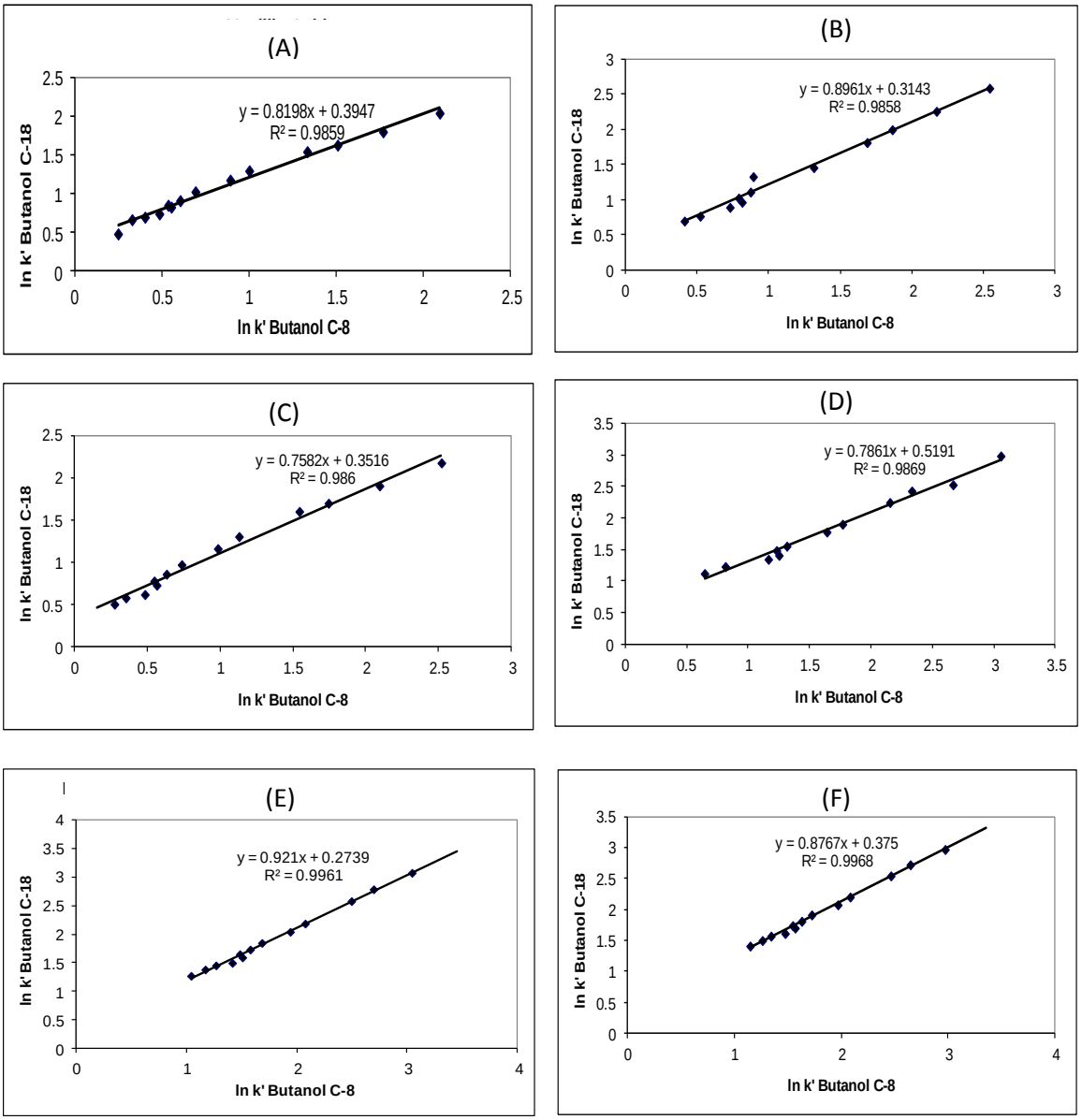

Figure 4.7. Log-Log plots for the vanillin test mixture compounds using butanol in water with 0.2% acetic acid as the mobile phase for A) vanillic acid, B) isovanillin, C) vanillin, D) o-vanillin, E) ethylvanillin, F) coumarin.

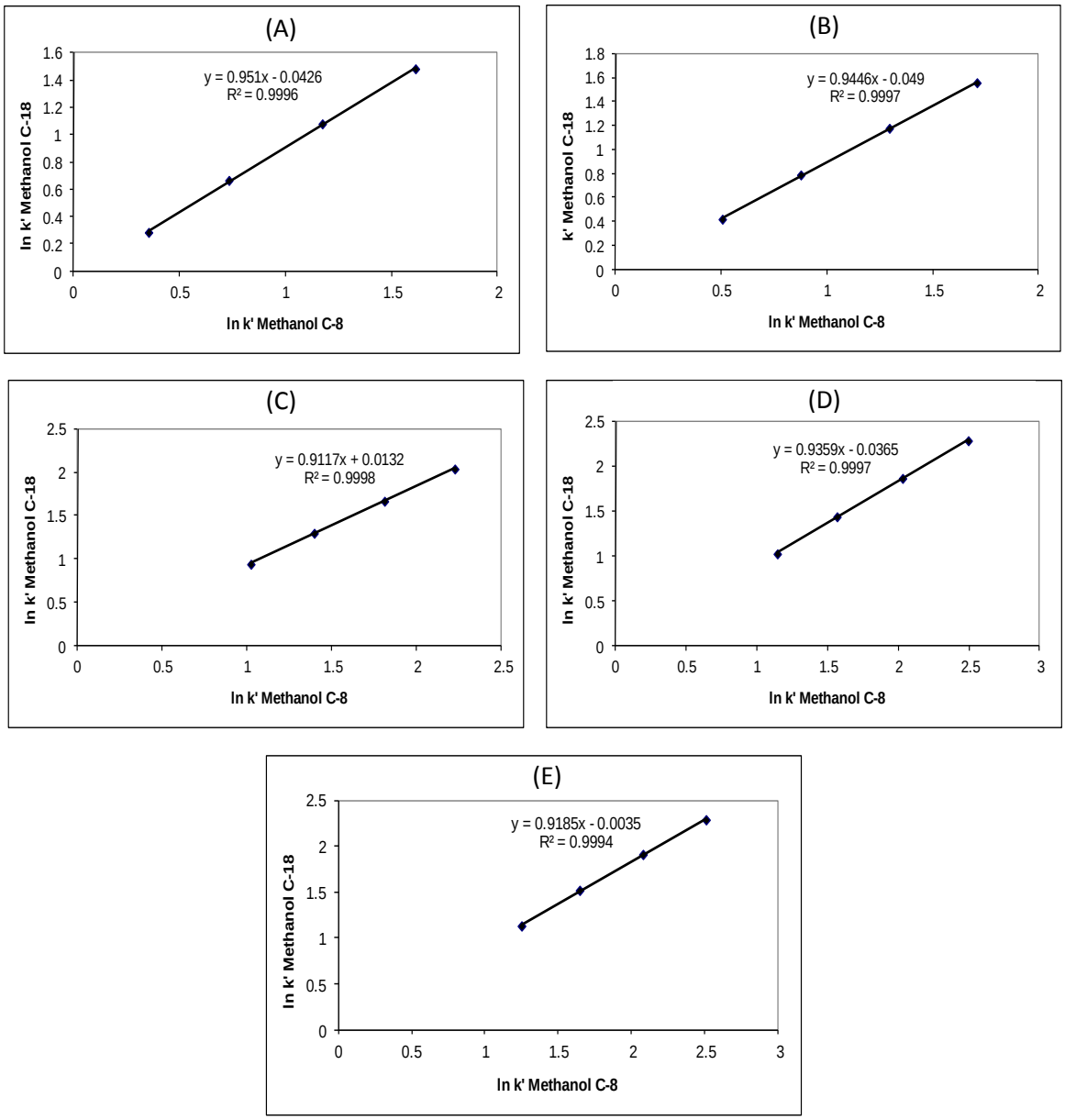

Figure 4.8. Log-Log plots for the vanillin test mixture compounds using methanol in water without acetic acid as the mobile phase for A) isovanillin, B) vanillin, C) o-vanillin, D) ethylvanillin, E) coumarin.

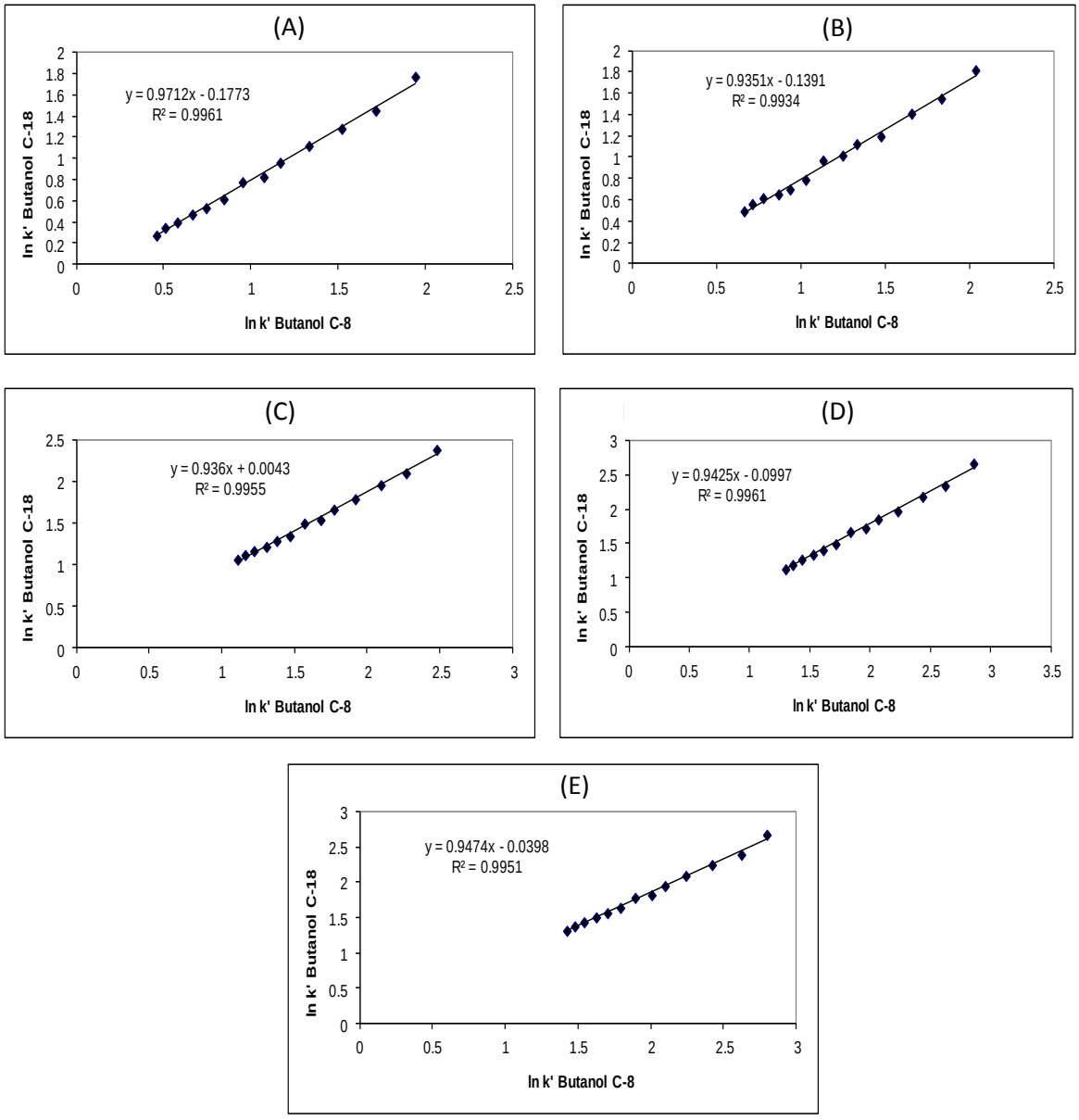

Figure 4.9. Log-Log plots for the vanillin test mixture compounds using butanol in water without acetic acid as the mobile phase for A) isovanillin, B) vanillin, C) o-vanillin, D) ethylvanillin, E) coumarin.

4.3.3 Controlling Selectivity through pH

Figure 10a shows a chromatogram of the vanillin test mixture using the butanol in water mobile phase without acetic acid (2.75% butanol in water) that yielded the best separation of the vanillin test mixture on the BDS C_{18} column. Figure 4.10b shows a chromatogram of the same test mixture using the butanol- water mobile phase (3.75% butanol in water) without acetic acid that yielded the best separation on the BDS C_8 column. A comparable but faster separation of the vanillin test mixture compounds was achieved using butanol-water mobile phases when acetic acid was not present in the mobile phase. Because vanillic acid coelutes with the dead marker when acetic acid is not present in the mobile phase, the adjustment of pH in the butanol-water mobile phase is crucial to ensure that vanillic acid does not coelute with the dead marker while ensuring adequate (baseline) resolution for all components. By judiciously controlling the pH of the mobile phase, the separation of vanillic acid, isovanillin, and vanillin in the test mixture can be tuned by controlling the retention time of vanillic acid through deprotonation of its carboxylic acid group and the retention of vanillin and isovanillin through its interactions with unreacted silanol groups. This will allow for the use of mobile phases with higher concentrations of butanol resulting in faster separations.

Figure 4.11 shows the separation of the vanillin test mixture on the BDS C_{18} column using 2.75% butanol in water mobile phases at pH 2.92 (0.2% acetic acid), pH 3.57, pH 4.07, and pH 6 (no acetic acid), and Figure 4.12 shows the separation of the same test mixture using the same mobile phases on the BDS C_8 column. Figures 4.13 and 4.14 show the separation of the same test mixture using a 3.75% butanol in water mobile phase at pH 2.92 (0.2% acetic acid), pH 3.57, pH 4.07, and pH 6 (no acetic acid) on the BDS C_{18} and

BDS C_8 columns respectively. The amount of butanol in each of these mobile phases corresponds to the composition of the butanol in water mobile phase without acetic acid that yielded the best separation of the vanillin test mixture on the BDS C_{18} and C_8 alkyl bonded phases. By controlling the pH of the mobile phase in the range of 3.5 to 4.0, problems associated with the co-elution of vanillic acid with the dead marker (which occurs at higher pH) or overlap with isovanillin (which occurs at lower pH) were obviated. Judicious control of pH of the butanol in water mobile phase provided greater benefit for the separation of the vanillin test mixture on C_{18}. For this reason, the 3.75% butanol in water at pH 4.03 on the BDS C_{18} column was used to characterize extract of vanilla in commercial products obtained from super markets in the local area.

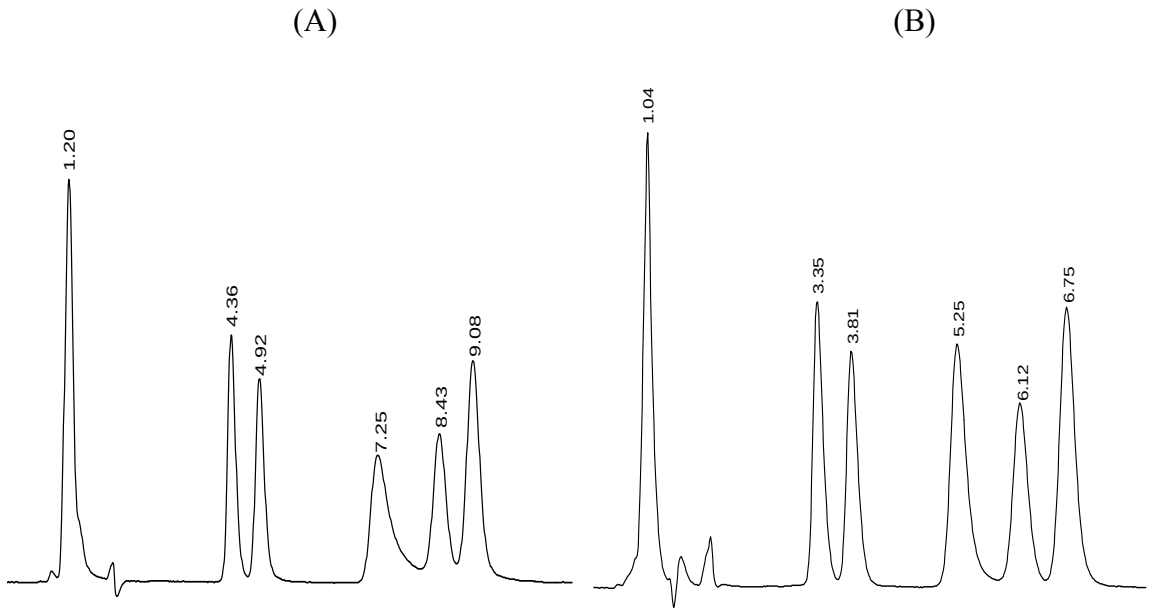

Figure 4.10. Chromatograms of the vanillin test mixture. Elution order was vanillic acid, isovanillin, vanillin, o-vanillin, ethylvanillin and coumarin. a) butanol in water mobile phase without acetic acid (2.75% butanol in water) that yielded the best separation of the vanillin test mixture on the BDS C_{18} column. b) butanol- water mobile phase (3.75% butanol in water) without acetic acid that yielded the best separation on the BDS C_8 column.

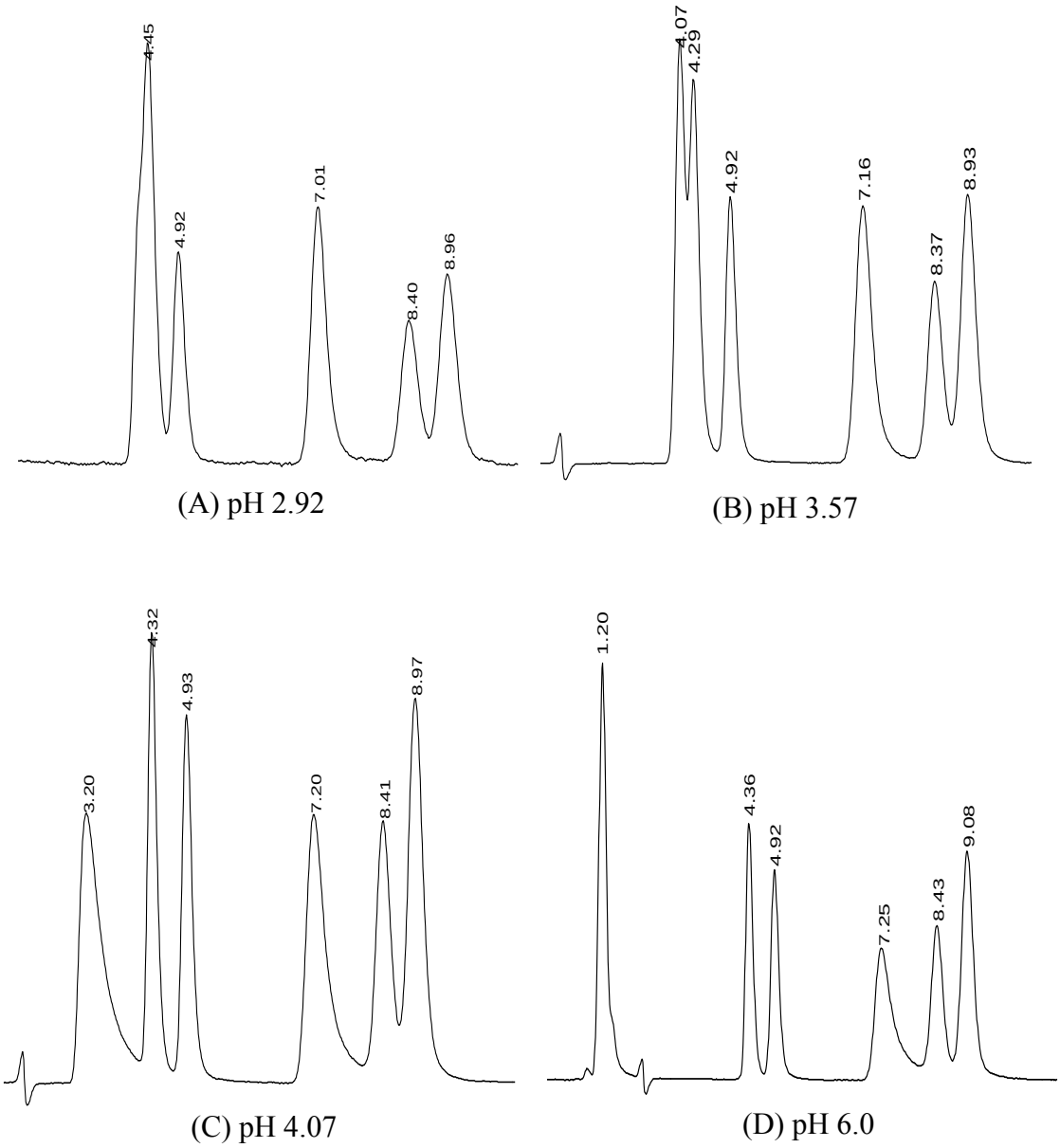

Figure 4.11. Chromatograms of the vanillin test mixture on the BDS C_{18} column using 2.75% butanol in water mobile phases at a) pH 2.92 (0.2% acetic acid), b) pH 3.57, c) pH 4.07, and d) pH 6 (no acetic acid).

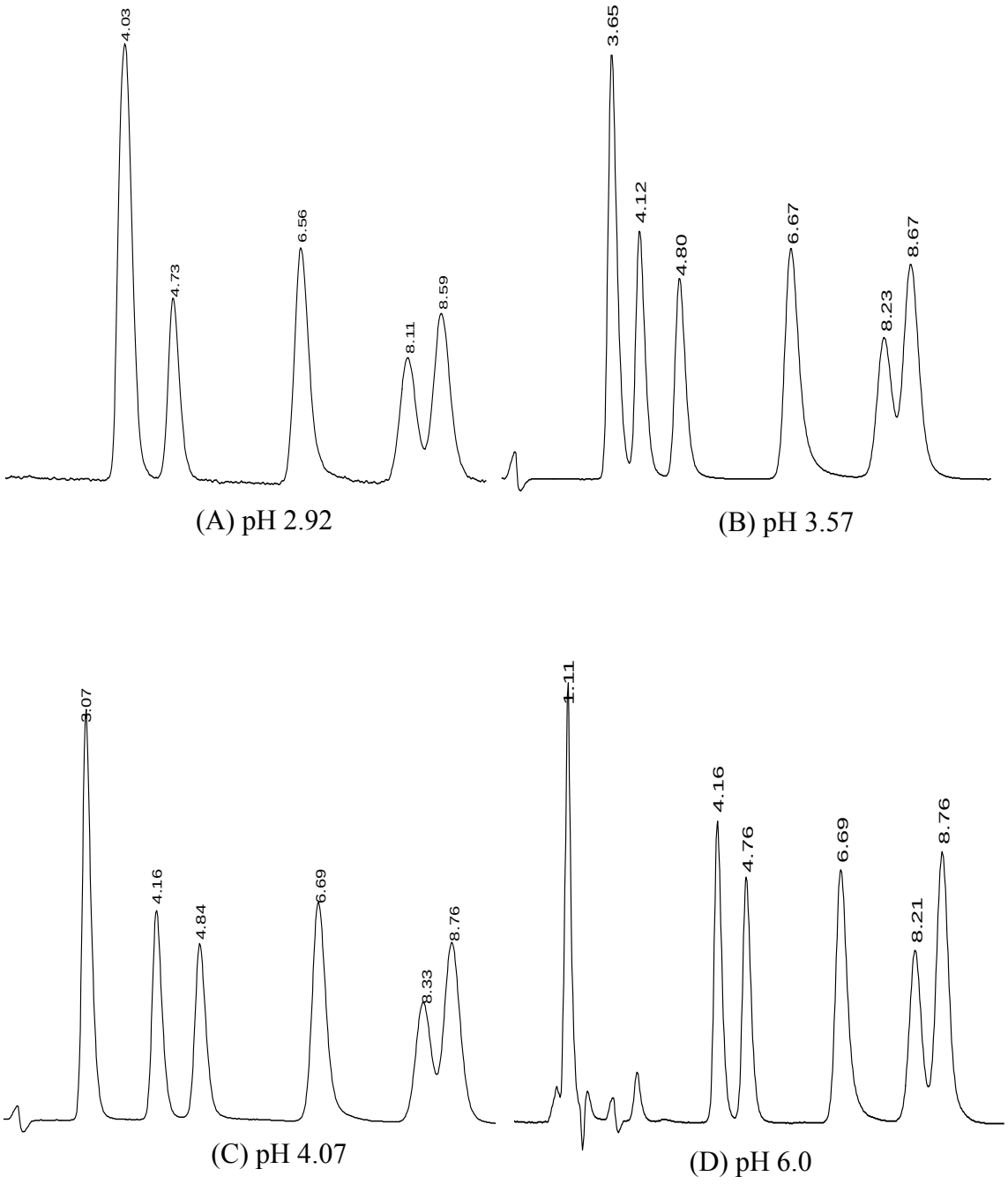

Figure 4.12. Chromatograms of the vanillin test mixture on the BDS C_8 column using 2.75% butanol in water mobile phases at a) pH 2.92 (0.2% acetic acid), b) pH 3.57, c) pH 4.07, and d) pH 6 (no acetic acid).

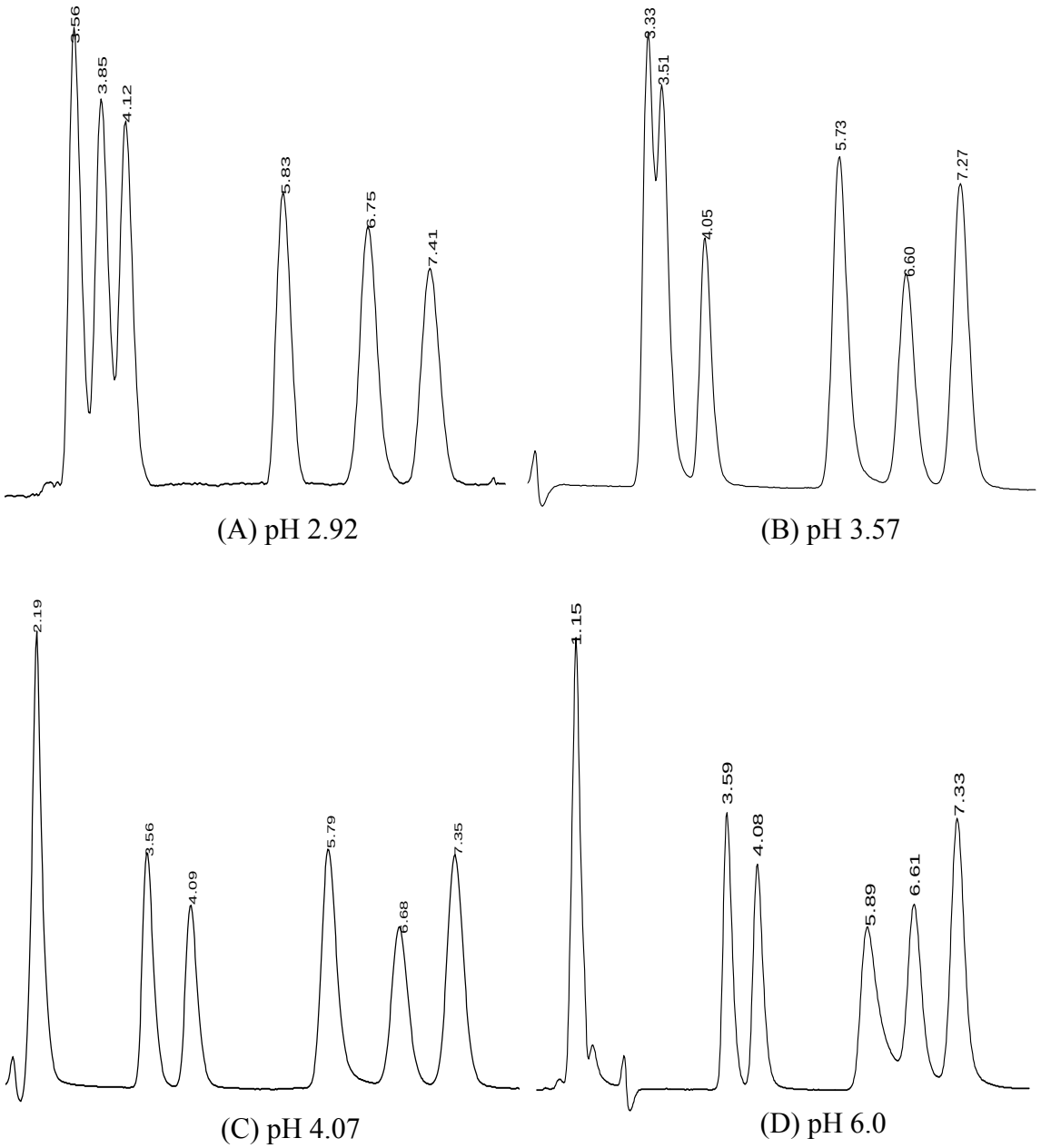

Figure 4.13. Chromatograms of the vanillin test mixture on BDS C_{18} column using 3.75% butanol in water mobile phase at a) pH 2.92 (0.2% acetic acid), b) pH 3.57, c) pH 4.07, and d) pH 6 (no acetic acid).

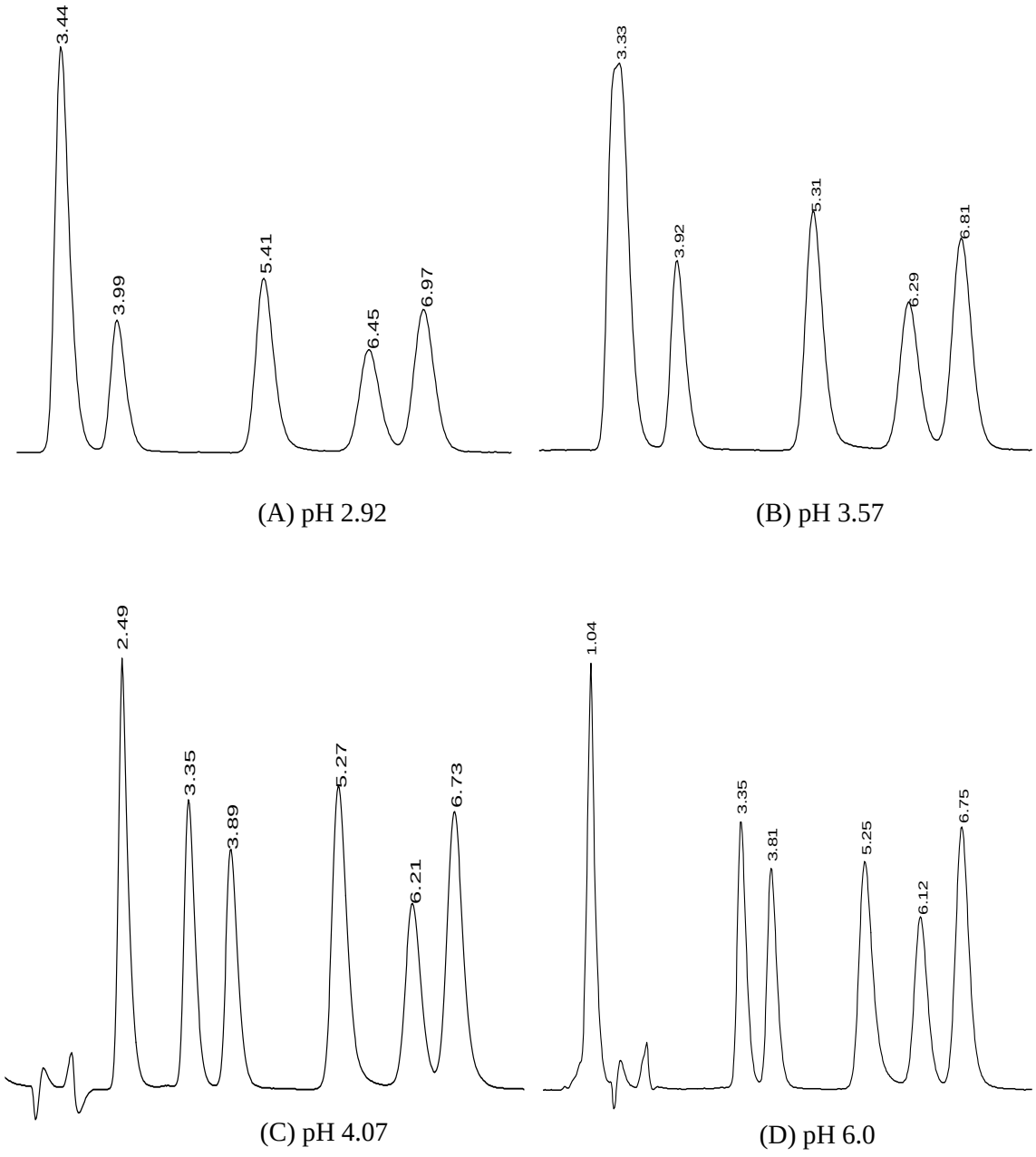

Figure 4.14. Chromatograms of the vanillin test mixture on BDS C_8 column using 3.75% butanol in water mobile phase at a) pH 2.92 (0.2% acetic acid), b) pH 3.57, c) pH 4.07, and d) pH 6 (no acetic acid).

4.3.4 Surveying Products Containing Extract of Vanilla.

Table 4.1 lists 36 commercial products (both foreign and domestic brands) containing extract of vanilla that were analyzed using the RPLC method developed as part of this study. Vanillic acid, vanillin, ethyl vanillin and coumarin were found to be present in some or all of these brands. As coumarin has been shown to cause hepatoxicity in animals, this result is of importance to the general public. The presence of vanillic acid in some of these products can be attributed to oxidation of vanillin suggesting problems with the initial formulation, the shelf life of the product or some combination of the two.

Figure 4.15 shows a principal component (PC) plot [69] of the 36 commercial products containing extract of vanilla. Each product was represented by 13 unique retention time windows identified based on the shape of the peak and its retention time. Thus, each chromatogram for PCA was represented as a data vector, $x = (x_1, x_2, x_3, \ldots x_{13})$ where each vector component was the peak area of one of the 13 peaks. Five products appeared as outliers in the PC plot: Caravelle (artificial extract), Best Choice (real vanilla extract), Always Save, Singing Dog, and Clover Valley (real vanilla extract). After deleting these five products from the analysis with the remaining 31 samples reanalyzed, four distinct clusters were detected using principal component analysis (see Figure 4.16). Cluster 1 consisted of 12 real extracts of vanilla: Spice Club, Nielsen Massey, Watkins (real extract), Rodelle, McCormick (Real Extract), Great Value (Real Extract), Market Pantry, Simply Organic, Blackbay, Now, Danncy Vainilla, and Archer Farms. Cluster 2 consisted of 9 products: 6 artificial, 2 real and 1 combination of real and artificial vanilla extract. Molina, Griffins, Francelin, Molino, Watkins (artificial extract), Mi Huerta, Adams, Alicante, and McCormick (artificial extract). Cluster 3 consisted of 4 artificial

extracts of vanilla: SAC, Viola, Dr. Oetke, and Aroma Pasta Vaneli, and cluster 4 consisted of 4 artificial and real extracts of vanilla: Clover Valley (artificial extract), Great Value (artificial extract), Mama Lycha (combination of artificial and real extract) and Universal.

Table 4.1. Vanilla Extract Products Analyzed by RPLC

Product	Vanillic Acid	Isovanillin	Vanillin	O-vanillin	Ethylvanillin	Coumarin
Danncy Vainilla	Detected	Not Detected	Detected	Not Detected	Detected	Detected
Molino (Real Extract)	Detected	Not Detected	Detected	Not Detected	Detected	Not Detected
Caravelle (Artificial)	Detected	Not Detected	Detected	Not Detected	Detected	Not Detected
Watkins (Artificial)	Detected	Not Detected	Detected	Not Detected	Detected	Not Detected
Adams (Artificial)	Detected	Not Detected	Detected	Not Detected	Detected	Not Detected
Mi Huerta (Artificial + Real)	Not Detected	Not Detected	Detected	Not Detected	Not Detected	Not Detected
Clover Vally (Artificial)	Detected	Not Detected	Detected	Not Detected	Detected	Not Detected
Great Value (Artificial)	Detected	Not Detected	Detected	Not Detected	Detected	Detected
Griffins (Artificial)	Detected	Not Detected	Detected	Not Detected	Detected	Not Detected
Great Value (Real Extract)	Detected	Not Detected	Detected	Not Detected	Not Detected	Not Detected
Best Choice (Real Extract)	Not Detected	Not Detected	Detected	Not Detected	Not Detected	Not Detected
Mc Cormick (Real Extract)	Detected	Not Detected	Detected	Not Detected	Not Detected	Not Detected
Rodelle (Real Extract)	Detected	Not Detected	Detected	Not Detected	Not Detected	Not Detected
SAC	Detected	Not Detected	Detected	Not Detected	Not Detected	Detected
Watkins (Real Extract)	Detected	Not Detected	Detected	Not Detected	Not Detected	Not Detected
Always Save (Artificial)	Not Detected	Not Detected	Detected	Not Detected	Detected	Not Detected
Molina (Real Extract)	Detected	Not Detected	Detected	Not Detected	Detected	Not Detected
Viola	Detected	Not Detected	Detected	Not Detected	Detected	Not Detected
Archer Farms (Real Extract)	Detected	Not Detected	Detected	Not Detected	Detected	Not Detected

Black Bay Real	Detected	Not Detected	Detected	Not Detected	Not Detected	Not Detected
Mama Lycha (Artificial)+ (Real Extract)	Not Detected	Not Detected	Detected	Not Detected	Detected	Not Detected
Alicante (Artificial)	Not Detected	Not Detected	Detected	Not Detected	Detected	Not Detected
Francelin	Not Detected	Not Detected	Detected	Not Detected	Detected	Not Detected
Universal (Real Extract)	Not Detected	Not Detected	Detected	Not Detected	Detected	Not Detected
Dr Oetke	Not Detected	Not Detected	Detected	Not Detected	Detected	Not Detected
Nielsen Massy	Detected	Not Detected	Detected	Not Detected	Not Detected	Not Detected
Singing Dog (Real Extract)	Not Detected	Not Detected	Detected	Not Detected	Not Detected	Not Detected
Spice Club (Real Extract)	Detected	Not Detected	Detected	Not Detected	Detected	Not Detected
Simply Organic (Real Extract)	Detected	Not Detected	Detected	Not Detected	Not Detected	Not Detected
Clover Vally (Real Extract)	Not Detected	Not Detected	Detected	Not Detected	Not Detected	Not Detected
Market Pantry (Real Extract)	Detected	Not Detected	Detected	Not Detected	Detected	Not Detected
Aroma Pasta Vaneli	Detected	Not Detected	Detected	Not Detected	Detected	Detected
Frontier (Real Extract)	Not Detected	Not Detected	Detected	Not Detected	Detected	Not Detected
Griffins Fake	Detected	Not Detected	Detected	Not Detected	Detected	Not Detected
Now (Real Extract)	Detected	Not Detected	Not Detected	Not Detected	Detected	Not Detected
McCormick (Artificial)	Not Detected	Not Detected	Detected	Not Detected	Not Detected	Not Detected

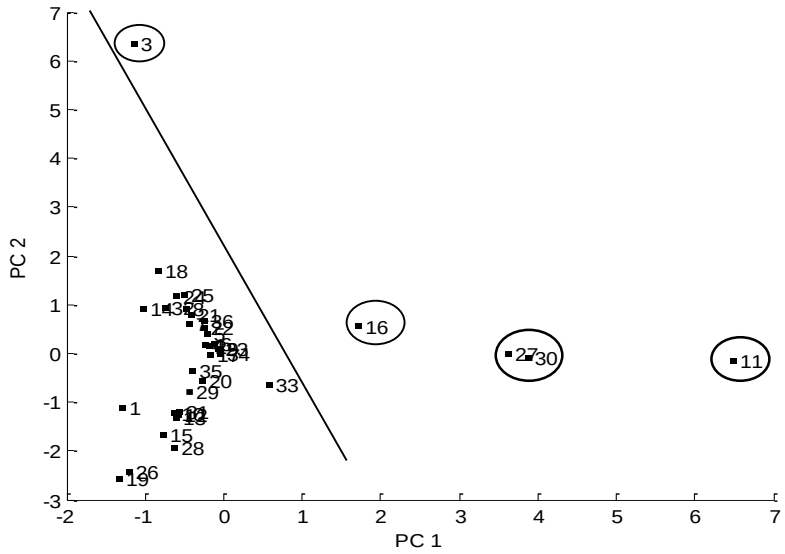

Figure 4.15. PC plot of the 36 extract of vanilla products. Each product was represented by 13 unique retention time windows identified based on the shape of the peak and its retention time. Outliers are circled.

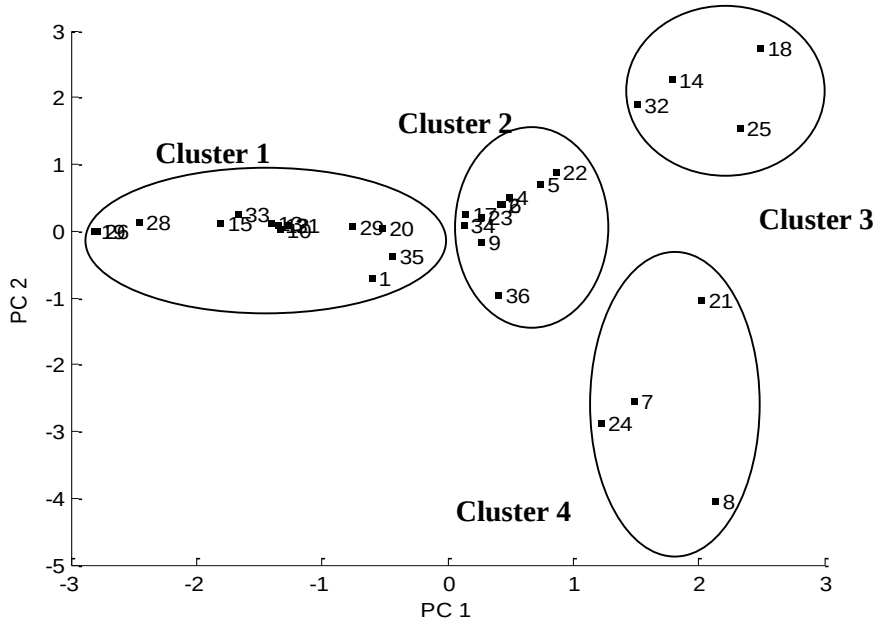

Figure 4.16. PC plot of the 31 products (with 5 outliers removed). Four distinct clusters of points are evident in the PC plot.

Chromatograms representative of each cluster are shown in Figure 4.17. The chromatograms of the so-called outliers are shown in Figure 4.18. Evidently, there is more than one class of real vanilla extract using chemical constitution as the variable to differentiate between extracts. Furthermore, several products containing artificial vanillin extract have chromatographic profiles similar to those of real vanilla extract. As for the so-called outliers, there was no pattern evident in the data as 3 were real vanilla extracts and 2 were artificial vanilla extracts.

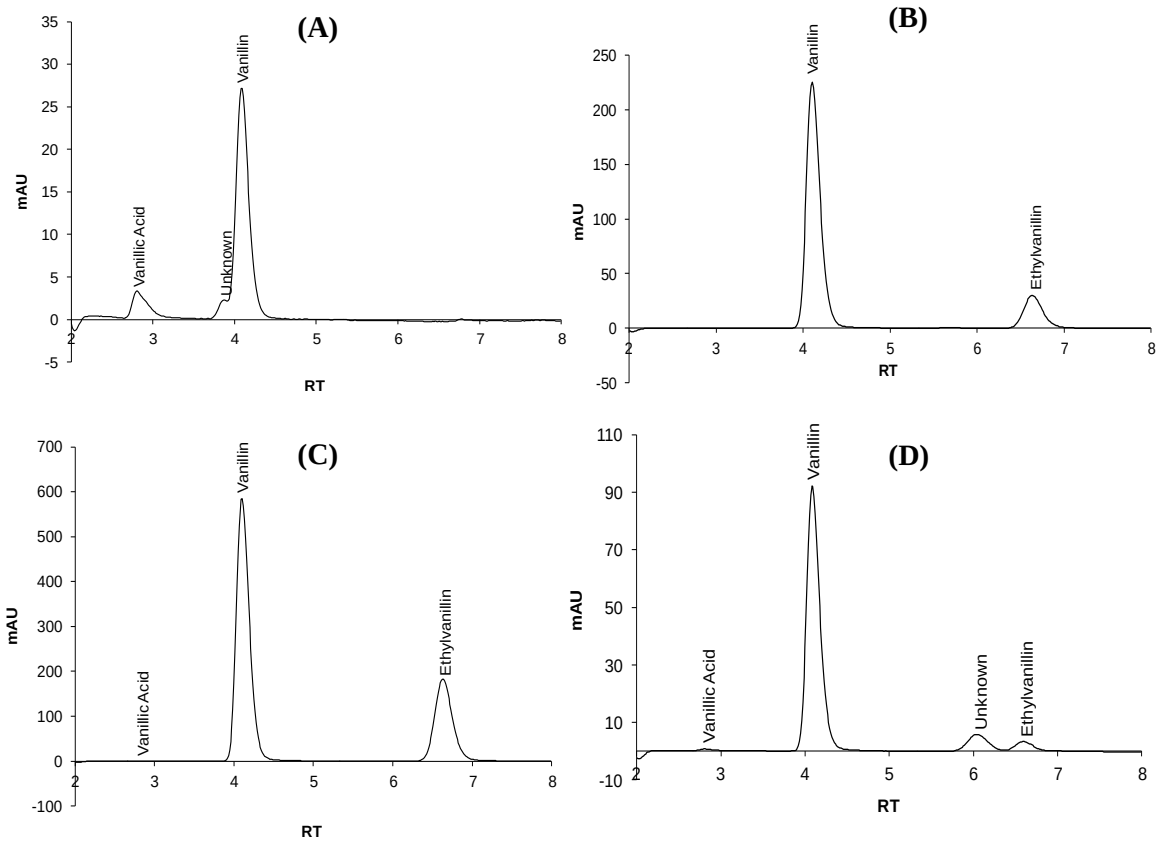

Figure 4.17. Chromatograms of the clusters A) cluster 1, B) cluster 2, C) cluster 3, D) cluster 4, detected by principal component analysis

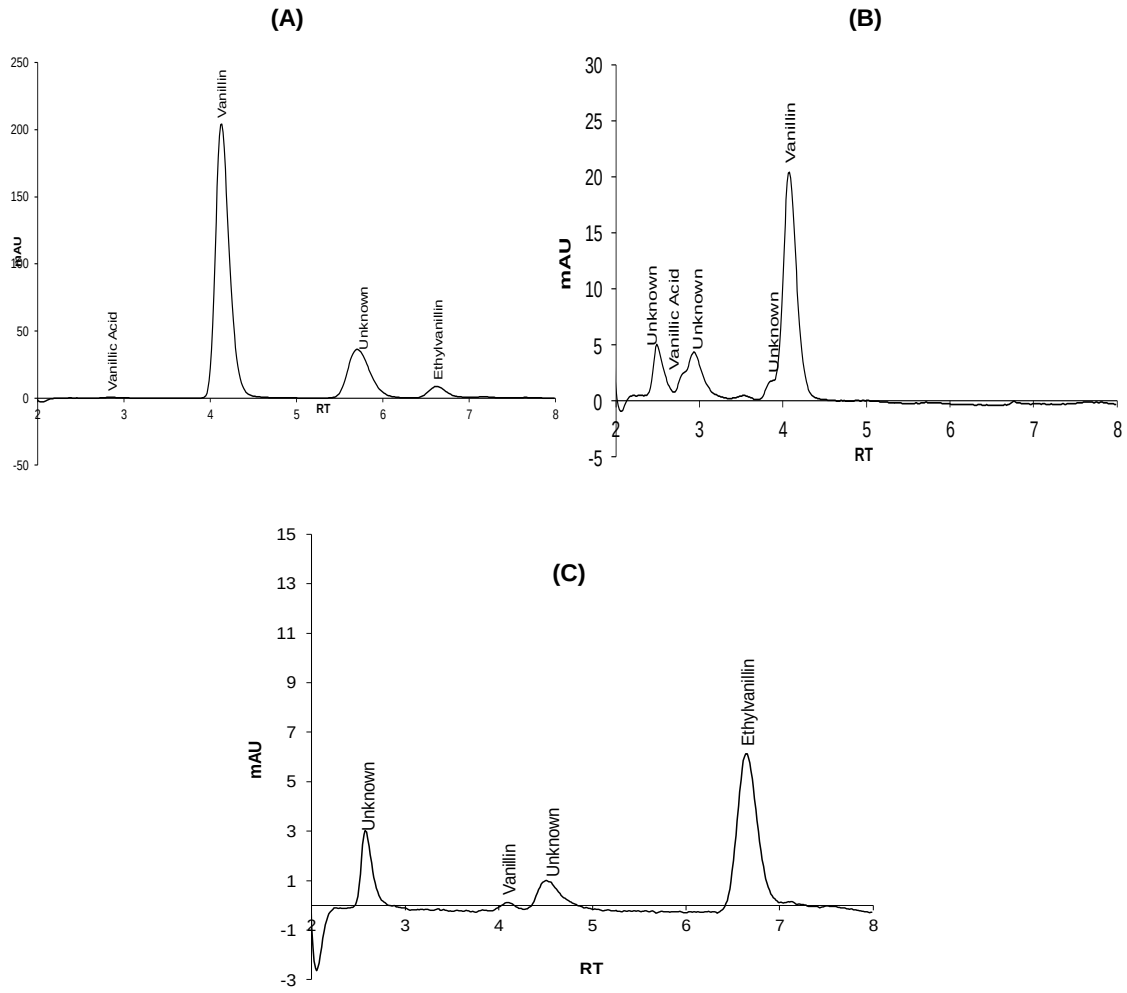

Figure 4.18. Chromatograms of the outliers detected by principal component analysis. A) Caravelle (artificial extract), B) Singing Dog real extract, Clover Valley real extract and Best Choice real extract, C) Always Save artificial extract

Several compounds not part of the original vanillin test mixture and consequently designated as unknown in the vanilla extract chromatograms obtained using the Varian Prostar HPLC were identified by LC/MS. The results of the LC/MS study are summarized in Table 4.2. All reported compounds are consistent with the reported molecular weights,

retention times, and the observed isotope patterns. The compounds listed in this table had not been previously reported as constituents of extract of vanilla. However, they had been reported at parts per million levels in vanilla beans [70]. In all likelihood, the detection of these compounds in vanilla extract is linked to the use of water rich mobile phases, which yielded better separations for these water soluble compounds.

Table 4.2. LC/MS Analysis of Unknown Chromatographic Peaks

Product	**Acetovanillone**	**Anisyl formate**	**p-hydroxy-benzaldehyde**	**2-phenylethanol**	**Glucose**
Caravelle	Detected	Detected	Not detected	Not detected	Detected
Danncy Vainilla	Not detected	Not detected	Detected	Detected	Detected
Great Value (Artificial)	Not detected	Not detected	Detected	Detected	Not detected
Universal Real Extract	Not detected	Not detected	Detected	Detected	Detected
Singing Dog (Real Extract)	Not detected	Not detected	Detected	Detected	Detected
Watkins (Real Extract)	Not detected	Not detected	Detected	Detected	Detected
Adams Double Strength	Not detected	Not detected	Not detected	Not detected	Detected

References

55. L. S. de Jager, G. A. Perfetti and G. W. Diachenko, Determination of coumarin, vanillin, and ethyl vanillin in vanilla extract products: liquid chromatography/mass spectrometry method development, J. Chromatogr. A. 1145 (2007) 83-88.

56. A. K. Sinha, S. C. Verma, and U. K. Sharma, Development and validation of an RP-HPLC method for quantitative determination of vanillin and related phenolic compounds in vanilla planifolia, J. Sep. Sci., 30 (2007) 15-20.

57. A. M. van Nederkassel, C. J. Xu, P. Lancelin, M. Sarraf, D. A. MacKenzie, N. J. Walton, F. Bensaid, M. Lees, G. J. Martin, J. R. Desmurs, and D. L. Massart, Chemometric treatment of vanillin fingerprint chromatograms – Effect of different signal alignments on principal component analysis plots, J. Chromatogr. A, 1120 (2006) 291-298.

58. G. Lamprecht, F. Pichlmayer, and E. R. Schmid, Determination of the authenticity of vanilla extracts by stable isotope ratio analysis and component analysis by HPLC, J. Agric. Food Chem., 42 (1994) 1722-1727.

59. B. K. Lavine, J. P. Ritter, and S. Peterson, Enhancement of selectivity in reversed-phase liquid chromatography, J. Chromatog. A., **946** (2002) 83-90.

60. K. Valko, L. R. Snyder, and J. L. Glajch, Retention in reversed phase liquid chromatography as a function of mobile phase composition, J. Chromatogr., **656**, (1993) 501-511.

61. N. Chen, Y. K. Zhang, and P. C. Lu, Effect of molecular structure on the log k_w index and linear S-logk_w correlation in reversed phase liquid chromatography, J. Chromatogr., **633** (1993) 31-38.

62. J. Dolan, L. R. Snyder, R. G. Wolcott, P. Haber, T. Baczek, and R. Kaliszan, Reversed phase liquid chromatographic separation of complex samples by optimizing temperature and gradient time, J. Chromatogr. A. **857** (1999) 41-68.

63. R. P. W. Scott, and C. F. Simpson, Solute-solvent interactions on the surface of reversed phases, Faraday Symp. Chem. Soc., 15 (1980) 69-82.

64. A. Tchapla, H. Colin, and G. Guiochon, Linearity of homologous series of retention plots in reversed phase liquid chromatography, Anal. Chem., **56**, (1984) 621-626

65. M. M. Hseih and J. G. Dorsey, Accurate determination of log k_w in reversed phase liquid chromatography – implications for quantitative structure-activity retention relationships, J. Chromatogr.A 631 (1993) 63-78.

66. P. J. Schoenmakers, H. A. H. Billiet, R. Tussen, and L. DeGalan, Description of solute retention over the full range of mobile phase compositions in reversed phase liquid chromatography, J. Chromatogr., **282**, (1983) 107-115.

67. P. J. Schoenmakers, H. A. H. Billiet, R. Tussen, and L. DeGalan, Gradient selection in Reversed phase liquid chromatography, J. Chromatogr., **149** (1978) 519-528.

68. W. T. Cooper and L.-Y. Lin, Effect of stationary phase polarity on retention in reversed phase liquid chromatography, Chromatographia, 21 (1986) 335-341.

69. J. E. Jackson, A User's Guide to Principal Component Analysis, Wiley Interscience, NY 1991.

70. A. Perez-Silva, E. Odoux, P. Brat, F. Ribeyre, G. Rodriguez-Jumenes, V. Robles-Olvera, M. A. Garcia-Alvarado, and Z. Gunata, GC-MS and GC-olfactometry analysis of aroma components in a representative organic aroma extract from cured vanilla beans, Food Chem., 99 (2006) 728-735.

CHAPTER V

SIMULATION OF ATTENUATED TOTAL REFLECTION INFRARED SPECTRA OF AUTOMOTIVE CLEAR COATS

5.1 Introduction

Automotive vehicles can be identified from paint fragments transferred onto another vehicle or onto the clothing of a pedestrian involved in a hit-and-run accident by comparing the color, layer sequence, and chemical composition of each individual layer of the automotive paint [71, 72]. To make these comparisons possible, the Royal Canadian Mounted Police (RCMP) have developed a comprehensive database for forensic automotive paint analysis known as the paint data query (PDQ) database. PDQ is a database that contains the complete color, the chemical composition and the infrared (IR) spectrum of each layer of the original manufacturer's automotive paint system. If the original automotive paint system is present in the recovered paint fragment, PDQ can assist in identifying both the make and model of the automotive vehicle within a limited production year range. Currently, PDQ contains 21,000 samples (street samples and factory panels) corresponding to over 84,000 individual paint layers representing the paint systems used in most domestic and foreign vehicles marketed in North America. Each year over 500 samples are painstakingly collected, analyzed and added to the PDQ database by the RCMP.

To use PDQ, the forensic chemist must translate the topcoat color and the chemical composition of each automotive paint layer based on the IR spectrum of each layer into specific text codes. The text based search and retrieval system of PDQ searches the database, comparing all records for make, model and year having a paint system similar to the coded information provided by the user. The final step in the process is to confirm these hits manually (as direct searching of IR spectra in PDQ does not exist) by comparing the IR spectrum of each unknown paint layer against IR spectra in the database hit list. Topcoat color is compared to topcoat color charts to narrow down this hit-list to those manufacturers known to have used a similar topcoat color in those samples identified by the database search.

A major problem with the PDQ database is its use of text to code the chemistry of each layer. Searches of the PDQ database require the user to code their FTIR spectrum according to the guidelines set out by the database, and to search these codes against the codes in the database. The coding used in PDQ is generic, and can lead to non-specific search criteria which results in a large number of spurious hits that a scientist must then work through and eliminate. This impairs the accuracy of a search. For example, modern automotive clear coats in PDQ have one of only two possible formulations: acrylic melamine styrene or acrylic melamine styrene polyurethane. Furthermore, modern automotive paints contain a thin color coat and on a microscopic fragment it may be too thin to obtain accurate chemical information. The small size of the fragment makes it difficult to accurately compare it against manufacturer's paint color standards. Most forensic laboratories rely on PPG or DuPont color refinish books for making color comparisons on paint chips recovered from crime scenes. The color represented in these

books is intended for use by the refinish/auto body industry and are accurate on a macroscopic scale. While the color can be viewed microscopically, such as under a sterero-microscope, details such as effect flake size and distribution are not accurately reproduced and do alter the appearance of the color somewhat on a microscopic scale. The accuracy of such comparisons diminishes with the size of the paint chip recovered from the crime scene. In cases where the automotive paint sample is limited to the clear coat paint layer which all too often occurs as modern automotive paints use thinner undercoat and color coat layers protected by a thicker clear coat layer, the text based portion of PDQ cannot identify the automotive vehicle because modern clear coats in PDQ are coded as either acrylic melamine styrene or acrylic melamine styrene polyurethane.

Another problem with PDQ stems from modern forensic laboratories using attenuated total reflection (ATR) spectroscopy for infrared analysis of automotive paints. Although ATR is a widely used sampling technique in infrared (IR) spectroscopy because minimal sample preparation is required, the IR spectrum of an automotive paint sample obtained by ATR exhibits distortions. Specifically, band broadening and lower relative intensities and skewed peaks at higher wavenumbers occur when compared with its transmission counterpart. This hinders library searching as all PDQ library spectra are measured in transmission mode.

In the study described in this chapter, IR search prefilters were developed from IR transmission spectra in the PDQ library that were transformed into ATR spectra using the ATR simulation algorithm (described in Chapter 2) for the purpose of identifying the assembly plant of the vehicle involved in a hit-and-run accident from an ATR spectrum of its clear coat paint smear. 456 transmission spectra from the PDQ library spanning 22 GM

assembly plants were converted into ATR spectra using the simulation algorithm. The spectral region used to formulate these search prefilters was the fingerprint region (1500 cm^{-1} to 600 cm^{-1}). In this study, both simulated and experimental ATR spectra were preprocessed using the discrete wavelet transform, which increased the signal to noise of both the real and simulated data by concentrating the signal in specific wavelet coefficients. Using a genetic algorithm (GA) for pattern recognition, wavelet coefficients characteristic of the assembly plant of the vehicle were identified. Even in challenging trials where the paint samples evaluated were all from the same manufacturer (General Motors) within a limited production year range (2000-2006), the respective assembly plant of the vehicle was correctly identified. Search prefilters to identify assembly plants were successfully validated using 14 samples provided by the RCMP as part of a study to populate PDQ to current production years.

5.2 Materials and Methods

PDQ IR spectra of 456 clear coats applied to the metal surfaces of automobiles and trucks assembled at 22 General Motors (GM) assembly plants within the limited production year range of 2000 - 2006 were measured on four different spectrometers: two Thermo-Nicolet 6700s FTIR spectrometers, one BioRad 40A and one BioRad 60 FTIR spectrometer. All four spectrometers were equipped with DTGS detectors and all samples were measured in transmission mode using high pressure diamond anvil cells. For the two BioRad instruments, Harrick 4x beam condensers were used, whereas a Harrick 6x beam condenser was used in each Thermo-Nicolet 6700s instrument.

Data preprocessing was crucial in the development of the search prefilters. In this study, data preprocessing consisted of aligning the IR spectra along the wavelength axis, converting the transmission spectra into ATR spectra, applying the discrete wavelet transform to resolve overlapping spectral bands in ATR spectra, and variable selection to identify informative wavelet coefficients using a genetic algorithm for feature selection and classification. Each step is described in detail below.

5.2.1 Wavelength Alignment.

Transmission spectra of the 456 clear coats from the PDQ database were not properly aligned by wavelength as these spectra were collected on four different spectrometers from two different vendors (Nicolet and Bio-Rad) manufactured in different years. To remedy this problem, we renormalized the x-axis of each interferogram to the helium neon laser frequency of 15798.0 cm^{-1} using OMNIC. Renormalizing the interferograms in this manner ensured that all data points occur at the same frequency positions allowing data from different spectrometers to be combined without the problems associated with inconsistent point spacing. For the measured absorbance to be very nearly equal to the true absorbance, all interferograms were multiplied by the Norton-Beer medium apodization function before application of the Fourier transform.

5.2.2. ATR Simulations

A program to implement the ATR simulation algorithm described in Chapter 2 was developed using Matlab (MathWorks, Nautick, MA U.S.A.) Since the double Fourier transform technique was used to implement Equation 2, the spectral data size was adjusted to 2^n points in excess of the original data length (analogous to zero filling) to the lower

and higher frequency sides. In these calculations, the thickness of the paint sample is required. IR spectra in the PDQ library were collected using thin microtomed films of the surface materials of the individual paint layers compressed between diamond-windows at 40 psi with the film thickness estimated to be below 10 micrometers thick. To estimate the film thickness, 10 transmission spectra were selected from the PDQ library, and ATR spectra of these same samples were measured using the built-in diamond single-reflection ATR accessory of the Nicolet iS50 FTIR spectrometer and compared with calculated ATR spectra for these samples using a sample thickness varying from 3 to 10 micrometers in 1 micrometer increments. In all cases, the best match in both ordinate intensities and peak positions was observed when the sample thickness was between 4 and 5 micrometers. For this reason, a thickness of 4.5 micrometers for the sample film was used throughout these simulations.

In these simulation studies, ATR analysis was limited to the clear coat paint layer. Because the penetration depth of an ATR analysis is shallow and is considerably less than the thickness of an automotive clear coat, this layer can be preferentially analyzed directly on intact paint chips with little or no sample preparation. Use of an ATR objective on an infrared microscope is also the method of choice for the analysis of very thin automotive paint smears. Such smears may consist primarily of the clear coat paint layer transferred onto the impacted vehicle or other object such as a pedestrian. The Forensic Laboratory of the Royal Canadian Mounted Police who utilize high pressure diamond cells to acquire transmission IR spectra of automotive paint layers for the PDQ database have estimated that the thickness of the clear coat layer, once it is pressed between the two diamonds, as 5 micrometers.

For the Matlab program, it was also necessary to provide the incident angle of the ATR accessory in the equations used to compute the ATR spectrum. The incident angle of the iS50 ATR accessory was estimated using a simulation. As explained above, it is possible to simulate ATR spectrum when the optical constants of the sample (e.g., refractive index) are known. We have selected the optical constants of toluene published by Jones and coworkers [3]. The best match for the ATR spectrum of toluene measured on the iS50 built-in ATR accessory at $1cm^{-1}$ spectral resolution was determined when the incident angle was changed from 43^0 to 50^0. For medium strength (~0.53 Abs.) absorption such as the absorption band at 463 cm^{-1}, the best match in intensity was achieved using an incident angle of 47^0, while for the strong band (~0.96 Abs.) at 725 cm^{-1}, 49^0 gave the best match in intensity. In this study, we have selected 47^0 for the effective incident angle of the built-in ATR accessory for our clear coat paint spectra as it is best for weak to medium strength absorptions.

All transformations of transmission spectra to corresponding ATR spectra were performed with the following input data to the above-mentioned MATLAB codes: refractive index of diamond is 2.38, the refractive index at high wavenumber where there is no absorption of the sample n (∞), is 1.50, and the incident angle (relative to the normal) in the IRE is 47^0. The value of 1.50 was searched from the list of refractive indices corresponding to the Sodium D-line. The clear coats used in this study are composed of acrylate polymer with modification by polyurethane and polystyrene. The refractive indices of these compounds are near 1.50, and this value was employed for n(∞) throughout our entire study.

5.2.3 Wavelets.

The fingerprint region of each ATR simulated spectrum (600 cm^{-1} to 1500 cm^{-1}), which is comprised of 468 points, was normalized to unit length and subject to wavelet analysis using the MATLAB Wavelet toolbox 3.0.4 (MathWorks, Natick, MA). Outside of the fingerprint region, each IR spectrum consisted of only C-H stretching bands present in all clear coat paint spectra and noise (2100 cm^{-1} to 2500 cm^{-1}) due to the uncompensated absorption of IR radiation by the diamond anvil cell. Applying the discrete wavelet transform to the fingerprint region, the 456 clear coats that served as the training set for the development of search prefilters for the PDQ database were decomposed into wavelet coefficients representing both the high and low frequency components of the signal. In this study, the Symlet6 mother wavelet at the 8^{th} level of decomposition, i.e., 8Sym6, was used to denoise and to resolve overlapping spectral responses in the fingerprint region of each IR spectrum. Preprocessing of IR spectra by wavelets produced 1080 wavelet coefficients for each IR spectrum.

5.2.4 Genetic Algorithm for Variable Selection.

Wavelet coefficients that contain information about the assembly plant of the automotive vehicle were identified by a genetic algorithm (GA) for pattern recognition analysis. The pattern recognition GA identifies a set of wavelet coefficients that optimizes the separation of the classes in a plot of the two or three largest principal components of the aligned and wavelet transformed data. Because principal components maximize variance, the bulk of the information encoded by the selected coefficients is about the classification problem of interest. The principal component (PC) plot functions as an

embedded information filter. A good PC plot can only be generated by coefficients whose variance or information content is primarily about class membership differences. Hence, the principal component analysis routine incorporated into the fitness function of the pattern recognition GA limits the search to these types of feature sets, thereby significantly reducing the size of the search space. In addition, the pattern recognition GA focuses on those classes and/or samples that are difficult to classify as the pattern recognition GA trains by boosting the relative importance (i.e., weights) of those classes and/or samples (i.e., vehicles). Samples that consistently classify correctly are not as heavily weighted as samples that are difficult to classify. Over time, the pattern GA is able to learn its optimal parameters in a manner similar to a neural network. The pattern recognition GA integrates aspects of artificial intelligence and evolutionary computations to yield a "smart" one-pass procedure for variable selection and classification. Further details about the operation of the pattern recognition GA can be found elsewhere [74, 75].

5.3 Results and Discussion

Comparison of ATR simulated spectra and experimentally obtained ATR spectra was made to assess the utility of the ATR simulation algorithm for search prefilter development. ATR spectra of automotive clear coat samples were obtained using a Thermo NICOLET iS50 FTIR spectrometer and compared with simulated ATR spectra developed from transmission spectra of the corresponding samples (see Figure 5.1).

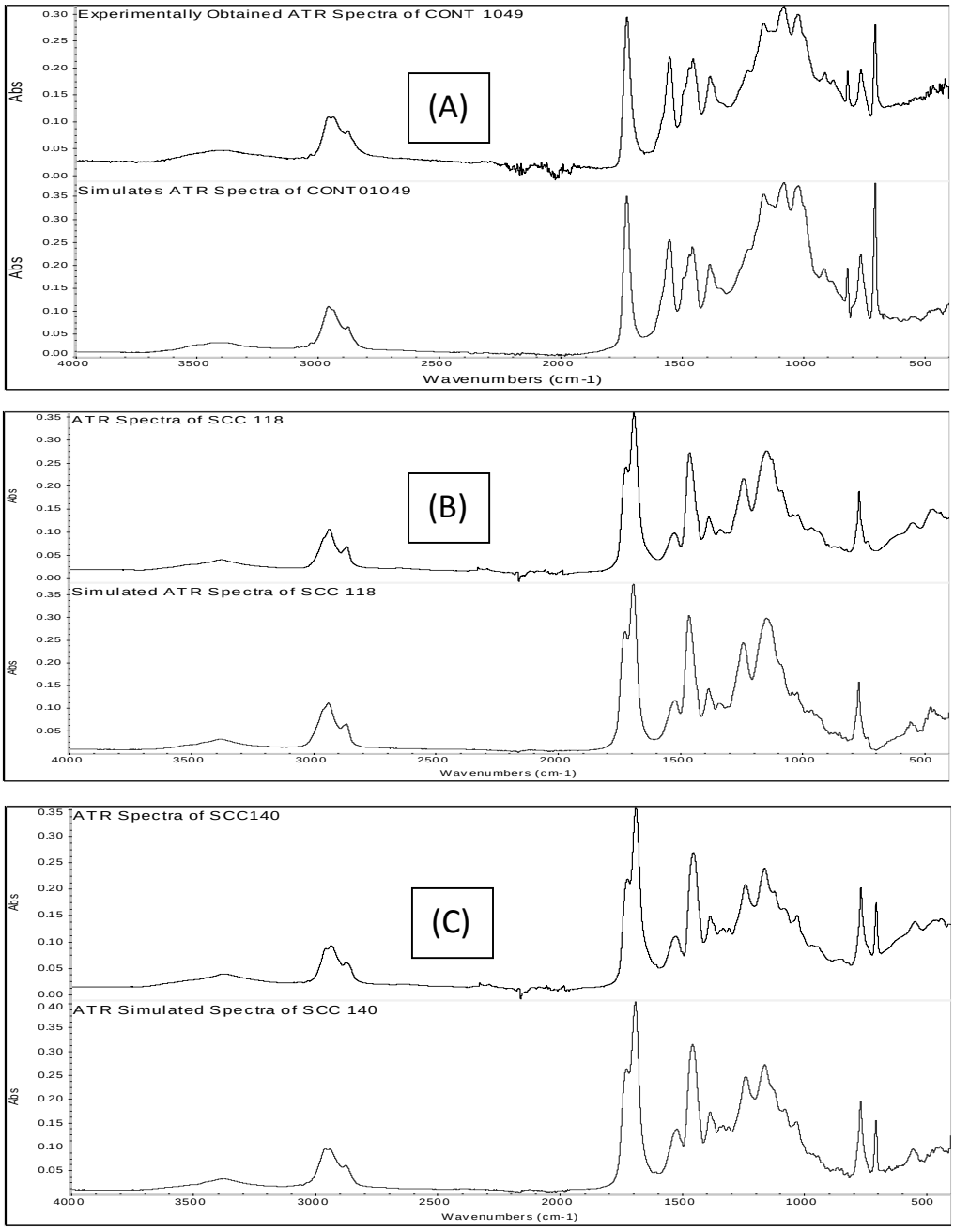

Figure 5.1. ATR spectra of automobile clear coats designated as (A) CONT1049, (B) SCC 118 and (C) SCC 140 in the PDQ database (upper), and simulated ATR simulated spectra developed from transmission spectra of the same sample (lower)

To evaluate the suitability of the ATR simulation algorithm in automotive paint analysis, search prefilters were developed for the purpose of identifying the assembly plant of a vehicle from an ATR spectrum of its clear coat paint smear using the same hierarchical classification scheme from a previous study [76] involving IR transmission data for GM assembly plants. 456 transmission spectra from the PDQ library spanning 22 GM assembly plants (see Table 5.1) were transformed into ATR spectra using the ATR simulation algorithm. First, an unknown was classified as to its plant group and then a search prefilter was used to identify a specific assembly plant or assembly plants within the plant group to which membership of the unknown was assigned. The assembly plants comprising each plant group are listed in Table 5.2. In the previous study, the IR spectra were initially divided into two categories based on the carbonyl band at 1709 cm^{-1}. In one category, the carbonyl band in each transmission spectrum was a singlet (Plant Groups 1, 3, and 5) which corresponds to acrylic melamine styrene and in the other category the carbonyl band was a doublet (Plant Groups 2 and 4) which corresponds to acrylic melamine styrene polyurethane. An examination of the expanded fingerprint region revealed five distinct spectral patterns with each pattern corresponding to a specific plant group.

The first step in this study was to apply principal component analysis (PCA) to the 456 wavelet transformed ATR spectra. Figure 5.2 shows a principal component (PC) plot of the 456 ATR spectra and the 1178 wavelet coefficients representing each simulated ATR spectrum. Each sample is represented as a point in the PC plot. The overlap of several plant groups in the PC plot of the data is evident.

Table 5.1. GM Plants used to develop the Search Prefilters

Plant ID	Plant	Model	Line
1	Arlington	CAD, CHE, GMC	SUB,YUK,ESD,CTA
3	Bowling Green	CAD,CHE	CVT,XLR
4	Doraville	PON	VTR,SIL,MTA,UPL,TAR
5	Fairfax	CHE,OLD,PON	GRA,MAL,ITR
6	Flint	CHE,GMC	SLV,SIE
8	Fort Wayne	CHE,GMC	SLV,SIE
9	Fremont	GMC	VIB,TAC,PVB,COA,GPR
10	Hamtramck	BUI,CAD,PON	BON,DEV,LUC,LES,SEV,ELD
11	Ingersoll	CHE, PON	EQU, MGM, TRA, TOR
12	Janesville	GMC	CTA,SUB,YUK
14	Lansing	PON	STS
16	Linden	CHE,GMC	BZR,JMY,S10
17	Lordstown	PON	SFR,CAV,COB,PST
18	Moraine	CHE,GMC,SAA	JMY,ENV,9S7,BZR,TBZ,SON
20	Oklahoma City	CHE, GMC	MAL,TBZ,ENV,EQU, XUV
21	Orion	PON,BUI	BON,PG6,LES,AUR, PKA
22	Oshawa	GMC,PON	ALL,REG
23	Pontiac	CHE,GMC	SLV,SIE,SIL
24	Ramos Arizpe	BUI,CHE,PON	CAV,SFR,RZV,AZT,HHR
25	Shreveport	CHE,GMC	S10,COL,SON
26	Silao	CHE,GMC,SAA	AVL,SUB,YXL
27	Spring Hill	STR	SSL,ION,SC1,SC2,SL1,VUE

The next step was feature selection. The pattern recognition GA identified wavelet coefficients characteristic of the plant group by sampling key feature subsets, scoring their PC plots and tracking those plant groups and/or spectra that were most difficult to classify. The boosting routine used this information to steer the population to an optimal solution. After 200 generations, the pattern recognition GA identified 27 wavelet coefficients whose PC plot (see Figure 5.3) showed clustering of the spectra on the basis of plant group.

Table 5.2. Assembly Plants Comprising Each Plant Group

Plant Group	Plant ID Number	Assembly Plant
1	1, 4, 5, 8, 14, 18, 23	Arlington, Doraville, Fairfax, Lansing, Moraine, Pontiac
2	3, 10, 21	Bowling Green, Hamtramck, Orion
3	6, 9, 11, 16, 17, 20, 22, 25	Flint, Fremont, Linden, Lordstown, Oklahoma City, Oshawa, Shreveport
4	12	Janesville
5	24, 26, 27	Ramos Arizpe, Silao, Spring Hill

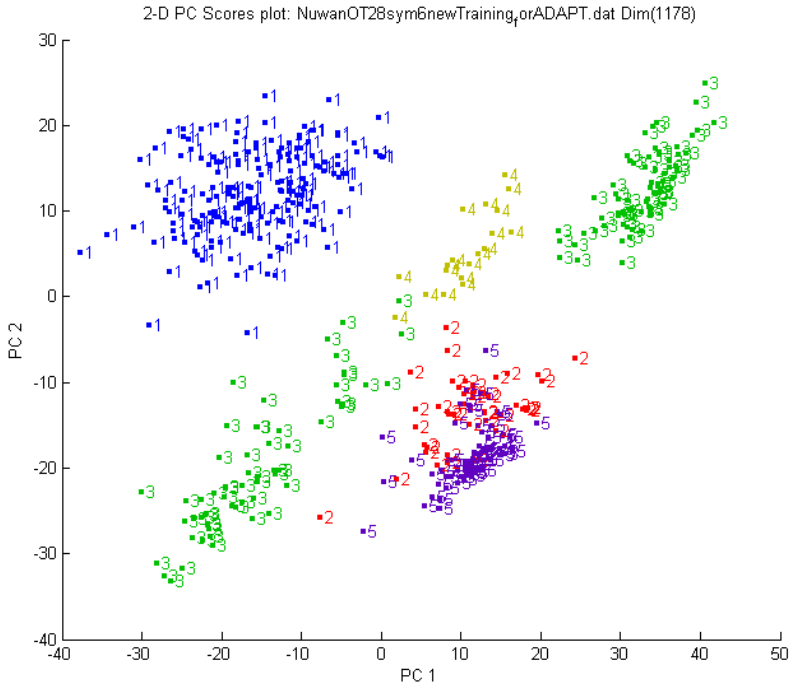

Figure 5.2. PC plot of the two largest principal components of the 456 ATR spectra and the 1178 wavelet coefficients comprising the training set. Each clear coat paint sample is represented as a point in the PC plot of the data (1 = Plant Group 1, 2 = Plant Group 2, 3 = Plant Group 3, 4 = Plant Group 4, and 5 = Plant Group 5).

To assess the predictive ability of these 27 wavelet coefficients, a validation set of 14 clear coat paint samples whose ATR spectra were obtained using a Nicolet iS50 FTIR

spectrometer served as the validation set. ATR spectra from the validations set were projected onto the PC plot developed from the 456 simulated ATR spectra of the training set and the 27 wavelet coefficients identified by GA using the transverse learning routine of the pattern recognition GA. Figure 5.4 shows the projection of the 14 validation set samples onto the PC plot of the training set data. All 14 clear coats were correctly classified.

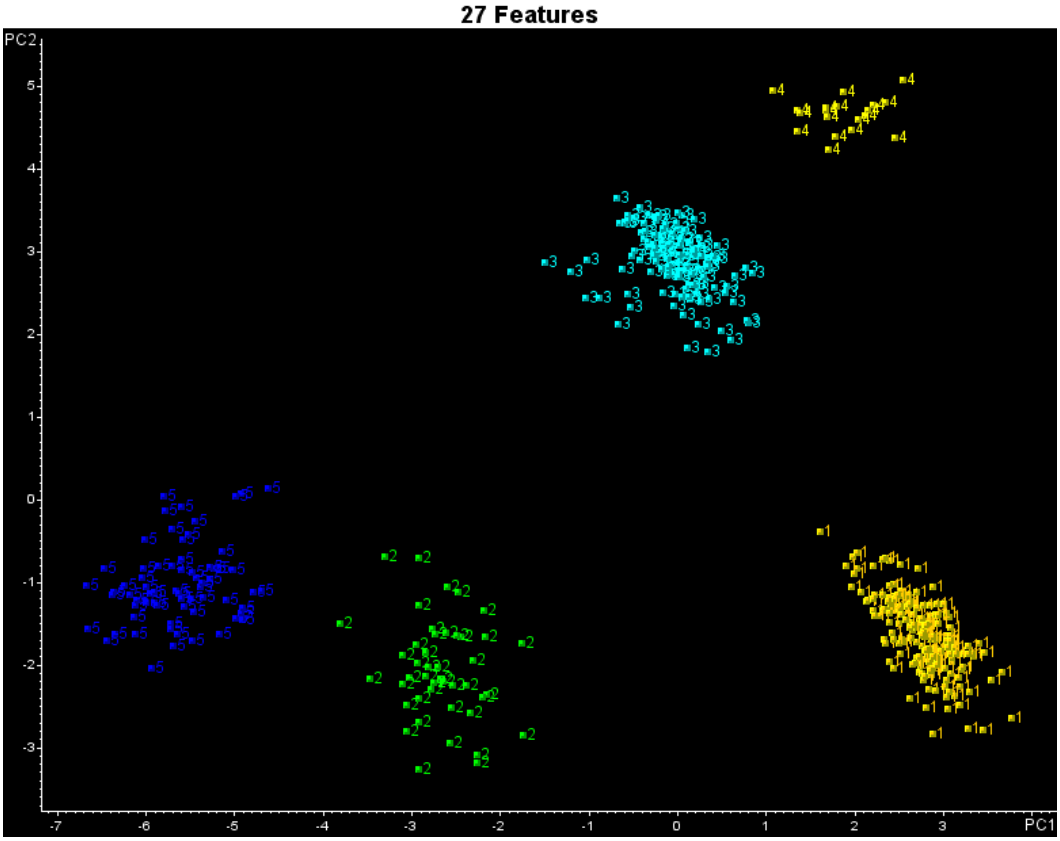

Figure 5.3. PC plot of the two largest principal components of the 456 ATR training set spectra and the 27 wavelet coefficients identified by the pattern recognition GA. Each clear coat paint sample is represented as a point in the PC plot of the data (1 = Plant Group 1, 2 = Plant Group 2, 3 = Plant Group 3, 4 = Plant Group 4, and 5 = Plant Group 5).

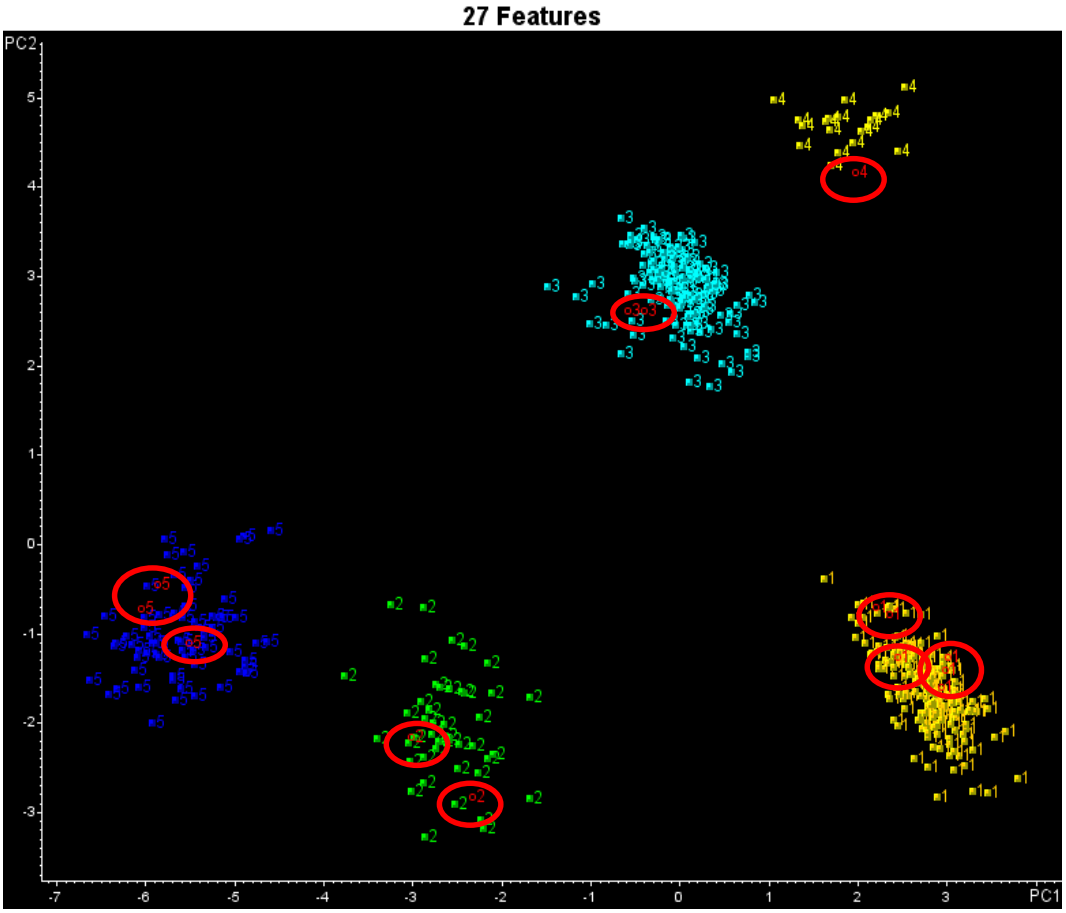

Figure 5.4. PC plot of the two largest principal components of the 456 ATR training set spectra and the 27 wavelet coefficients identified by the pattern recognition GA. Each clear coat paint sample is represented as a point in the PC plot of the data. Validation set samples are circled. (1 = Plant Group 1, 2 = Plant Group 2, 3 = Plant Group 3, 4 = Plant Group 4, and 5 = Plant Group 5).

The next step was to develop search prefilters to identify the spectra of the validation set samples by assembly plant. For each plant group, a search prefilter was developed to discriminate spectra by assembly plant within a plant group. Figure 5.5 shows a PC plot of the two largest principal components of 29 wavelet coefficients identified by the pattern recognition GA for Plant Group 1 (see Table 5.2). Each simulated spectrum is represented as a point in the PC plot of the data. Plant 18 (Moraine, OH) is well separated from the other assembly plants in the PC plot. The spectra from the other 6 assembly plants (Arlington TX, Doraville GA, Fairfax KS, Fort Wayne IN, Lansing MI, and Pontiac MI)

were similar, which prevented further discrimination by assembly plant of these clear coats. Projecting the validation set samples assigned to Plant Group 1 onto this PC plot via transverse learning showed that each projected sample was located in a region of the map with paint samples of the same class label: either plant 18 or plants 1, 4, 5, 8, 14, and 23.

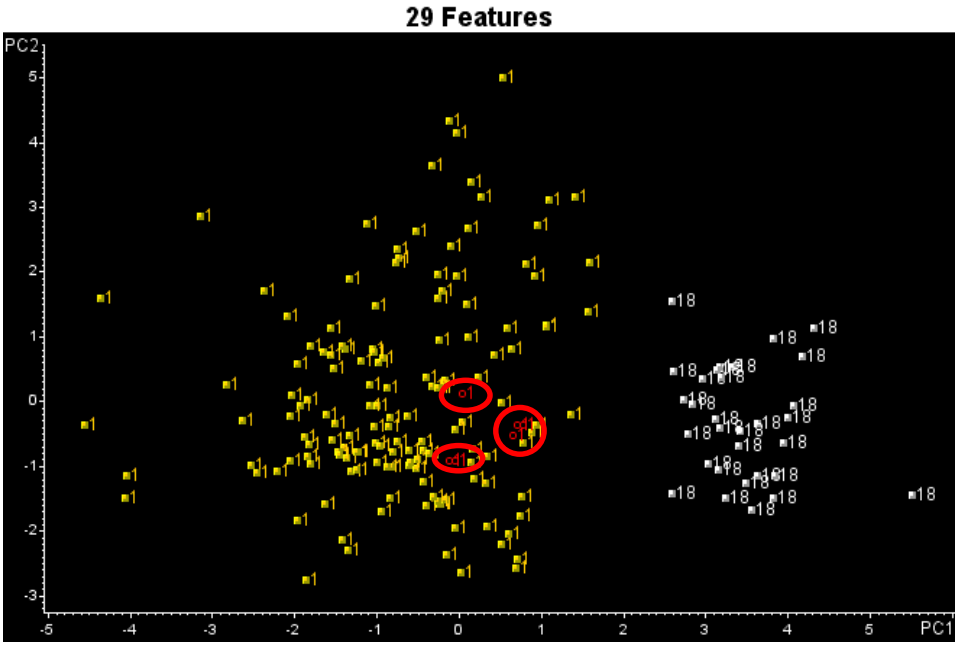

Figure 5.5. PC plot of the two largest principal components of the 180 Plant Group 1 simulated spectra and the 27 wavelet coefficients identified by the pattern recognition GA. Each simulated or experimental ATR spectrum is represented as a point in the PC plot of the data. Validation set samples are in red and circled. (1 = Arlington, Doraville, Fairfax, Fort Wayne, Lansing, Pontiac, and 18 = Moraine).

Figure 5.6 shows a plot of the two largest principal components of the 52 simulated ATR spectra and the 28 wavelet coefficients identified by the pattern recognition GA for the assembly plants comprising Plant Group 2. All 3 assembly plants (Bowling Green KY, Hamtramck MI, and Orion MI) are well separated from each other in the PC plot of the data. The two validation set samples assigned to Plant Group 2 also projected onto

this plot lie in a region of the PC map that contains simulated spectra with the same class label.

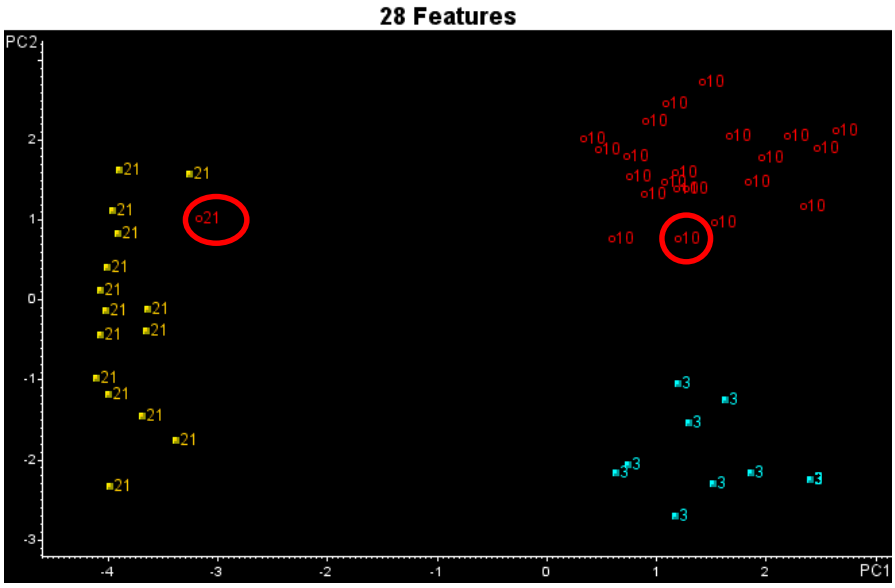

Figure 5.6. PC plot of the two largest principal components of the 52 Plant Group 2 simulated spectra and the 28 wavelet coefficients identified by the pattern recognition GA. Each simulated or experimental ATR spectrum is represented as a point in the PC plot of the data. Validation set samples are in red and circled. (3 = Bowling Green, 10 = Hamtramck, and 21 = Orion).

Figure 5.7 shows a plot of the two largest principal components of the 138 simulated ATR spectra from Plant Group 3 and the 33 wavelet coefficients identified by the pattern recognition GA. Clustering of the simulated spectra by assembly plant and model in the PC plot is evident for the spectra comprising the training set. Fremont California (Plant 9) and Lordstown Ohio (Plant 17) form distinct clusters in the PC plot as do the trucks from Oshawa (Plant 22). The two validation set samples assigned to Plant Group 3 are projected onto the PC plot in a region that contains simulated spectra from the same assembly plant.

Plant Group 4 contains only one assembly plant, and the three assembly plants from Plant Group 5 cannot be discriminated due to the similarity of their spectra. A summary of the results obtained for the 14 validation samples using the search prefilters developed from the simulated ATR spectra is shown in Table 5.3. For validation set samples 91001, 91013, 91027, and 92005, differences between the experimental ATR spectrum and the simulated ATR spectrum derived from the corresponding transmission spectrum of the same sample in the PDQ library (see Figures 5.8-5.11) can be attributed to weathering. The increase in the 1630 cm^{-1} band and the decrease and change in the spectral pattern for the 1030 cm^{-1} – 1085 cm^{-1} region can be attributed to the formation of primary amines and the loss of the C-O-C groups attached to the triazine ring of acrylic melamine in acrylic melamine styrene [77, 78]. By exposing a fresh surface of the clear coat automotive paint layer to the spectrometer (see Figure 5.12), interference due to weathering can be eliminated.

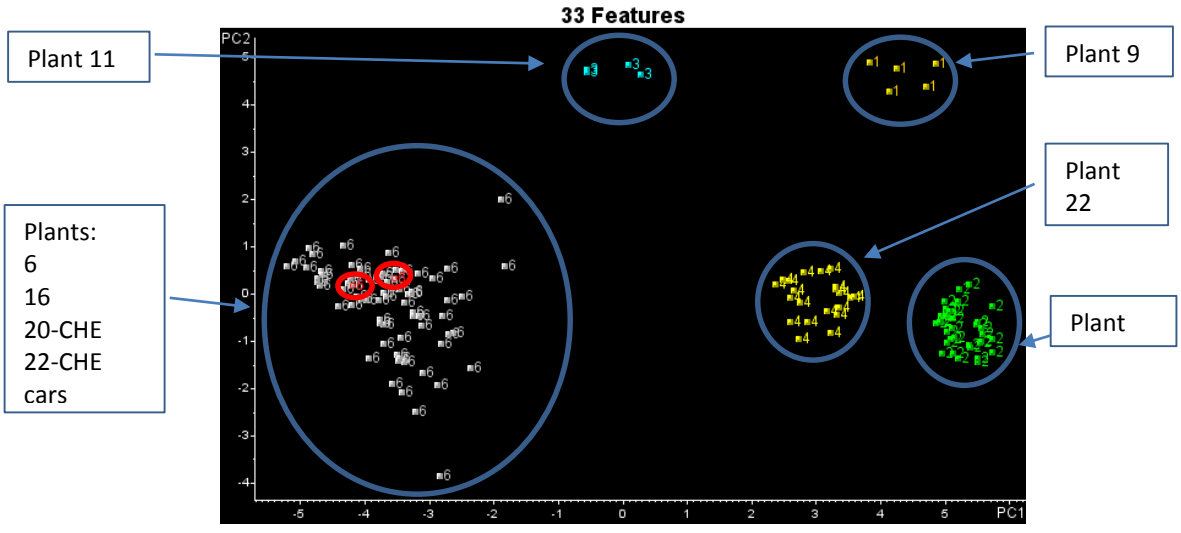

Figure 5.7. PC plot of the two largest principal components of 138 Plant Group 3 simulated ATR spectra and the 33 wavelet coefficients identified by the pattern recognition GA. Each simulated or experimental ATR spectrum is represented as a point in the PC plot of the data. Validation set samples are in red and circled. (1 = Fremont, 2 = Lordstown, 3 = Ingersoll, 4 = Oshawa, and 6 = Flint, Linden, Oklahoma City, Oshawa, Shreveport).

Table 5.3. Summary of Results for Validation Set Samples

Validation Sample	Assigned Plant Group	Assigned Plant(s)	ID of Validation Sample
91001	1	1,4,5,8,14, 22(Buick cars), 20(Trucks)	14
91011	5	24,26,27	26
91012	5	24,26,27	26
91013	1	1,4,5,8,14, 22(Buick cars), 20(Trucks)	14
91025	2	10	10
91027	1	1,4,5,8,14, 22(Buick cars), 20(Trucks)	14
91028	1	1,4,5,8,14, 22(Buick cars), 20(Trucks)	14
92001	1	1,4,5,8,14, 22(Buick cars), 20(Trucks)	1
92003	4	12	12
92004	3	6,16,20(CHE),22(CHE cars),25	6
92005	1	1,4,5,8,14, 22(Buick cars), 20(Trucks)	22
92006	5	24,26,27	24
92007	2	21	21
92008	3	6,16,20(CHE),22(CHE cars),25	25

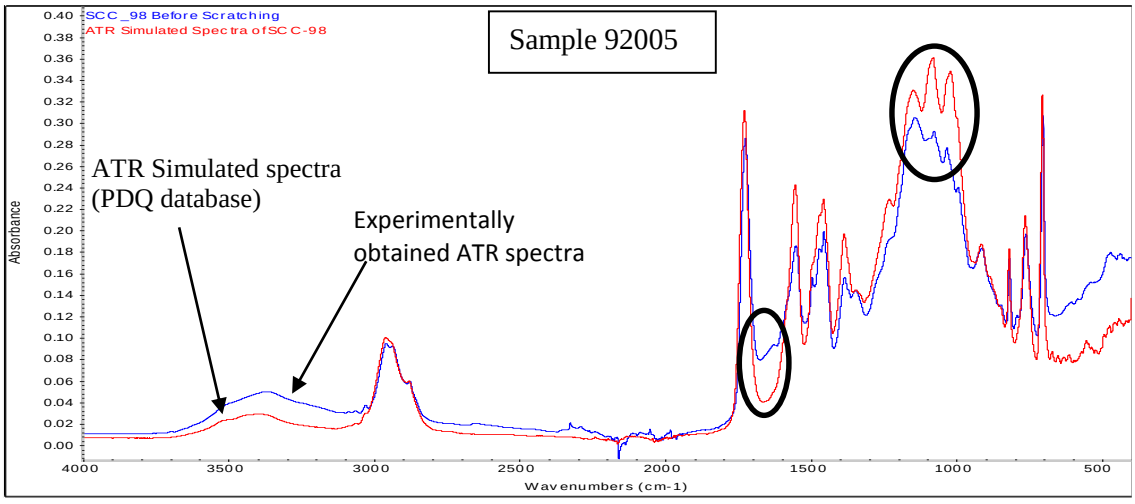

Figure 5.8. Simulated (red) and experimental (blue) ATR spectra for Sample 92005. For the experimental ATR spectrum, the increase in the 1630 cm^{-1} band and the decrease in the 1030 cm^{-1} and 1085 cm^{-1} bands are attributed to weathering of the clear coat layer.

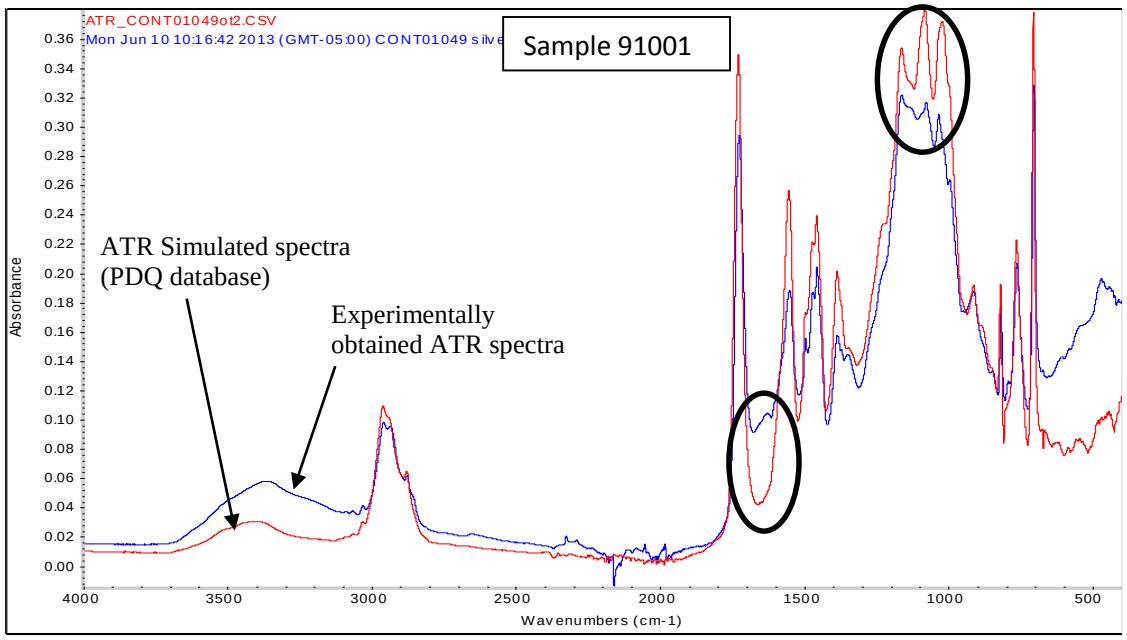

Figure 5.9. Simulated (red) and experimental (blue) ATR spectra for Sample 91001. For the experimental ATR spectrum, the increase in the 1630 cm^{-1} band and the decrease in the 1030 cm^{-1} and 1085 cm^{-1} bands are attributed to weathering of the clear coat layer.

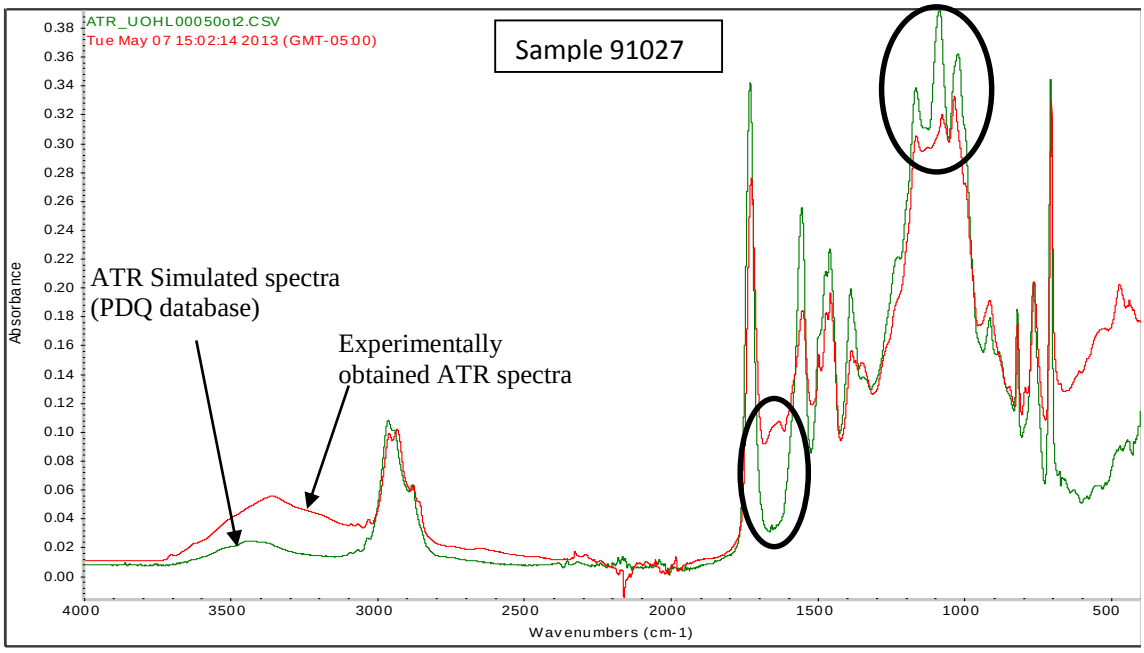

Figure 5.10. Simulated (green) and experimental (red) ATR spectra for Sample 91027. For the experimental ATR spectrum, the increase in the 1630 cm^{-1} band and the decrease in the 1030 cm^{-1} and 1085 cm^{-1} bands are attributed to weathering of the clear coat layer.

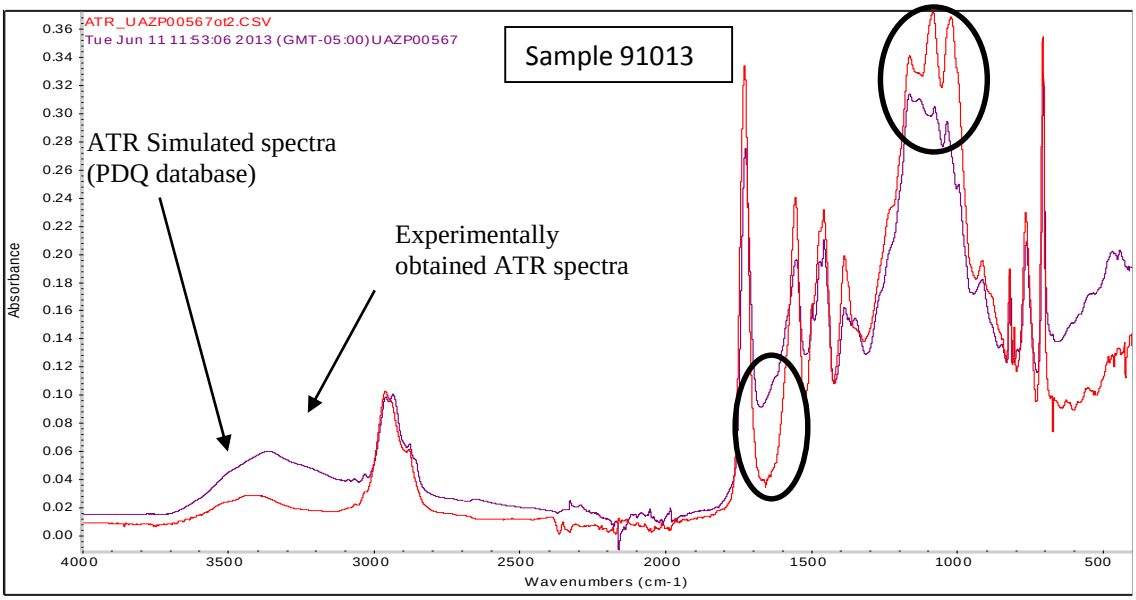

Figure 5.11. Simulated (red) and experimental (purple) ATR spectra for Sample 91013. For the experimental ATR spectrum, the increase in the 1630 cm^{-1} band and the decrease in the 1030 cm^{-1} and 1085 cm^{-1} bands are attributed to weathering of the clear coat layer.

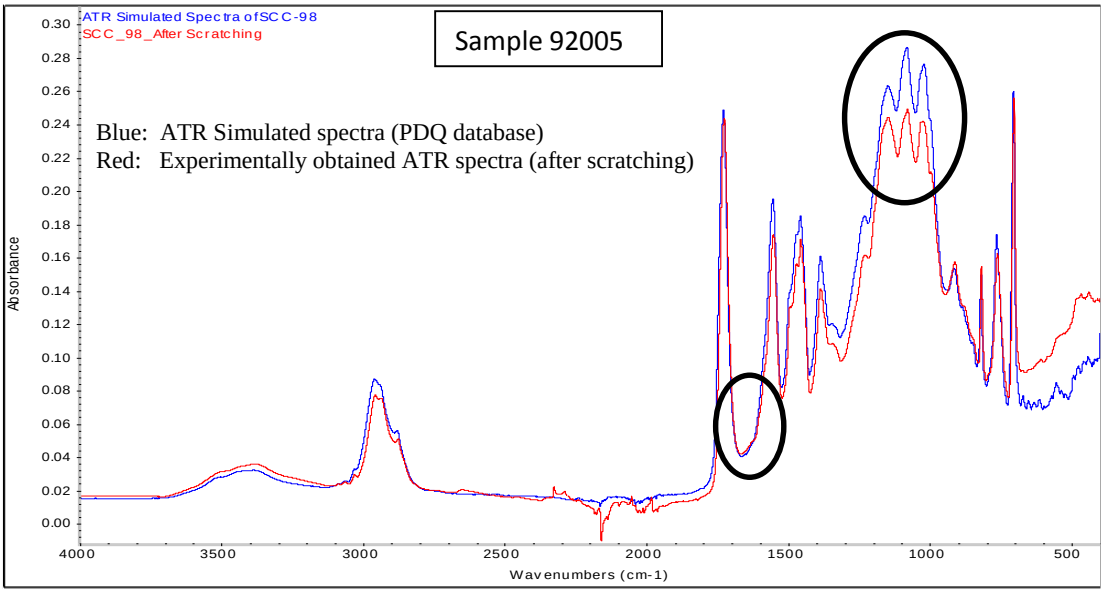

Figure 5.12. Simulated (red) and experimental (blue) ATR spectra for Sample 92005. For the experimental ATR spectrum, a fresh surface of the clear coat layer was exposed to the spectrometer to minimize the effects of weathering. The circled regions (1630 cm^{-1}, 1030 cm^{-1} and 1085 cm^{-1}) indicative of weathering are consistent with the simulated ATR spectrum.

To further understand the weathering of clear coats, an IR imaging experiment was performed using Thermo Nicolet iN10 MX infrared imaging microscope. The surface of an automotive paint chip (SCC 0988) was scratched using a sharp blade to expose a fresh surface for the analysis. Using a germanium micro-tip ATR accessory, the spectra of both the fresh (scratched) and the original surface of the sample were collect with 8 wavenumber resolution. 364 spectra were collected with 16 scans run for each spectrum. A liquid nitrogen cooled mercury–cadmium–telluride (MCT) detector was employed. For better visualization of the IR data, an image of the interrogated area of the paint chip was generated by dividing the area of the peak at 1075 cm^{-1} by the area of the peak at 700 cm^{-1} (Figure 5.13 (B)). The peak at 1075 cm^{-1} , which is affected by weathering, corresponds to C-O-C, which is attached to the triazine ring of acrylic melamine in acrylic melamine styrene resin, whereas the 700 cm^{-1} peak corresponds to the C-H bending mode of styrene which does not show any changes due to weathering. The FTIR image clearly shows that this peak ratio is higher for the scratched (fresh) surface of the paint chip than for the non-scratched surface. This confirms that the area of the peak at 1075 cm^{-1} is comparatively small on the weathered (old) surface compared to the fresh (scratched) surface. This image supports our previous conclusions about the weathering of clear coat layer. Sample spectra of both old and fresh surfaces are shown in Figure 5.14.

(A)

(B)

(C)

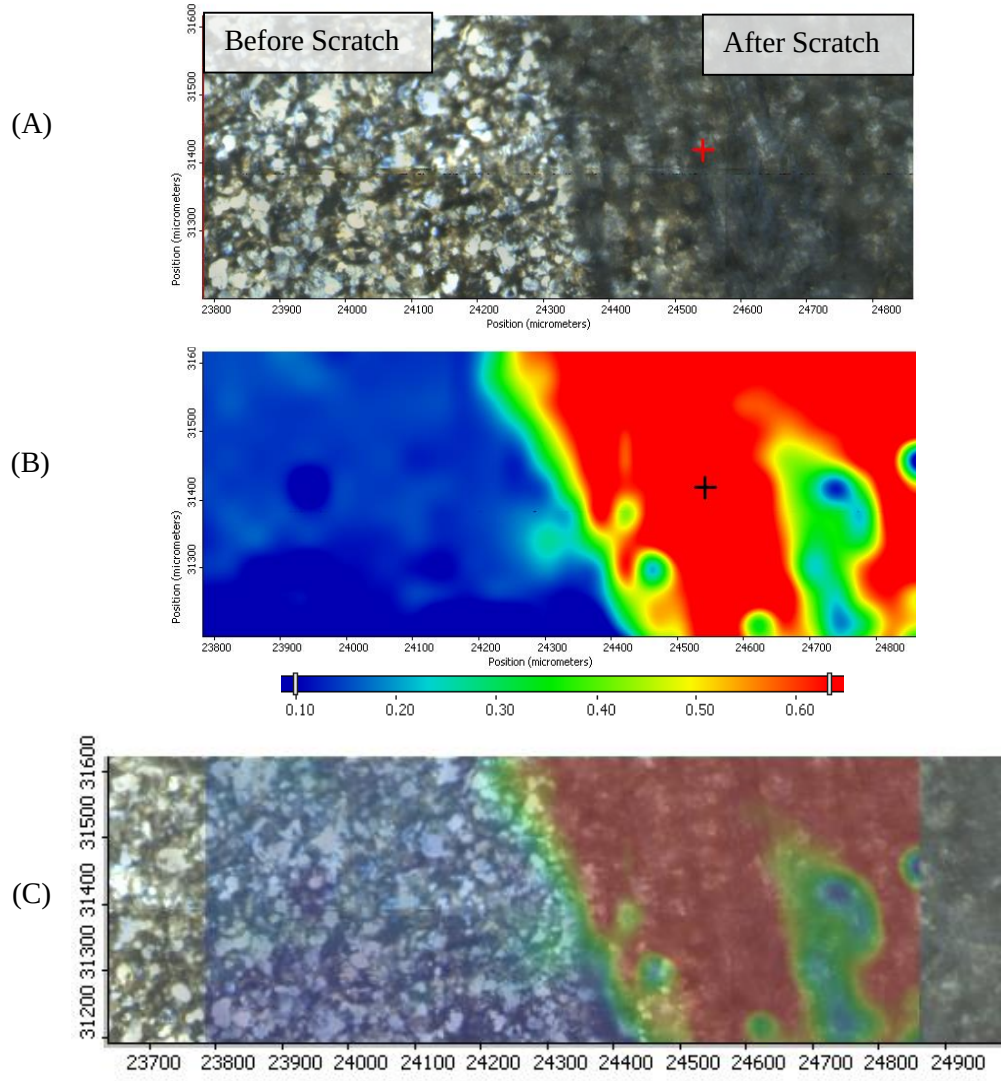

Figure 5.13, (A) Area map of the paint chip (B) FTIR image showing peak area ratio between peaks at the peak at 1075 cm^{-1} and peak at 700 cm^{-1} for the same area (C) Blended image of (A) and (B)

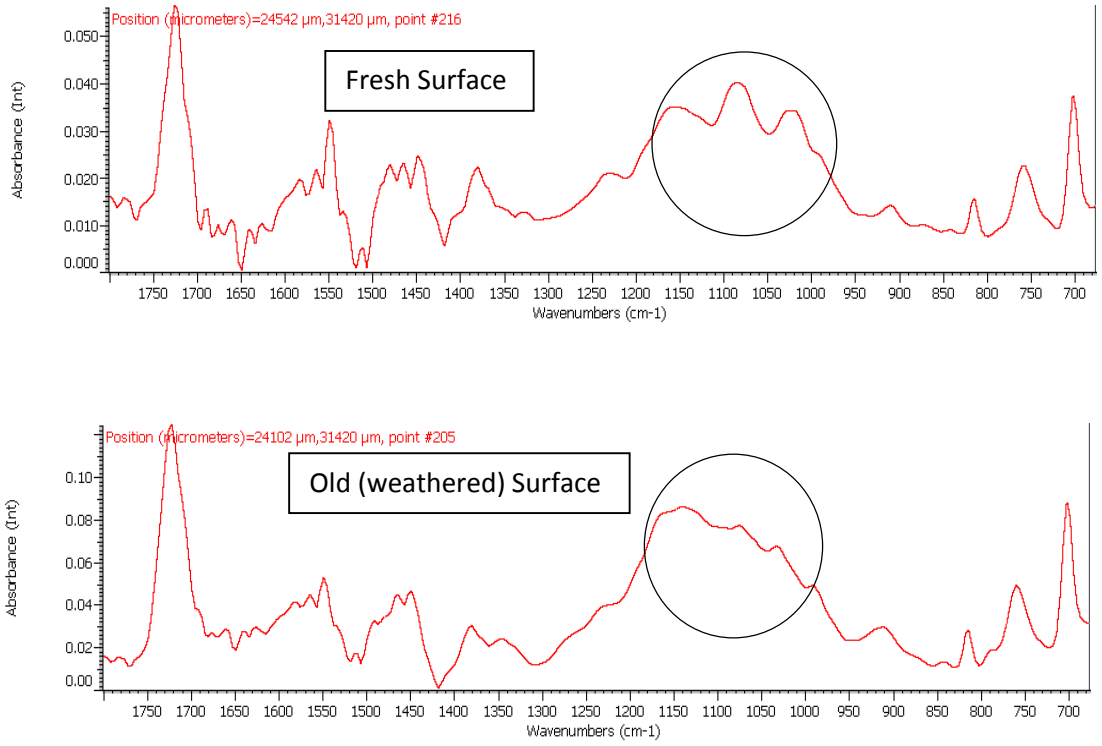

Figure 5.14, FTIR spectra from scratched side of the paint chip (above) and non-scratched side of the paint chip (below)

Spectral libraries of archived transmission data of automotive paint samples can be transformed into ATR libraries using the correction algorithm. As ATR is a surface sensitive technique, changes in the composition of the clear coat layer at or near the surface due to weathering, which will not be a problem with transmission spectra, can pose a problem for ATR. Careful consideration of the effects of weathering on clear coats is crucial to quantify the general discrimination power of original automotive paint comparisons limited to the clear coat paint layer when ATR spectroscopy is used to characterize automotive paint samples recovered from a crime scene.

References

71. G. Fettis (Editor), Automotive Paints and Coatings, VCH Publications, New York, 1995.

72. S. Ryland, T. Jegovich, K. P. Kirkbride, "Current Trends in Forensic Paint Examination" Forensic Sci. Rev. 2006, 18, 97-117.

73. J. E. Bertie, R. N. Jones, Y. Apelblat, and C. D. Keefe, "Infrared Intensities of Liquids XIII: Accurate Optical Constants and Molar Absorption Coefficients Between 6500 and 435 cm^{-1} of Toluene at 25^0C from Spectra Recorded in Several Laboratories," Appl. Spec., 1994, 48(1), 127-143.

74. B. K. Lavine, K. Nuguru, and N. Mirjankar, "One Stop Shopping - Feature Selection, Classification, and Prediction in a Single Step," **Journal of Chemometrics,** 2011, 25, 116-129

75. B. K. Lavine, J. Ritter, A. J. Moores[*1], M. Wilson, A. Faruque, and H. T. Mayfield, "Source Identification of Underground Fuel Spills by Solid Phase Micro-extraction/High-Resolution Gas Chromatography/Genetic Algorithms," **Anal. Chem**., 2000, 72(2), 423-431

76. B. K. Lavine, A. Fasasi, N. Mirjankar, and M. Sandercock, "Development of Search Prefilters for Infrared Library Searching of Clear Coat Paint Smears," **Talanta**, 2014, 119, 331–340.

77. J. F. Larche, P. O. Bussiere, P. Chung, and J. L. Gardette, Chemical Structure Evolution of Acrylic-Melamine Thermoset upon Photo-Ageing, European Polymer Journal, 2012, 48, 172-182.

78. T. Nguyen, J. Martin, E. Byrd and N. Embree, Relating Laboratory and Outdoor Exposure of Coatings: II, J. Coating Technology, 2002, 74, 65-80.

CHAPTER VI

CONCLUSION

Swellable polymer particles that respond to pH have been prepared by free radical dispersion polymerization using *N*-isopropylpolyacrylamide (NIPA), methylene-bis acrylamide, 2-dimethoxy-2 phenyl-acetophenone, *N*-tert-butylacrylamide (NTBA), and acrylic acid methacrylic acid, ethacrylic acid or propacrylic acid. The polymer particles are incorporated into hydrogel membranes prepared by mixing the pH sensitive polyNIPA particles with aqueous polyvinyl alcohol solutions followed by cross linking using glutaric dialdehyde. When the polymer particles are dispersed in a hydrogel, there are large changes in the turbidity of the membrane as the pH of the solution in contact with the membrane is varied. These changes can be monitored using visible or near infrared absorbance spectroscopy. These copolymers show a large response over a narrower pH range. Furthermore, the degree of swelling and the apparent pK_a of these polymer particles increase with temperature. Swelling is nonionic as the degree of swelling is independent of ionic strength of the solution in contact with the membrane. The pK_a of these particles can be tuned to respond sharply in the physiological pH range (5.0 to 7.4) by varying the degree of cross-linking, the amount of NTBA used or the alkyl chain length of the pH sensitive co-monomer. Proposed applications of these polymer particles include gastric

pH sensing using magnetoelastic sensing, bioconjugation, and pH monitoring of the progress of open heart surgery using optical fibers where pH serves as a measure of tissue ischemia.

Vanillin is the major constituent of vanilla extract, a flavoring ingredient used in food and beverages. Natural vanilla extract prepared from the bean of the tropical orchid, *Vanilla planifolia*, is expensive due to the limited supply of the vanilla bean. For this reason, synthetic vanilla extracts are popular. Synthetic vanilla extracts are less complex and usually contain vanillin, ethyl vanillin, and other related compounds prepared from inexpensive starting materials. Several liquid chromatographic methods have been developed to quantitate coumarin, vanillin, and ethylvanillin in vanilla extract. The use of water rich mobile phases in reversed phase liquid chromatography (RPLC), e.g., 1% butanol in water with 0.2% acetic acid with C_{18}, C_8, and cyanopropyl columns, has been investigated as a potential method to characterize the composition of synthetic vanilla extracts. Better resolution is achieved in the separation of vanillin compounds when hydrophobic alcohols are used as organic modifiers. This can be attributed to butanol partitioning into the bonded phase, which provides a more extended ordered surface increasing the contact surface area of the stationary phase and thereby increasing the selectivity of the separation. Using water rich mobile phases, constituents of vanilla extract in 36 commercial products obtained from markets in the local area (Stillwater and Oklahoma City) were identified demonstrating the efficacy of using water rich mobile phases as the basis of an RPLC method.

A correction algorithm to allow ATR spectra to be matched using the IR transmission spectral library of the PDQ database has also been investigated as part of the research described in this dissertation. ATR is a widely used sampling technique in FTIR because minimal sample preparation is required. As the penetration depth of the ATR analysis beam is shallow, the outer layers of a multi-layered automotive paint sample is preferentially analyzed with the entire sample intact. For this reason, forensic laboratories have utilized ATR to collect IR spectra of automotive paint systems which may consist of three or more layers. However, the IR spectrum of a paint sample obtained by ATR will exhibit distortions, e.g., band broadening and lower relative intensities at higher wavenumbers, when compared with its transmission counterpart. This hinders library searching as most library spectra are measured in transmission mode. The correction algorithm to convert transmission spectra from the PDQ library into ATR spectra is shown to be able to address distortion issues such as the relative intensities and broadening of the bands, and introduction of wavelength shifts at lower frequencies, which prevent library searching of ATR spectra using archived IR transmission data.

To assess the efficacy of the ATR correction algorithm, search prefilters were developed from simulated ATR spectra for the purpose of identifying the assembly plant of a vehicle from an ATR spectrum of its clear coat. 456 transmission spectra from the PDQ library spanning 22 GM assembly plants which served as the training set cohort were transformed into ATR spectra using the correction algorithm. The spectral region used to formulate the search prefilters was the fingerprint region (1500 cm^{-1} to 600 cm^{-1}). Both the simulated and experimental ATR spectra were preprocessed using the discrete wavelet

transform, which increased the signal to noise of the data by concentrating the signal in specific wavelet coefficients. Fourteen clear coat paint samples whose ATR spectra were obtained using a Nicolet iS50 FTIR spectrometer served as the validation set. All 14 samples were correctly classified on the basis of the vehicle's assembly plant.

For 4 of the validation set samples, there were marked differences between the experimental ATR spectrum and the computed ATR spectrum derived from the corresponding transmission spectrum of the same sample in the PDQ library which we attributed to weathering. By exposing a fresh surface of the clear coat automotive paint layer to the ATR probe, interference due to weathering was obviated. This facilitated the accurate classification of this validation set sample by the search prefilters developed from simulated ATR spectra of automotive clear coats.

VITA

Undugodage Don Nuwan Tharanga Perera

Candidate for the Degree of

Doctor of Philosophy

Thesis: COMPUTER ENHANCED SPECTROCHEMICAL AND CHROMATOGRAPHIC ANALYSIS APPLIED TO PROBLEMS IN ANALYTICAL AND FORENSIC CHEMISTRY

Major Field: Chemistry

Biographical:

Education:

Completed the requirements for the Doctor of Philosophy in Chemistry at Oklahoma State University, Stillwater, Oklahoma in July, 2015.

Completed the requirements for the Post Graduate Diploma in Analytical Chemistry at University of Peradeniya, Peradeniya, Sri Lanka in 2009.

Completed the requirements for the Bachelor of Science at University of Kelaniya, Kelaniya, Sri Lanka in 2006.

Experience: Teaching/Research Assistant, Depertment of Chemistry, Oklahoma State University (January 2010-July 2015), Standards/ Testing Officer, Sri Lanka Standards Institution, Ministry of Science and Technology, Sri Lanka. (January 2008-December 2009), Management Trainee/ISO Coordinator, Multichemi Exports (Pvt) Ltd, Biyagama, Sri Lanka (July 2006-January 2008)